JMO

Journal for Modeling in Ophthalmology

Journal for Modeling in Ophthalmology (JMO) was created in 2014 with the aim of providing a forum for interdisciplinary approaches integrating mathematical and computational modeling techniques to address open problems in ophthalmology.

The Editorial Board members include experts in ophthalmology, physiology, mathematics and engineering and strive to ensure the highest scientific level of the contributions selected for publication. JMO aims to be the voice for this rapidly growing interdisciplinary research and we hope you will join us on this exciting journey.

JMO welcomes articles that use modeling techniques to investigate questions related to the anatomy, physiology and function of the eye in health and disease.

For further information on JMO's focus & scope, and manuscript submissions:

www.modeling-ophthalmology.com
info@modeling-ophthalmology.com

Copyright

Manuscript submissions
Author guidelines & templates are available via the website, through which all manuscripts should be submitted. For inquiries please contact us via e-mail.

Publication frequency
JMO is published four issues per year (quarterly) electronically. A selection is published in print twice a year and distributed free of charge at congresses through Kugler Publications or partners.

Advertising inquiries
JMO offers online and in print sponsorship and advertising opportunities. Please contact Kugler Publications to for inquiries.

b. After 12 months from the date of publication, authors are able to enter into separate, additional contractual arrangements for the non-exclusive distribution of JMO's published version of the work, with an acknowledgement of its initial publication in JMO.

Open access policy

The first volume of JMO is fully open access (after registration) without requiring any publication fee from the authors. However, we are currently evaluating various models to cover the publications costs while keeping knowledge as accessible as possible, which remains our first priority. Possible models include subscription fees, publication fees and advertisement venues, or a combination. Please share your thoughts with us on this hot topic via e-mail.

Disclaimers

All articles published, including editorials and letters, represent the opinions of the authors and do not reflect the official policy of JMO, its sponsors, the publisher or the institution with which the author is affiliated, unless this is clearly specified. Although every effort has been made to ensure the technical accuracy of the contents of JMO, no responsibility for errors or omissions is accepted. JMO and the publisher do not endorse or guarantee, directly or indirectly, the quality or efficacy of any product or service described the advertisements or other material that is commercial in nature in any issue. All advertising is expected to conform to ethical and medical standards. No responsibility is assumed by JMO or the publisher for any injury and/or damage to persons or property as a matter of products liability, negligence or otherwise, or from any use or operation of any methods, products, instructions, or ideas contained in the material herein. Because of rapid advances in the medical Sciences, independent verification of diagnoses and drug dosages should be made.

Table of contents

Original article

Review article

Ophthalmology and mathematics: crossroad or scientific interface?

The progress of science is discontinuous. However, accepting the dynamic nature of science, most of us have experienced the point of research crossroads when it was hard to choose the correct path. In 1962, Thomas Samuel Kuhn published his controversial book *The Structure of Scientific Revolutions* introducing the term 'paradigm shift' raising the idea that progress is not a continuous accumulation, but rather a revolutionary process where brand new ideas are adopted and old ideas are abandoned.[1]

Without trying to accept or argue philosophical aspects, today we experience a rapidly-growing amount of research in ophthalmology. The goal of the current evidence-based approach in medicine is to optimize everyday clinical practice based on comprehensive research. However, results coming from the basic sciences sometimes may not be directly applicable to an individual patient. The latest developments, scientific achievements and research in ophthalmology steer to the exciting new perspective based on a multidisciplinary approach. Bringing together scientists whose expertise encompasses ophthalmology, physiology, mathematics, physics and engineering and who explore different aspects of the same problems empowering to make scientific progress.

Can ophthalmologists think mathematically? Is it possible to provide a quantitative representation of the biophysical processes in the eye? Application of objective scientific methods and subjective perspectives can open up a wide range of educational and professional opportunities leading to a better understanding of the pathogenesis and the natural course of the disease, progression and new ways of treatment.

Introducing the second issue of Journal for Modeling in Ophthalmology, we hope the reader will enjoy both clinical and theoretical insights on glaucoma in short papers that followed the International Congress on Advanced Technologies and Treatments for Glaucoma (ICATTG15) held in Milan (Italy), October 29-31, 2015 (http://www.icatto.com/archive/icattg2015/).

Normal-tension glaucoma is a particularly difficult type of glaucoma both in terms of diagnosis and treatment. Iester points out that different types of glaucoma exist and are probably based on the presence of different risk factors. The cut-off value of 21 mmHg is not used anymore to differentiate healthy subjects from glaucoma patients. The paper by Quaranta *et al.* analyses the rationale for IOP measurements throughout the 24-hour cycle. IOP is not a static number; rather, it exhibits time-de-

pendent variations that can reach up to 6 mmHg over a 24-hour period in healthy eyes, and even more in eyes with glaucoma.[2-5] Regarding 24-hour IOP character-istics, only IOP peak was correlated to visual field progression, while 24-hour IOP fluctuation was not an independent risk factor.[6] Indeed, 24-hour mean, peak and fluctuation were all associated and a strong correlation was found between mean and peak IOP, and between fluctuation and peak IOP. Mean IOP is a strong predictor of glaucomatous damage. A desired therapeutic target is therefore a uniform reduction of IOP throughout the 24 hours. A reliable method of continuous IOP measurement would be desirable, making 24-hour IOP phasing easier and opening new pathways for research.

Interestingly, the papers by Szopos *et al.* and Mauri et al. lead to new perspec-tives of mathematical modeling of aqueous humor flow and intraocular pressure towards individualized glaucoma management. Szopos *et al.* aim to provide both a qualitative description and a quantitative assessment of how variations in aqueous humor flow parameters influence IOP and the outcome of IOP lowering medications. They developed a mathematical model that describes the steady state value of IOP as the result of the balance between aqueous humor production and drainage and performing stochastic simulations to assess the influence of different factors on the IOP distribution in ocular normotensive and ocular hypertensive subjects and also on the IOP reduction following medications. This model may help identify patient specific factors that influence the efficacy of IOP lowering medications and aid the development of novel, effective, and individualized therapeutic approaches to glaucoma management.

Mauri *et al.* theoretically analyzed new aspects of electro-fluid dynamics of aqueous humor production. The connection between HCO_3, Na^+ and topical medications in the regulation of aqueous humor production is still controversial and difficult to study experimentally by trying to isolate the role of a single electrolyte in regulating aqueous humor production. The use of a mathematical model appeared to be a promising approach to help unravel such a connection through simulation and comparison of different predicted scenarios.

Groups of authors from Indianapolis and Milan universities contributed to glaucoma progression analysis. The paper by Hutchins *et al.* on clinical evaluation of baseline characteristics predictive of structural and functional progression in open-angle glaucoma patients with different demographic characteristics aims to examine ocular blood flow parameters that may predict structural and functional disease progression in open angle glaucoma patients of different diabetic status, gender, ethnicity, and body mass index. Messenio *et al.* evaluated the variations of IOP, morphometric papillary characteristics, perimetric indices and electrophysio-logical parameters before and after topical IOP lowering therapy in patients with

suspect normal tension glaucoma. They showed that electrophysiological tests could provide a more sensitive measure of retinal ganglion cell integrity and help distinguish between suspect normal-pressure glaucoma patients before perimetric alterations are evident and normal subjects with apparent larger disc cupping.

Over the past decades, color Doppler imaging (CDI) has gained popularity as a reliable tool to measure blood flow in a variety of vascular beds throughout the body. The use of CDI to measure blood flow parameters in retrobulbar vessels has become very common. Carichino et al. introduce a computer-aided identification of novel ophthalmic artery waveform parameters. The computed-aided analyses of ophthalmic artery velocity waveforms obtained via CDI were able to distinguish arterial waveform parameters values between healthy subjects and glaucoma patients, as well as between gender. Authors foresee further studies investigating the potential to predict severity and progression of glaucoma.

An interesting contribution by Cassani *et al.* on theoretical predictions of metabolic flow regulation in the retina aims to better understand the regulating mechanisms in health and disease. This study uses a theoretical model to investigate the response of retinal blood flow to changes in tissue oxygen demand. The increase in blood flow predicted by the model due to an increase in oxygen demand was not in the same proportion as the change in blood flow observed with the same decrease in oxygen demand, suggesting that vascular regulatory mechanisms may respond differently to different levels of oxygen demand.

Several studies have suggested an association between vascular factors and glaucoma.[7-11] Several epidemiological studies demonstrated the influence of ocular perfusion pressure on the prevalence, incidence and progression of glaucoma.[12] Ocular perfusion pressure refers to the pressure available to drive blood through the intraocular vasculature, with the degree of perfusion being influenced by the resistance to flow, which is a function of the vessel caliber or the vessel tone.[13] While it seems a very complex parameter, Guglielmi et al. utilized statistical techniques and analysis to show that it is the joint effect of IOP, ocular perfusion pressure and blood pressure, or, more precisely, of all the covariates in the selected logistic model, that determines the probability of disease, rather than the value of an individual covariate. Importantly, the main statistical interest should be the prediction of disease probabilities for new patients entering the study, presenting specific values of the covariates included in the model, rather than the estimated individual effect of a single predictor.

It has been shown that glaucoma, proliferative vitreoretinopathy, posterior capsule opacification, diabetic retinopathy, age-related macular degeneration, pterygium and keratoconus have been associated with modulation of Transforming Growth Factor beta (TGF-β) protein expression.[14-20] Therapeutic intervention targeting TGF-β2 protein expression may have multifold effects on relevant intraocular

tissues such as trabecular meshwork (cell invasion/migration), retina (scarring and wound-healing processes) and/or optic nerve head (neuroprotection), and warrant further evaluation in patients suffering advanced glaucoma and undergoing trabeculectomy. Hasenbach et al. used a murine model of glaucoma filtration surgery to evaluate the effect of intraocular ISTH0036 administration. They showed that treatment with ISTH0036 resulted in prolonged bleb survival and decreased scarring (downregulation of collagen-1 and -3 fibers) in a murine glaucoma filtration surgery model. Initial results rose a strong rationale that patients with glaucoma or other ocular diseases may benefit from treatment with TGF-β2 antisense oligonucleotides.

Paulaviciute-Baikstiene et al. performed a prospective 12-month study aiming to find the correlation between anterior segment OCT and functional outcomes of trabeculectomy by describing morphological features of successful and limited success filtering blebs. The detection of early postoperative scarring and the continuing development of surgical measures to reduce this risk represent a major challenge of filtering surgery. Authors suggest that larger internal fluid filled cavity, total bleb height, bigger bleb wall thickness and multiform bleb wall reflectivity are good indicators of successful bleb function.

The second Issue of the Journal for Modeling in Ophthalmology uniquely combines and balances clinical and mathematical aspects in the study of glaucoma and we believe that both ophthalmologists and modeling experts will find in it interesting aspects and new information on glaucoma and its risk factors. Enjoy your reading!

Ingrida Januleviciene

References

1. Kuhn TS. The Structure of Scientific Revolutions. 3rd ed. Chicago, IL: University of Chicago Press, 1996. (Asking new questions of old data on pages 139, 159. Moving beyond 'puzzle-solving' on pages 37, 144.)
2. Drance SM. Diurnal Variation of Intraocular Pressure in Treated Glaucoma. Significance in Patients with Chronic Simple Glaucoma. Arch Ophthalmol 1963;70:302-311.
3. Duke-Elder S. The phasic variations in the ocular tension in primary glaucoma. Am J Ophthalmol 1952;35(1):1-21.
4. Langley D, Swanljung H. Ocular tension in glaucoma simplex. Br J Ophthalmol 1951;35(8):445-458.
5. Loewen NA, Liu JH, Weinreb RN. Increased 24-hour variation of human intraocular pressure with short axial length. Invest Ophthalmol Vis Sci 2010;51(2):933-937.
6. Fogagnolo P, Orzalesi N, Centofanti M, et al. Short- and long-term phasing of intraocular pressure in stable and progressive glaucoma. Ophthalmologica 2013;230(2):87-92.
7. Bill A. Blood circulation and fluid dynamics in the eye. Physiol Rev 1975;55:385-417.
8. Drance SM, Douglas G, Wijsman K, et al. Response of blood flow to warm and cold in normal and low-tension glaucoma patients. Am J Ophthalmol1988;105:35-39.
9. Flammer J. The vascular concept in glaucoma. Surv Ophthalmol 1988;38(Suppl):S3-S6.
10. Bonomi L, Babighian S, Bonadimani M, et al. Correlation between glaucoma and vascular factors, and circumstances leading to the diagnosis of glaucoma. Acta Ophthalmol Scand Suppl 2000:34-35.
11. Harris A, Rechman E, Siesky B, et al. The role of optic nerve blood flow in the pathogenesis of glaucoma. Ophthalmol Clin North Am 2005; 18: 345-353.
12. Costa V , Harris A, Anderson D, et al. Ocular perfusion pressure in glaucoma. Acta Ophthalmol Scand 2013. doi: 10.1111/aos.12298.
13. Caprioli J, Coleman AL. Blood Flow in Glaucoma Discussion: Blood pressure, perfusion pressure, and glaucoma. AmJ Ophthalmol 2010;149:704-712.
14. Connor TB Jr, Roberts AB, Sporn MB, et al. Correlation of fibrosis and transforming growth factor-beta type 2 levels in the eye. J Clin Invest 1989;83(5):1661-1666. 10.1172/JCI114065.
15. Kria L, Ohira A, Amemiya T. Immunohistochemical localization of basic fibroblast growth factor, platelet derived growth factor, transforming growth factor-beta and tumor necrosis factor-alpha in the pterygium. Acta Histochem 1996;98(2):195-201.
16. Kon CH, Occleston NL, Aylward GW, Khaw PT. Expression of vitreous cytokines in proliferative vitreo-retinopathy: a prospective study. Invest Ophthalmol Vis Sci 1999;40(3):705-712.
17. Wormstone IM. Posterior capsule opacification: a cell biological perspective. Exp Eye Res 2002;74(3):337-347. 10.1006/exer.2001.1153.
18. Engler C, Chakravarti S, Doyle J, et al. Transforming growth factor-beta signaling pathway activation in Keratoconus. Am J Ophthalmol 2011;151(5):752-759 e2. 10.1016/j.ajo.2010.11.008.
19. Prendes MA, Harris A, Wirostko BM, Gerber AL, Siesky B. The role of transforming growth factor beta in glaucoma and the therapeutic implications. Br J Ophthalmol 2013;97(6):680-686. 10.1136/bjophthalmol-2011-301132.
20. Hirase K, Ikeda T, Sotozono C, et al. Transforming growth factor beta2 in the vitreous in proliferative diabetic retinopathy. Arch Ophthalmol 1998;116(6):738-741.

Filtering blebs structure and function evaluation using optical coherence tomography

Daiva Paulaviciute-Baikstiene, Renata Vaiciuliene, Ingrida Januleviciene

Eye Clinic of Kaunas Medical Academy of Lithuanian University of Health Sciences, Kaunas, Lithuania

Abstract

Purpose: To assess the ability of a noncontact optical coherence tomography to evaluate the morphological features of filtering blebs one year after glaucoma surgery.
Design: Prospective study.
Methods: Eighteen patients (18 eyes) with diagnosed primary open-angle glaucoma (POAG) assigned for trabeculectomy were included in the 12-month study carried out in the Eye clinic of the Lithuanian University of Health Sciences. All participants underwent trabeculectomy with 5-fluorouracil (5-FU). Bleb function was considered to be successful if the intraocular pressure (IOP) was ≤ 18 mmHg without glaucoma medications and a limited success if: 18 < IOP ≤ 21 mmHg with or without glaucoma medications at 12 months after surgery.
The filtering blebs were imaged by anterior segment optical coherence tomography (AS-OCT) to evaluate the bleb wall reflectivity and measured bleb structures 12 months after trabeculectomy. Level of significance: $p < 0.05$ was considered significant.
Results: The mean preoperative IOP was 25.7 (6.5) mmHg and the mean number of topical glaucoma medications was 3.0 (1.2). After surgery the mean IOP was 13.8 (3.4) mmHg and glaucoma medication was 0.3 (1.0) (Wilcoxon test, $p < 0.001$).
Analyzing bleb morphology and bleb function it was found that with uniform wall reflectivity 0 out of 3 eyes (0%) had successful bleb function and with multiform wall reflectivity 14 out of 15 eyes (93.3%) had successful bleb function 12 months after surgery ($p = 0.005$).

Correspondence: Daiva Paulaviciute-Baikstiene, Eye Clinic of Kaunas Medical Academy of Lithuanian University of Health Sciences, Eivenių g. 2A, LT 50009, Kaunas, Lithuania. E-mail: daiva_paulaviciute@yahoo.com

We found positive correlation between IOP changes and bleb wall thickness, height of internal fluid-filled cavity (bleb height) and total bleb height (r = 0.875, 0.897, 0.939, p < 0.001).
Conclusion: AS-OCT is a useful device to assess the structure of the filtering bleb. Larger internal fluid-filled cavity, total bleb height, bigger bleb wall thickness and multiform bleb wall reflectivity were found to be good indicators of bleb function.

Key words: AS-OCT, intraocular pressure, filtering bleb, primary open-angle glaucoma, trabeculectomy

1. Introduction

Trabeculectomy is indicated for eyes with POAG that have an inadequate IOP with maximum tolerated medical therapy. The principle of the surgery is to reduce IOP by circumventing the outflow tract and allowing aqueous humor to exit beneath the scleral flap and under the conjunctiva where it forms a filtering bleb.[1] The success of this surgery depends on the functionality of the filtering bleb, aqueous humor drainage and IOP lowering effect.[2] However, in a significant number of cases aqueous humor filtration does not occur, because of obstruction of intrascleral aqueous flow and bleb fibrosis.[3] Bleb morphology has always been an important clinical parameter as an indicator for bleb function.[2] The description of bleb morphology and function is usually based on clinician's subjective judgment. Bleb appearance, as assessed by slit-lamp biomicroscopy, is widely used to predict the possible functionality and the structure of blebs, but it is difficult to see internal structures, which may have an effect on bleb function.[3]

Cross-sectional imaging modality such as AS-OCT with high axial resolution (18 µm), allows to see the bleb's internal structures, improves the analysis of the function of filtering blebs[4-6] and gives additional information of the morphology.[7-10] Understanding the bleb function, objectively identifying and quantifying early signs of failure after glaucoma surgery, would enable clinicians to choose proper treatment and/or preclude possible complications such as bleb leak or scarring, blebitis, and bleb-related endophthalmitis.[11-13]

It is important to know what features of mature blebs are associated with bleb function. The purpose of the present study was to assess the ability of OCT to evaluate morphological features of filtering blebs one year after trabeculectomy with 5FU. We aimed to find the correlation between AS-OCT and functional outcomes by describing morphological features of successful and limited success blebs.

2. Methods

This prospective study was performed in the Eye clinic of the Lithuanian University of Health Sciences. Eligible patients with POAG were recruited between January and December 2014. The study was conducted in accordance with the ethical standards of the Declaration of Helsinki and approved by Kaunas clinical research ethics committee. Written informed consent was obtained from all the patients.

The inclusion criteria were POAG patients over 18 years with medically uncontrolled IOP and progressing glaucoma, scheduled for surgical treatment. Pregnant or nursing women, patients with uncontrolled systemic diseases, previous ocular surgery, secondary glaucoma, congenital glaucoma and patients with a history of other eye diseases or trauma were excluded from the study.

Goldmann applanation tonometry was performed before and 12 months after surgery. An average of three separate IOP measurements was taken.

All participants underwent trabeculectomy with 5-FU. In all cases a fornix-based conjunctival flap was created, after which a sponge soaked in 5-FU was applied to the sclera. A scleral flap of approximately 5 x 5 mm was made. After trabeculectomy the scleral flap was closed with several (4-5) nylon 10-0 sutures. The conjunctiva was closed with a nylon 10-0 running suture.

Bleb function was considered to be successful if IOP was ≤ 18 mmHg without glaucoma medications and a limited success if: 18 < IOP ≤ 21 mmHg with or without glaucoma medications 12 months after surgery.

The filtering blebs were examined by slit-lamp biomicroscopy, photography and by AS-OCT (Nidek, RS-3000). This optical device is adapted to analyze the anterior segment of the eye. Work principle is based on low coherence interferometry, which measures the delay and intensity of backscattered infrared light using a super luminescent diode with a six-mm tissue penetration and the reflection signal at a wavelength of approximately 1310 nm.[14]

Patients were asked to look down, and the upper lid was manually elevated to expose the bleb as much as possible for better visualization and taking care to avoid pressure on the globe or bleb.

All blebs were assessed by wall reflectivity. Depending on the presence or absence of hyporeflective spaces in the bleb wall we divided blebs into the multiform or uniform. There was noted presence of small hyporeflective areas (various sizes and shapes fluid-filled spaces) in blebs with multiform walls. Uniform blebs wall looked hyperreflective (no visible fluid filling spaces in the wall).[15]

Bleb structures (wall thickness, total height, length and height of internal fluid-filled cavity (bleb length and height)) were evaluated in the AS-OCT images (Fig. 1). The optical aperture of the AS-OCT was centered to the maximal elevation of the filtering bleb with the aid of a joystick. Then four standard AS-OCT images (vertical, horizontal, oblique to the right, oblique to the left) were obtained simultaneously for each bleb and one randomly chosen section was used for analysis.
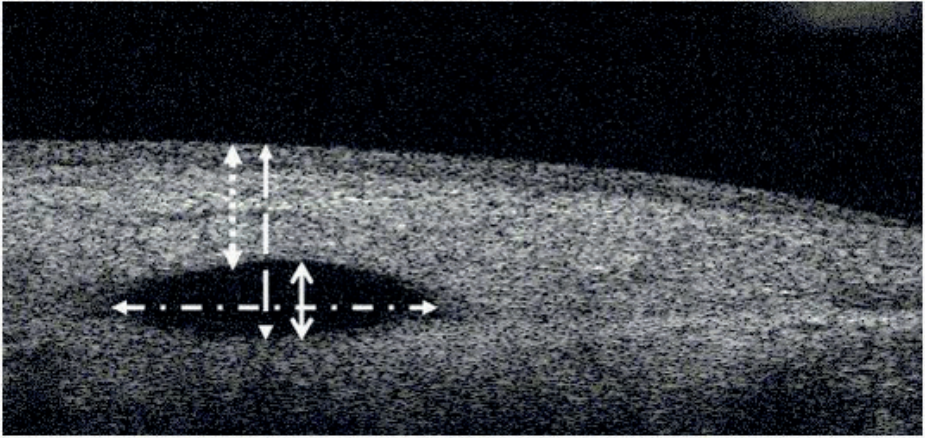
Fig. 1. Parameters describing bleb morphology: wall thickness (dot line), total bleb height (dash line), bleb height (solid line); bleb length (dash-dot line).

The AS-OCT images were evaluated in order to assess bleb morphologic features by a single, skilled observer (D.P.B), who was blinded to the clinical data.

Statistical analysis were performed using SPSS version 20.0 for Windows (IBM Corporation, Armonk, NY, USA). Qualitative variables were described as arithmetic mean and standard deviation (M (SD)). In this pilot study, variables of patients were described using the general statistical concepts for small sample size of the position, distribution and symmetry. The level of significance $p \leq 0.05$ was considered significant.

The Kolmogorov-Smirnov test was used to test for normal distribution. Preoperative and postoperative data were analyzed with the nonparametric Wilcoxon test for continuous variables (IOP, number of glaucoma medications) and chi-square test for categorical variables (correlation of bleb wall morphology with bleb functions). To calculate a difference in IOP reduction between multiform and uniform filtering blebs, Mann-Whitney test was performed. Correlation between IOP reduction and bleb structure parameters was analyzed using the Spearman`s correlation.

3. Results

Eighteen eyes of 18 patients (13 males (66.7%) and six females (33.3%)) with a mean age of 67.5 (7.8) were included in the study.

The mean preoperative IOP was 25.7 (6.5) mmHg after trabeculectomy decreased to 13.8 (3.4) mmHg (Wilcoxon test, $p < 0.001$) (Fig. 2). The mean number of topical glaucoma medications at the preoperative visit was 3.0 (1.2) and 0.3 (1.0) after surgery (Wilcoxon test, $p < 0.001$). According to surgical outcome success criteria there were 14 (77.8%) successful blebs (mean IOP = 12.4 (2.4) mmHg) and 4 (22.2%)
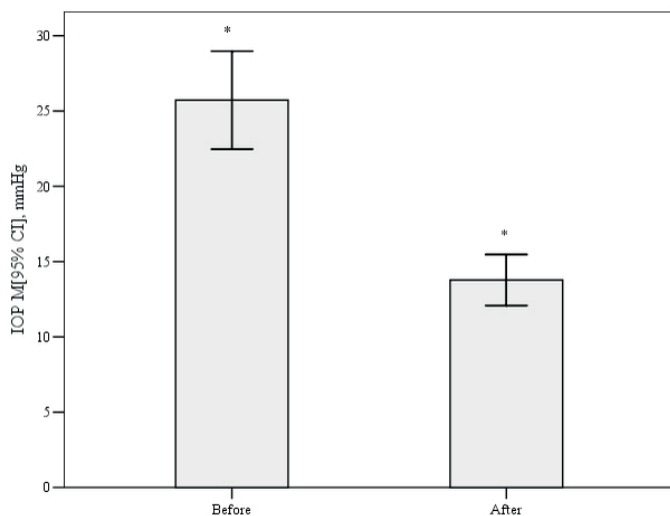
Fig. 2. IOP reduction 12 months after trabeculectomy. * p < 0.001 by Wilcoxon test.

limited success (mean IOP = 18.5 (1.7) mmHg).

Uniform bleb wall reflectivity was in three eyes (16.7%) and multiform in 15 eyes (83.3%). Analyzing bleb morphology and function it was found that none of blebs with uniform wall reflectivity has successful function. While blebs with multiform wall reflectivity 93.3% had successful function at 12 months (p = 0.005) (Table 1).

One year after surgery decrease in IOP was statistically significantly higher in eyes with multiform as compared to uniform bleb wall reflectivity (p = 0.008) (Fig. 3).

Measurements of bleb structure are shown in Figure 4. We found positive correlation between IOP changes and bleb wall thickness (r = 0.875, p < 0.001), height of internal fluid-filled cavity (r = 0.897, p < 0.001) and total bleb height (r = 0.939, p < 0.001) (Fig. 5).

Table 1. Correlation of bleb wall morphology with bleb functions at 12 months after surgery.

Bleb wall reflectivity/ function	Success (%)	Limited success (%)	Total (%)
Uniform	0 (0)	3 (16.7)	3 (16.7)
Multiform	14 (93.3)	1 (6.7)	15 (83.3)
Total (%)	14 (77.8)	4 (22.2)	18 (100)

p = 0.005 by Chi-square test.
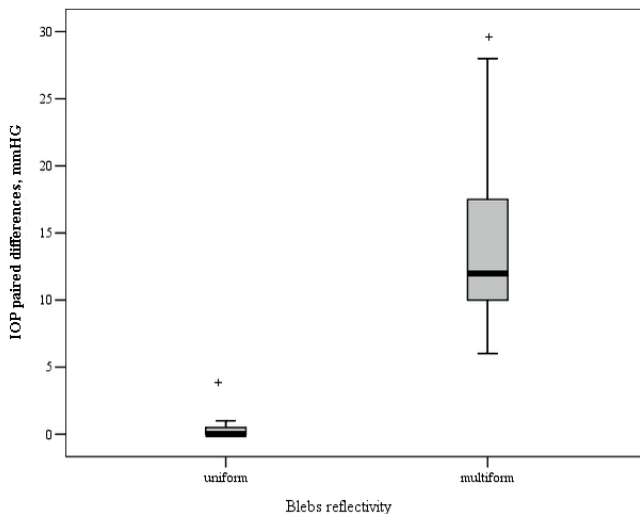
Fig. 3. IOP changes after trabeculectomy depending on bleb wall morphology. + p = 0.008 by Mann-Whitney Test.
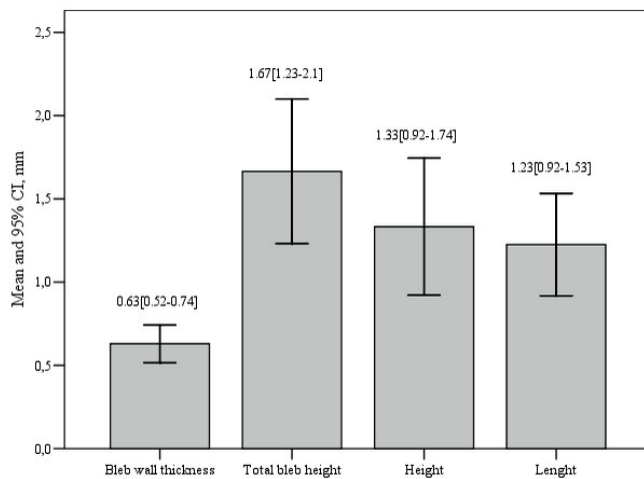
Fig. 4. Bleb structure measurements (mean and 95% CI).
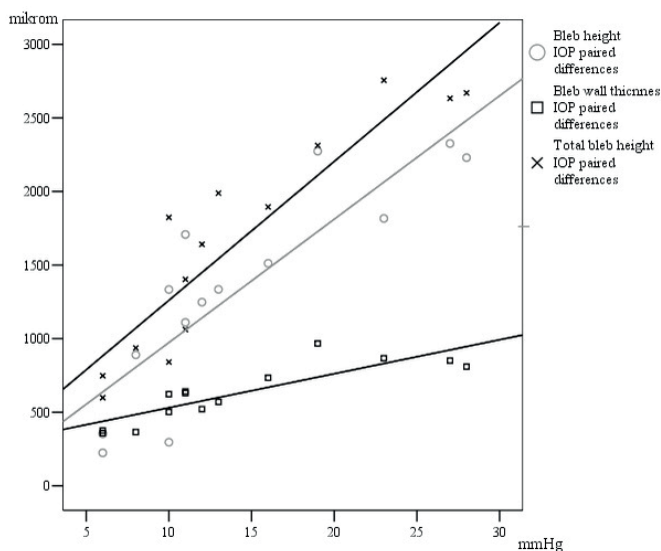
Fig. 5. Scattergram showing the relationship between the changes of IOP and bleb structure parameters. Spearman`s correlation: O 0.897, p < 0.001; □ 0.875, p < 0.001; × 0.939, p < 0.001.

4. Discussion

We found that the vast majority of investigated eyes (93.3%) retained multiple layer appearance (areas of hyporeflectivity) and had good bleb function 12 months after the glaucoma surgery. It has been reported that most of the filtering blebs found on AS-OCT imaging, with good IOP control had thicker bleb walls with microcysts, wider hyporeflective areas and higher blebs.[10,17-24] Several studies used a variety of cross-sectional imaging modalities (*e.g.*, UBM or AS-OCT) and found associations between bleb wall reflectivity and bleb function.[14-24] It is known that it is possible from AS-OCT images to recognize features that may help to find the process and location of bleb failure.[10] Ciancaglini et al. observed that successful blebs reveal a low bleb wall reflectivity.[4] Filtering blebs showed average bleb wall thickness 0.51 mm, height of internal fluid cavity 0.67 mm in observational case-series study of Devika *et al.*[24] In our successful cases bleb wall thickness were 0.63 mm, height of internal fluid cavity 1.35 mm. Our advantage is that we also measured the length and the total height of the filtering bleb. Results suggested that higher IOP reduction and better bleb function were associated with higher bleb, bigger wall thickness and total height. Contrarily Tominaga *et al.* did not find any correlation between the IOP and height of bleb cavity. However a negative correlation was found between postoperative IOP and bleb wall thickness.[25]

The limited success blebs had a non-thickened, low bleb wall, high reflectiv-

ity between the conjunctiva and scleral flap, a small spaces beneath the flap and occluded internal ostium.[26] These small optically empty spaces beneath the flap inform about the level of aqueous outflow interrupting process between the sclera and subconjunctival space.[10] Another useful information is thickness of bleb wall after the surgery. It possibly reflects flow of aqueous through conjunctiva-episclera.[25]

IOP control after trabeculectomy depends on both the aqueous outflow to the bleb and its absorption from the bleb.[2] In our study, a mean IOP reduction was 46.3% after the surgery. Singh et al. in a prospective cross-sectional study revealed that in successful cases mean IOP was 12.2 (2.9) mmHg with no ocular hypotensive medications. In failed cases, mean IOP was 17.9 (2.0) mmHg.[27] Our study shows similar results. Mean IOP was 12.4 (2.4) mmHg in successful cases, and 18.5 (1.7) in limited success cases. This proves that trabeculectomy is very effective surgical method for the majority of glaucoma patients.

Napoli and coworkers reported that the reflectivity of filtering blebs associated very well to the postoperative IOP and to the reduction of IOP.[28] Based on IOP and glaucoma medication criteria we determined that successful blebs had multiform wall reflectivity while limited success blebs had uniform wall reflectivity. Furthermore, multiform bleb wall reflectivity had higher IOP change from baseline 12 months after the surgery.

Nakano and colleagues observed that uniform bleb wall reflectivity in the early postoperative period associated with worse function of the mature bleb. This information might predict future bleb failure. They also noticed that there is no correlation between IOP of developing blebs and blebs function at six months.[3]

It is known that high wall reflectivity indicated scarring of the bleb.[29] The success of trabeculectomy depends on the long-term preservation of the aqueous drainage, healing process and the use of 5-FU and mitomycin C.[29,30] These antimetabolites are used to prevent fibrosis and significantly lowers high scarring of the bleb by reducing the population of goblet cells.[32,32]

The detection of early postoperative scarring and the continuing development of surgical measures to reduce this risk represent a major challenge of filtering surgery.

Possible limitations of our study are small sample size and relatively short follow-up. A small number of limited success blebs, may have influenced the significance of statistical findings in this group. Limitation of the AS-OCT is the disability to image bleb vascularity, which may be an important prognostic factor of bleb survival postoperatively.

Further long-term studies are needed in order to evaluate stabilization of glaucoma progression based on morphological parameters of filtering blebs.

5. Conclusion

Anterior segment imaging is a valuable tool in the detailed assessment of the morphological changes in the bleb tissue. Larger internal fluid-filled cavity, total bleb height, bigger bleb wall thickness and multiform bleb wall reflectivity were found to be good indicators of bleb function. These findings may aid clinicians to predict surgical treatment outcomes and to make correct decisions regarding postoperative bleb management.

References

1.   Weinreb RN, Crowston JG. Glaucoma surgery: Open-angle glaucoma. WGA Consensus Series 2, pp. 57-62. The Netherlands: Kugler Publications 2005.
2.   Wells AP, Crowston JG, Marks J, Kirwan JF, Smith G, Clarke JC, et al. A pilot study of a system for grading of drainage blebs after glaucoma surgery. J Glaucoma 2004;13:454-460.
3.   Nakano N, Hangai M, Nakanishi H, et al. Early trabeculectomy bleb walls on anterior-segment optical coherence tomography. Graefes Arch ClinExpOphthalmol 2010;248(8):1173-1182.
4.   Ciancaglini M, Carpineto P, Agnifili L, et al. Filtering bleb functionality: a clinical, anterior segment optical coherence tomography and in vivo confocal microscopy study. J Glaucoma 2008;17:308-317.
5.   Pfenninger L, Schneider F, Funk J. Internal reflectivity of filtering blebs versus intraocular pressure in patients with recent trabeculectomy. Invest Ophthalmol Vis Sci 2011;52:2450-2455.
6.   Picht G, Grehn F. Classification of filtering blebs in trabeculectomy: biomicroscopy and functionality. Curr Opin Ophthalmol 1998;9:2-8.
7.   Hirooka K, Takagishi M, Baba T, Takenaka H, Shiraga F. Stratus optical coherence tomography study of filtering blebs after primary trabeculectomy with a fornix-based conjunctival flap. Acta Ophthalmol 2010;88:60-64.
8.   Babighian S, Papizzi E, Galan A. Stratus-OCT of filtering bleb after trabeculectomy. Acta Ophthalmol Scand 2006;84:270-271.
9.   Savini G, Zanini M, Barboni P. Filtering blebs imaging by optical coherence tomography. Clin Experiment Ophthalmol 2005;33:483-489.
10. Singh M, Chew PT, Friedman DS, et al. Imaging of trabeculectomy blebs using anterior segment optical coherence tomography. Ophthalmology 2007;114:47-53.
11. Hu CY, Matsuo H, Tomita G, et al. Clinical characteristics and leakage of functioning blebs after trabeculectomy with mitomycin-C in primary glaucoma patients. Ophthalmology 2003;110:345-352.
12. DeBry PW, Perkins TW, Heatly G, et al. Incidence of late onset bleb-related complications following trabeculectomy with mitomycin. Arch Ophthalmol 2002;120:297-300.
13. Soltau JB, Rothman RF, Budenz DL, et al. Risk factors for glaucoma filtering bleb infections. Arch Ophthalmol 2000;118:338-342.
14. Yamamoto T, Sakuma T, Kitazawa Y. An ultrasound biomicroscopic study of filtering blebs after mitomycin C trabeculectomy. Ophthalmology 1995;102:1770-1776.
15. McWhae JA, Crichton AC. The use of ultrasound biomicroscopy following trabeculectomy. Can J Ophthalmol 1996;31:187-191.
16. Avitabile T, Russo V, Uva MG. Ultrasound-biomicroscopic evaluation of filtering blebs after laser suture lysis trabeculectomy. Ophthalmologica 1998;212:17-21.
17. Jinza K, Saika S, Kin K, Ohnishi Y. Relationship between formation of a filtering bleb and an intrascleral aqueous drainage route after trabeculectomy: evaluation using ultrasound biomicroscopy.

Ophthalmic Res 2000;32:240-243.

18. Savini G, Zanini M, Barboni P. Filtering blebs imaging by optical coherence tomography. Clin Experiment Ophthalmol 2005;33:483-489.

19. Babighian S, Rapizzi E, Galan A. Stratus OCT of filtering bleb after trabeculectomy. Acta Ophthalmol Scand 2006;84:270-271.

20. Müller M, Hoerauf H, Geerling G, et al. Filtering bleb evaluation with slit-lamp-adapted 1310-nm optical coherence tomography. Curr Eye Res 2006;31:909-915.

21. Leung CK, Yick DW, Kwong YY, et al. Analysis of bleb morphology after trabeculectomy with Visante anterior segment optical coherence tomography. Br J Ophthalmol 2007;91:340-344.

22. Kawana K, Kiuchi T, Yasuno Y, Oshika T. Evaluation of trabeculectomy blebs using 3-dimensional cornea and anterior segment optical coherence tomography. Ophthalmology 2009;116:848-855.

23. Addicks EM, Quigley HA, Green R, Robin AL. Histologic characteristics of filtering blebs in glaucomatous eyes. Arch Ophthalmol 1983;101:795-798.

24. Devika K, Girija K, Sindhu S. Analysis of bleb morphology after trabeculectomy with anterior segment optical coherence tomography. Kerala J Ophthalmol 2014;26(1):48-52.

25. Tominaga A, Miki A, Yamazaki Y, Matsushita K, Otori Y. The assessment of the filtering bleb function with anterior segment optical coherence tomography. J Glaucoma 2010; 19(8):551-555.

26. Zhang Y, Wu Q, Zhang M, et al. Evaluating subconjunctival bleb function after trabeculectomy using slit lamp optical coherence tomography and ultrasound biomicroscopy. Chin Med J 2008;121(14):1274-1279.

27. Singh M, See JL, Aquino MC, Thean LS, Chew PT. High-definition imaging of trabeculectomy blebs using spectral domain optical coherence tomography adapted for the anterior segment. Clin Experiment Ophthalmol 2009;37(4):345-351.

28. Napoli PE, Zucca I, Fossarello M. Qualitative and quantitative analysis of filtering blebs with optical coherence tomography. Can J Ophthalmol 2014;49(2):210-216.

29. Khalili MA, Diestelhorst M, Krieglstein GK. Langzeit untersuchungen von 700 Trabekulektomien. Klin Monatsbl Augenheilkd 2000;217:1-8.

30. Picht G, Mutsch Y, Grehn F. Nachbetreuung von Trabekulektomien. Ophthalmologe 2001;7:629-624.

31. Bindlish R, Condom GP, Schlosser MS, et al. Efficacy and safety of mitomycin-C in primary trabeculectomy. Ophthalmology 2002;109:1336-1342.

32. Katz GL, Higginbotham EJ, Lichter PR, et al. Mitomycin C versus 5 fluorouracil in high risk glaucoma filtering surgery. Extended follow up. Ophthalmology 1995;102:1263-1269.

Potent and selective antisense oligonucleotides targeting the transforming growth factor beta (TGF-β) isoforms in advanced glaucoma: a preclinical evaluation

Kathy Hasenbach[1], Tine Van Bergen[2], Evelien Vandewalle[2], Lies De Groef[2], Inge Van Hove[2], Lieve Moons[3], Ingeborg Stalmans[2], Petra Fettes[1], Eugen Leo[1], Katja Wosikowski[1], Michel Janicot[1]

[1]Isarna Therapeutics, Munich, Germany; [2]Laboratory of Ophthalmology, KU Leuven, Leuven, Belgium; [3]Department of Biology, Zoological Institute, KU Leuven, Leuven, Belgium

Abstract

Purpose: ISARNA Therapeutics is developing highly potent and selective LNA-modified ASO gapmers targeting TGF-β1 and TGF-β2 mRNA. In the field of ophthalmology, glaucoma, the second leading cause for blindness in the US, has been linked to TGF-β activation as a key driver. ISTH0036 is a 14-mer phosphorothioate Locked Nucleic Acid- (LNA) modified antisense oligonucleotide gapmer, targeting the sequence of TGF-β2 mRNA and was developed for therapeutic intervention in ocular diseases. It was shown to effectively and potently downregulate target mRNA in a dose-dependent manner in relevant cell-based assays, as well as leading to target engagement in anterior eye segment tissues upon intravitreal administration (Isarna proprietary information). The aim of this study was to evaluate the therapeutic potential of ISTH0036 in murine models of glaucoma filtration surgery (GFS) following different intraocular administrations.
Methods: A murine model of glaucoma filtration surgery has been used to evaluate the effect of intraocular ISTH0036 administration on post-operative wound healing. Bleb size and bleb survival were determined after different intraocular administra-

Correspondence: Dr. Michel Janicot. E-mail: m.janicot@isarna-therapeutics.com.

tions of saline, control scrambled oligonucleotide or ISTH0036 (at day of surgery and after two weeks).

Results: Intraocular administrations of ISTH0036 lead to a significant effect on bleb area and survival, as well as decreasing scarring (downregulation of collagen-1 and -3 fibers) in a murine glaucoma filtration surgery model.

Conclusion: Consistent with the expected molecular mechanism of action and demonstrated pharmacokinetic (PK) and pharmacodynamic (PD) properties following intraocular administration, preclinical data with ISTH0036 in murine glaucoma filtration surgery model support the current exploration of the drug candidate in advanced glaucoma patients undergoing trabeculectomy.

Key words: antisense oligonucleotide, glaucoma, intraocular administration, transforming growth factor beta

1. Introduction

In ophthalmology, several diseases have been associated with modulation of transforming growth factor beta (TGF-β) protein expression. In particular, a large body of scientific evidence has been generated for glaucoma, proliferative vitreoretinopathy, posterior capsule opacification, diabetic retinopathy, age-related macular degeneration and corneal diseases such as pterygium and keratoconus.[1-7] Furthermore, single TGF-β isoforms of the TGF-β family (*i.e.*, TGF-β1, -β2 and -β3) appear to be the core pathophysiologic molecular 'driving force' for various key ophthalmic diseases with high unmet medical need. TGF-β2 is the predominant cytokine expressed in the eye and is found in large amounts in the aqueous and vitreous humors, the neuronal retina and the retinal pigmented epithelium in the healthy eye.[8-12] Various studies have shown the potential significance of TGF-β2 signaling by observing that active TGF-β2 protein is significantly increased intraocularly in the ciliary body, the optic nerve and the trabecular meshwork in primary open-angle glaucoma (POAG) patients.[13-21] This effect is also reflected by increase in TGF-β levels 70- to 100-fold above normal in the optic nerve head in POAG patients.[22] TGF-β2-induced changes might contribute to deformation of the optic nerve axons by causing impairment of axonal transport and neurotrophic supply via the remodeling of the extracellular matrix (ECM) in the lamina cribrosa, leading to their permanent degeneration. The increase in intraocular pressure further adds mechanical stress and strain to optic nerve axons and accelerates degenerative changes.[6,23,24] TGF-β also plays a distinct driving role in fibrotic diseases[25] and epithelial-mesenchymal transition and is therefore most probably responsible for the increase of ECM and cellular transformation which is reported for the trabecular meshwork in glaucoma patients. POAG patients show a significant increase in sheath-derived plagues due to fine fibrils and other ECM components which adhere to the sheaths of the elastic fibers in the inner

wall endothelium.[26,27]

Antisense oligonucleotides are small synthetic single strands of DNA or RNA that are complementary to a chosen sequence which can be used to prevent protein translation of certain messenger RNA strands by binding to them and/or to target a specific, complementary (coding or non-coding) RNA. Antisense oligonucle-otides have been used for decades to achieve sequence-specific silencing of gene expression, and a wide range of chemical modifications (*e.g.*, locked nucleic acids) have been explored and implemented over the years to improve drug-like properties. ISTH0036 represents a 14-mer fully phosphorothioate Locked Nucleic Acid- (LNA) modified antisense oligodeoxynucleotide gapmer (nucleotide sequence: 5'-**ga**(Me)**c**CAGATGCA**gga**-3'; in which bold italics letters represent LNA-modified nucleotides in a '3+3 gapmer' pattern), for which potent and selective activity on TGF-β2 mRNA has been demonstrated in cell-based assays and *in vivo*, with consequent selective decrease in protein expression (data not shown).

Specifically for TGF-β2, a critical role in the pathophysiology of glaucoma has been demonstrated, making this isoform an obvious therapeutic target of high interest for a disease, which is the second leading cause for blindness in the Western world. As visually summarized in Figure 1, considering the pleiotropic
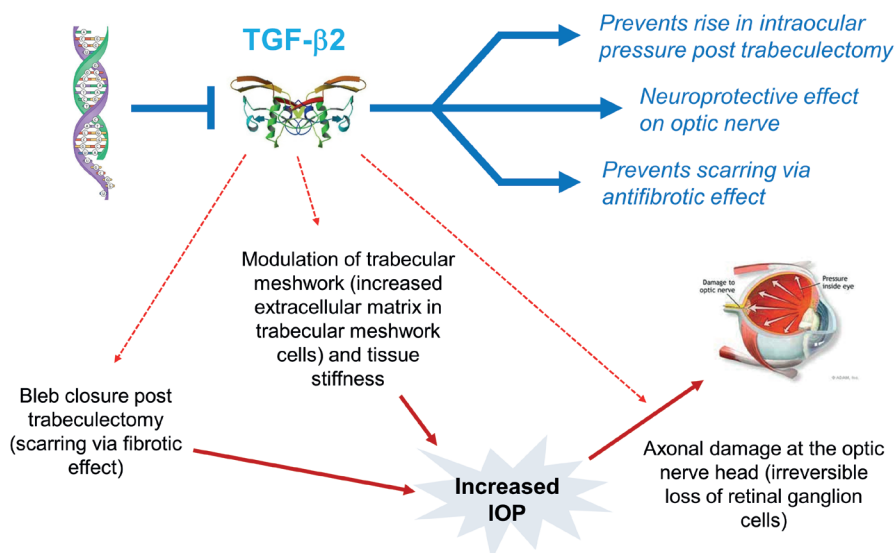
Fig. 1. Pleiotropic physiological mechanisms of action linked to targeting TGF-β2 protein expression claimed to support therapeutic intervention in advanced-staged glaucoma post-trabeculectomy. (Oligonucleotide/mRNA hybrid complex illustration has been adapted from a figure presented by Rigo *et al.* (2012);[28] TGF-β2 protein ribbon structure is from Schlunegger & Grutter (1992);[29] and the illustration of the glaucoma-induced intraocular pressure in human eye is from http://www.ftwortheyedoctor.com/glaucoma.html.)

physiological mechanisms of action, therapeutic intervention targeting TGF-β2 protein expression may have multifold effects on relevant intraocular tissues such as trabecular meshwork (cell invasion/migration), retina (scarring and wound-healing processes) and/or optic nerve head (neuroprotection), and warrant further evaluation in patients suffering advanced glaucoma and undergoing trabeculectomy.

2. Methods

Highly relevant to the initial clinical focus, a murine glaucoma filtration surgery model has been evaluated in which post-operative wound healing after glaucoma surgery is mimicked. Briefly, filtering surgery was performed under anesthesia on both eyes of eight to ten weeks old C57BL/6J mice resulting in a filtration bleb.[30-32] Shortly, the conjunctiva was first surgically dissected to expose the underlying sclera, and a small filtration subconjunctival space was created by running the surgical scissors underneath the dissected conjunctiva. Next, a 30-gauge needle was used to make an incision through the sclera into the anterior chamber of the eye to allow the aqueous humor to escape into the subconjunctival space. Finally, the conjunctiva was closed at the limbus by suturing over the newly created fistula. A topical steroids and antibiotics combination preparation was administered at the end of surgery to avoid opportunistic infections. Intraocular administrations [1-µL intravitreal (IVT) or intracameral (ICM) injections] of saline or about 1 µg of either control scrambled (mismatch) oligonucleotide or ISTH0036 were performed immediately after surgery and repeated after two weeks. Bleb size was measured via digital photographs about three times a week within the one-month experiment duration. Bleb survival was determined at the end of the study, while bleb failure was defined as the appearance of a scarred and flat bleb at two consecutive measurements.

3. Results

As illustrated in Figure 2, although no significant differences were observed between the saline- and the scrambled control oligonucleotide-treated groups on bleb area and survival (with blebs failing at day 17), ISTH0036 was shown to induce a statistically significant increase in bleb area and survival. Interestingly and consistent with the location of the bleb, following ICM administrations, a greater increase in bleb area and survival was observed as compared to IVT administrations, with potentially a significant effect of the second injection performed on day 14. However, it must be noted that considering the very low volume of the aqueous humor chamber (only 1-2 µL), accuracy of doses dispensed by ICM injection as compared to IVT administra-
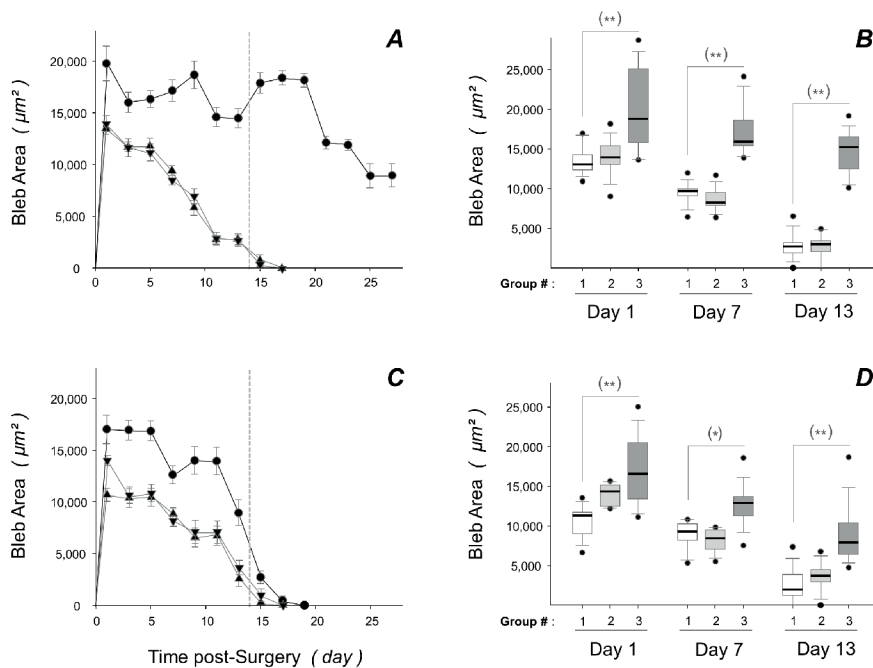
Fig. 2. Effect of ISTH0036 on bleb size and survival in an experimental mouse glaucoma filtration surgery model. C57BL/6J mice were used for a filtration surgery on both eyes, using a technique that has been described previously and that results in a filtering bleb.30 Bleb area (n = 8-10 eyes) was monitored after intracameral (**A, B**) or intravitreal (**C, D**) 1-µL injection(s) of either saline (▲, Group 1), 1-µg irrelevant scrambled mismatch control antisense oligonu-cleotide (▼, Group 2) or 1-µg ISTH0036 (●, Group 3) to mice after glaucoma filtration surgery (performed on day 0). Injections were repeated on day 14, and bleb size (expressed as µm²) was measured at the indicated times via digital photographs. Results are presented for each group as bleb area (mean ± SEM) at the indicated times (**A, C**), or as box plot on day 1, 7 and 14 (**B, D**), in which median value (solid line), 25-75% box, 10-90% percentiles and lowest and highest values in each group are presented. All experimental animal procedures were performed in accordance with the standards in the Association for Research in Vision and Ophthalmology (ARVO) Statement for the Use of Animals in Ophthalmic and Vision Research and the EC Directive 86/609/EEC for animal experiments. Non parametric 2-independent samples Wilcoxon-Mann-Whitney test was used to determine the significance of the differences between vehicle control and test item-treated groups (* p < 0.05; ** p < 0.01).

tion may be challenged. In addition, the very rapid turnover of the aqueous humor fluid (about 100 min[33]) compared to vitreous humor may strongly affect oligonu-cleotide concentrations over time. Therefore, direct side-by-side dose comparison between the two routes of administration may not lead to conclusive results.

Moreover, to evaluate the deposition of ECM (including collagen) in the bleb area, immunohistochemistry was performed to quantify Sirius Red (SR, collagen-1

and -3 fibers) positive area. Deposition of collagen was determined by measuring the percentage of the collagen positive area in the bleb area. Polarized light was used to distinguish mature from immature collagen fibers. Mature collagen fibers appear bright yellow or orange, whereas immature collagen fibers appear green. Analysis of the Sirius Red positive area in IVT and ICM injected mice showed that no differences in collagen deposition could be seen between saline- and control scrambled mismatch oligonucleotide-treated eyes at day 28. In contrast, treatment with the ISTH0036 was able to significantly reduce the deposition of extracellular matrix, namely collagen, after IVT or ICM injection (Fig. 3).
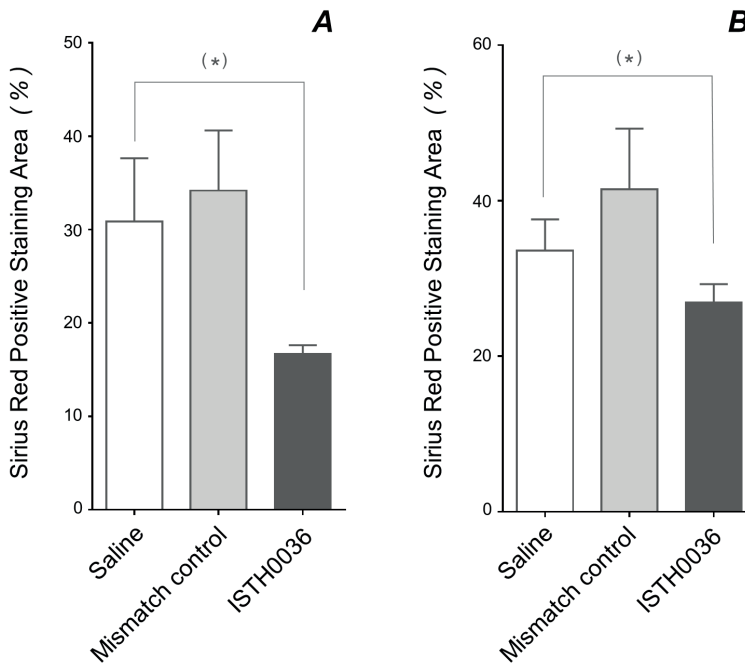
Fig. 3. Effect of ISTH0036 on collagen deposition in the bleb area in a murine experimental glaucoma filtration surgery model. Results represent the Sirius Red positive area (mean ± SD; n = 4) after intracameral (**A**) or intravitreal (**B**) administrations of either saline, mismatch/scrambled control oligonucleotide or ISTH0036 to mice following glaucoma filtration surgery (performed on day 0), as described in the legend of Figure 2. First injections of test items were performed at the time of surgery, and repeated on day 14. Sirius Red positive area (expressed as %) was measured in the bleb area via digital photographs on day 28. Student's t-test was used to determine the significance of the differences between vehicle control and test item-treated groups (* $p < 0.05$).

4. Discussion

We showed that the intraocular administration of ISTH0036, which is leading to sequence-specific TGF β2 downregulation (Isarna proprietary information), showed a significant effect on bleb size and survival, as well as fibrosis, in a murine glaucoma filtration surgery (GFS) model. Treatment with ISTH0036 resulted in prolonged bleb survival and decreased scarring (downregulation of collagen-1 and -3 fibers) in a murine glaucoma filtration surgery model. Considering the pleiotropic physiological mechanisms of action, therapeutic intervention targeting TGF-β2 protein expression in glaucoma patients may have many more effects on relevant intraocular tissues such as trabecular meshwork (cell invasion/migration and scarring), retina (scarring and wound-healing processes) and/or optic nerve head (neuroprotection).

5. Conclusion

These data provide a strong rationale that patients with glaucoma (or other ocular diseases), and potentially specifically those undergoing trabeculectomy, may benefit from treatment with TGF-β2 antisense oligonucleotides. Nevertheless, further comparative studies will be necessary to investigate different doses and treatment schedules. In addition, the reported anti-fibrotic, as well as the potential anti-invasive, anti-angiogenic and neuroprotective effects should be confirmed in other animal models of scarring and ocular diseases. Further studies should include animal models of diabetic retinopathy, wet macular degeneration/human neovascular chorioretinal diseases (choroidal and retinal neovascularization model) and other retinal vascular pathologies (oxygen-induced retinopathy model).

References

1.   Connor TB Jr, Roberts AB, Sporn MB, et al. Correlation of fibrosis and transforming growth factor-beta type 2 levels in the eye. J Clin Invest 1989;83(5):1661-1666. 10.1172/JCI114065.
2.   Kria L, Ohira A, Amemiya T. Immunohistochemical localization of basic fibroblast growth factor, platelet derived growth factor, transforming growth factor-beta and tumor necrosis factor-alpha in the pterygium. Acta Histochem 1996;98(2):195-201.
3.   Kon CH, Occleston NL, Aylward GW, Khaw PT. Expression of vitreous cytokines in proliferative vitreo-retinopathy: a prospective study. Invest Ophthalmol Vis Sci 1999;40(3):705-712.
4.   Wormstone IM. Posterior capsule opacification: a cell biological perspective. Exp Eye Res 2002;74(3):337-47. 10.1006/exer.2001.1153.
5.   Engler C, Chakravarti S, Doyle J, et al. Transforming growth factor-beta signaling pathway activation in Keratoconus. American journal of ophthalmology 2011;151(5):752-759 e2. 10.1016/j.ajo.2010.11.008.

6.   Prendes MA, Harris A, Wirostko BM, Gerber AL, Siesky B. The role of transforming growth factor beta in glaucoma and the therapeutic implications. Br J Ophthalmol 2013;97(6):680-686. 10.1136/bjophthalmol-2011-301132.

7.   Hirase K, Ikeda T, Sotozono C, et al. Transforming growth factor beta2 in the vitreous in proliferative diabetic retinopathy. Arch Ophthalmol 1998;116(6):738-741.

8.   Granstein RD, Staszewski R, Knisely TL. Aqueous humor contains transforming growth factor-beta and a small (less than 3500 daltons) inhibitor of thymocyte proliferation. J Immunol 1990;144(8):3021-3027.

9.   Jampel HD, Quigley HA, Kerrigan-Baumrind LA, et al. Risk factors for late-onset infection following glaucoma filtration surgery. Arch Ophthalmol 2001;119(7):1001-1008.

10. Pfeffer BA, Flanders KC, Guérin CJ, al. E. Transforming growth factor beta 2 is the predominant isoform in the neural retina, retinal pigment epithelium-choroid and vitreous of the monkey eye. Exp Eye Res 1994;59(3):323-333.

11. Saika S. TGFbeta pathobiology in the eye. Lab Invest 2006;86(2):106-115.

12. Freedman J, Iserovich P. Pro-Inflammatory Cytokines in Glaucomatous Aqueous and Encysted Molteno Implant Blebs and Their Relationship to Pressure. Invest Ophthalmol Vis Sci 2013;54:4851-4855. 10.1167/.

13. Tripathi RC, Li J, Chan WF, Tripathi BJ. Aqueous humor in glaucomatous eyes contains an increased level of TGF-beta 2. Exp Eye Res 1994;59(6):723-727.

14. Inatani M, Tanihara H, Katsuta H, et al. Transforming growth factor-beta 2 levels in aqueous humor of glaucomatous eyes. Graefes Arch Clin Exp Ophthalmol 2001;239(2):109-113.

15. Picht G, Welge-Luessen U, Grehn F, Lütjen-Drecoll E. Transforming growth factor beta 2 levels in the aqueous humor in different types of glaucoma and the relation to filtering bleb development. Graefes Arch Clin Exp Ophthalmol 2001;239(3):199-207.

16. Schlötzer-Schrehardt U, Zenkel M, Kuchle M, Sakai LY, Naumann GO. Role of transforming growth factor-beta1 and its latent form binding protein in pseudoexfoliation syndrome. Exp Eye Res 2001;73(6):765-780.

17. Ochiai Y, Ochiai H. Higher concentration of transforming growth factor-beta in aqueous humor of glaucomatous eyes and diabetic eyes. Jpn J Ophthalmol 2002;46(3):249-253.

18. Yamamoto N, Itonaga K, Marunouchi T, Majima K. Concentration of transforming growth factor beta2 in aqueous humor. Ophthalmic Res 2005;37(1):29-33.

19. Ozcan AA, Odzdemir N, Canataroglu A. The aqueous levels of TGF-β2 in patients with glaucoma. International Ophthalmology 2004;25:19-22.

20. Min SH, Lee TI, Chung YS, al. E. Transforming growth factor-beta levels in human aqueous humor of glaucomatous, diabetic and uveitic eyes. Korean J Ophthalmol 2006;20(3):162-165.

21. Trivedi RH, Nutaitis M, Vroman D, Crosson CE. Influence of race and age on aqueous humor levels of transforming growth factor-beta 2 in glaucomatous and nonglaucomatous eyes. J Ocul Pharmacol Ther 2011;27(5):477-480. 10.1089/jop.2010.0100.

22. Pena JD, Taylor AW, Ricard CS, Vidal I, Hernandez MR. Transforming growth factor beta isoforms in human optic nerve heads. Br J Ophthalmol 1999;83(2):209-218.

23. Quigley HA. Glaucoma. Lancet 2011;377(9774):1367-1377.

24. Fuchshofer R. The pathogenic role of transforming growth factor-beta2 in glaucomatous damage to the optic nerve head. Exp Eye Res 2011;347(1):279-290. S0014-4835(10)00225-3 [pii]

25. 10.1016/j.exer.2010.07.014 [doi].

26. Border WA, Noble NA. Transforming growth factor beta in tissue fibrosis. N Engl J Med 1994;331(19):1286-1292.

27. Rohen JW, Witmer R. Electron microscopic studies on the trabecular meshwork in glaucoma simplex. Graefes Arch Clin Exp Ophthalmol 1972;183(4):251-266.

28. Tektas OY, Lütjen-Drecoll E. Structural changes of the trabecular meshwork in different kinds of glaucoma. Exp Eye Res 2009;88(4):763-775.

29. Rigo F, Hua Y, Krainer AR, Bennett CF. Antisense-based therapy for the treatment of spinal muscular atrophy. J Cell Biol 2012;199(1):21-25. 10.1083/jcb.201207087.

30. Schlunegger MP, Grutter MG. An unusual feature revealed by the crystal structure at 2.2 A resolution of human transforming growth factor-beta 2. Nature 1992;358(6385):430-434.

31. Seet LF, Lee WS, Su R, et al. Validation of the glaucoma filtration surgical mouse model for antifibrotic drug evaluation. Mol Med 2011;17(5-6):557-567. 10.2119/molmed.2010.00188.

32. Van Bergen T, Jonckx B, Hollanders K, et al. Inhibition of placental growth factor improves surgical outcome of glaucoma surgery. J Cell Mol Med 2013;17(12):1632-1643. 10.1111/jcmm.12151.

33. Van Bergen T, Vandewalle E, Moons L, Stalmans I. Complementary effects of bevacizumab and MMC in the improvement of surgical outcome after glaucoma filtration surgery. Acta Ophthalmol 2015;93(7):667-678. 10.1111/aos.12766.

34. Aihara M, Lindsey JD, Weinreb RN. Aqueous Humor Dynamics in Mice. Invest Opthalmol Vis Sci 2003;44(12):5168. 10.1167/iovs.03-0504.

Mathematical modeling of aqueous humor flow and intraocular pressure under uncertainty: towards individualized glaucoma management

Marcela Szopos[1], Simone Cassani[2], Giovanna Guidoboni[1,2], Christophe Prud'homme[1], Riccardo Sacco[3], Brent Siesky[4], Alon Harris[4]

[1]Institut de Recherche Mathématique Avancée UMR 7501, Université de Strasbourg / CNRS, Strasbourg, France; [2]Department of Mathematical Sciences, Indiana University Purdue University Indianapolis, Indianapolis, USA; [3]Dipartimento di Matematica Politecnico di Milano, Milano, Italy; [4]Eugene and Marylin Glick Eye Institute, Indiana University School of Medicine, Indianapolis, USA.

Abstract

Purpose: The aim of the proposed analysis is to provide both a qualitative description and a quantitative assessment of how variations in aqueous humor (AH) flow parameters influence intraocular pressure (IOP) and the outcome of IOP-lowering medications.

Methods: We developed a mathematical model that describes the steady-state value of IOP as the result of the balance between AH production and drainage. We performed stochastic simulations to assess the influence of different factors on the IOP distribution in ocular normotensive and ocular hypertensive subjects and on the IOP reduction following medications.

Results: The distribution of the relative frequency of a given IOP value for ocular normotensive subjects fits a right-skewed Gaussian curve with a frequency peak of 25% at 15.13 mmHg and a skewness of 0.2, in very good agreement with the results from a population-based study on approximately 12,000 individuals. The model also shows that the outcomes of IOP-lowering treatments depend on the levels of

Correspondence: Marcela Szopos, Institut de Recherche Mathématique Avancée UMR 7501, Université de Strasbourg / CNRS, 7, rue René Descartes, 67084 Strasbourg Cedex, France. E-mail: szopos@math.unistra.fr

pre-treatment IOP and blood pressure. The model predicts mean IOP reductions of 2.55 mmHg and 4.31 mmHg when the pre-treatment IOP mean values are 15.13 mmHg and 20.12 mmHg, respectively; these predictions are in qualitative and quantitative agreement with clinical findings.

Conclusion: These findings may help identify patient-specific factors that influence the efficacy of IOP-lowering medications and aid the development of novel, effective, and individualized therapeutic approaches to glaucoma management.

Key words: aqueous humor flow, glaucoma management, intraocular pressure, mathematical modeling, sensitivity analysis

1. Introduction

Aqueous humor (AH) flow plays an important role in determining the level of intraocular pressure (IOP).[1-3] AH production and drainage can be modulated via topical medications aimed at lowering IOP in glaucoma patients.[4] Although clinical and experimental studies have elucidated some of the mechanisms of action of many IOP-lowering agents, important questions concerning the significant variability of their efficacy observed among individuals still remain unanswered.[5-8] For example, latanoprost, a prostaglandin analog (PGA), seems to induce larger IOP reductions when pre-treatment IOP is higher[7,8] and when the glaucomatous damage is at its early stages.[7] Travoprost, another PGA, seems to be more effective in lowering IOP in African American patients when compared to non-African Americans.[9] Age, gender and eye color have also been suggested as potential factors influencing the IOP-lowering efficacy, but the results are not consistent among the different studies.[5,7,10,11] In addition, the circadian rhythm has been shown to alter the drug efficacy between day and night for some IOP-lowering agents but not for others.[6,12-15]

The observed differences in drug efficacy may be explained by other physiological factors. Blood pressure in the capillaries of the ciliary body (*cBP*), total inflow facility (*L*), blood/AH osmotic pressure difference ($\Delta\pi_s$), trabecular outflow facility (C_0), uveoscleral outflow facility (k_1) and episcleral venous pressure (*EVP*) are just some examples of the parameters that contribute to establishing the balance between AH production and drainage.[3] Consequently, they can potentially influence the IOP level and the IOP-lowering effects of the drugs. Interestingly, these factors have also been shown to vary with age, gender, ethnicity and health conditions.[16,17]

Since it is extremely difficult to identify and isolate variations in *cBP, L, $\Delta\pi_s$, C_0, k_1* and *EVP* in clinical and experimental studies, we propose a complementary mathematical approach. Only a few modeling works have studied AH flow and its relation to IOP-lowering medications;[1-3,18-20] importantly, none of them explicitly accounted for uncertainties and variabilities in the model parameters. In this study, we compute IOP as the solution of a simplified mathematical model describing the

balance between AH production and drainage; we then perform a sensitivity analysis aimed at quantifying the influence of parameters' variations on the IOP distribution in various situations of clinical interest. Accounting for variability in a systematic manner can help identify some patient-specific factors that influence the efficacy of IOP-lowering medications and aid in the development of novel, effective, and individualized therapeutic approaches in glaucoma management.

2. Methods

To analyze AH flow, we utilized a mathematical model that describes the steady-state value of IOP as the result of the balance between AH production and drainage. Changes in ocular blood volume, mainly localized in the choroid, are conjectured to affect the time variations of IOP,[2] but they are not considered here.

AH is produced at the level of the ciliary body by a combination of a passive mechanism, the *ultrafiltration*, and an active mechanism, the *ionic secretion*, and is modulated by the total inflow facility (L).[1,3,19] Here the term facility indicates hydraulic conductance, namely a flow rate per units of pressure. The total flow J_{in} of AH entering the eye is therefore given by

$$J_{in} = J_{uf} + J_{secr}, \tag{1}$$

where J_{uf} and J_{sec} are the flows due to ultrafiltration and active secretion, respectively. The ultrafiltration from the ciliary circulation consists of flow of transparent fluid across semipermeable membranes (including vascular walls, stroma and epithelial cells) and is driven by blood/AH differences in hydrostatic pressures (cBP - IOP) and oncotic pressures ($\Delta\pi_p$): the latter is modulated by a protein reflection coefficient (σ_p). We thus model J_{uf} as

$$J_{uf} = L[(cBP\text{-}IOP)\text{-}\sigma_p) \, \Delta\pi_p \,]. \tag{2}$$

The inflow, as a result of the active ionic secretion, is proportional to the blood/AH osmotic pressure difference ($\Delta\pi_s$), via a reflection coefficient for low-molecular components (σ_s), and it is similarly modeled by

$$J_{sec} = L[\text{-}\sigma_s \, \Delta\pi_s \,]. \tag{3}$$

The drainage of AH from the eye is driven by passive mechanisms through two different pathways. The *trabecular pathway*, also known as conventional pathway, consists of AH flow through the trabecular meshwork, into the Schlemm's canal and the episcleral veins. The *uveoscleral pathway*, also known as the non-conventional pathway, consists of AH flow through the ciliary muscle and into the supraciliary

space. Thus, the total flow J_{out} of AH leaving the eye is given by

$$J_{out} = J_{tm} + J_{uv},$$ (4)

where J_{tm} and J_{uv} are the flows via the trabecular and uveoscleral pathways, respectively. As proposed by Brubaker,[18] the trabecular pathway model consists of a flow through a nonlinear resistor positioned between the anterior chamber (where pressure is equal to *IOP*) and the episcleral veins (where pressure is equal to EVP), with outflow facility (C_{tm}) and is given by the following equation:

$$J_{tm} = C_{tm}(IOP - EVP), \text{ with } C_{TM} = \frac{1}{R_0[1 + Q(IOP - EVP)]}$$ (5)

where R_0 is the resistance when *IOP* equals *EVP*, and *Q* is the outflow obstruction coefficient. The contribution of the uveoscleral pathway is modeled as the flow through a non-linear resistor connected to the ground,[3] with outflow facility (C_{us}) depending non-linearly on the pressure through the Michaelis-Menten-type relation[21]:

$$J_{tm} = C_{tm}(IOP - 0), \text{ with } C_{uv} = \frac{k_1}{k_2 + IOP},$$ (6)

where k_1 is the maximum value attainable by the uveoscleral flow rate. k_2 is the Michaelis constant for the uveoscleral flow rate, namely the pressure value for which the uveoscleral flow rate is half of k_1.

The steady state value of *IOP*, resulting from the balance between production and drainage of AH, namely $J_{in} = J_{out}$, can be written as:

$$J_{uf} + J_{secr} = J_{tm} + J_{uv},$$ (7)

or, equivalently:

$$L[(cBP - IOP) - \sigma_p \Delta\pi_p - \sigma_s \Delta\pi_s] = \frac{1}{R_0[1 + Q(IOP - EVP)]}(IOP - EVP) + \frac{k_1}{k_2 + IOP}IOP.$$ (8)

This is a scalar third-order polynomial equation in the sole unknown *IOP* and can be explicitly computed from the previous formula. Control state values for the parameters, defined to represent typical conditions of a healthy eye, are indicated with an overline bar in Table 1.

To include potential sources of uncertainties as well as to identify and rank parameters having the most important influence on *IOP*, we applied a global stochastic sensitivity analysis to the model described above. We considered stochastic variations in *cBP* following a normal distribution, and in *L*, $\Delta\pi_s$, $C_0 = 1/R_0$ (trabecular outflow facility), k_1 and *EVP* following a uniform distribution, both within physiological ranges. By using the probability distribution of *IOP*, we computed vari-

Table 1. Control state values for the parameters in the model for AH flow (8).

Parameter		Value	Unit	Source
Total inflow facility	*L*	0.3	μl/min/mmHg	Lyubimov *et al*.[19]
Blood pressure in the capillaries of the ciliary body	*cBP*	27.5	mmHg	Kiel[2], Kiel *et al*.[3], Lyubimov et al.[19]
Blood/AH oncotic pressure difference	$\Delta\pi_p$	25	mmHg	Lyubimov *et al*.[19]
Reflection coefficient for proteins	σ_p	1	[-]	Lyubimov *et al*.[19]
Blood/AH osmotic pressure difference	$\Delta\pi_s$	-450	mmHg	Lyubimov *et al*.[19]
Reflection coefficient for low-molecular components	σ_s	0.0515	[-]	Lyubimov *et al*.[19]
Episcleral venous pressure	*EVP*	8	mmHg	Kiel *et al*.[3]
Trabecular outflow resistance (when pressure gradient equals 0)	R_0	2.2	mmHg min/μl	Brubaker[18]
Trabecular outflow obstruction coefficient	*Q*	0.012	mmHg^{-1}	Brubaker[18]
Maximum uveoscleral flow rate	k_1	0.4	μl/min	Kiel *et al*.[3]
Pressure at which uveoscleral flow rate is at half maximum	k_2	5	mmHg	Kiel *et al*.[3]

ance-based sensitivity indices, also known as Sobol indices[22] and the probability density function,[23] which describes the relative frequency of a given *IOP* value. For each parameter, its direct influence on *IOP* is quantified in terms of *first-order Sobol indices,* and the influence through interactions with other parameters is identified by means of the *total Sobol indices*. The values of first-order and total indices can be estimated via Monte Carlo simulations,[22] or via reduced order models using polynomial chaos expansion.[24] The former method is very costly from the computational viewpoint as it requires many evaluations to ensure convergence, whereas the latter requires considerably less evaluations. Both methods have been compared and provide similar results. We report in the sequel the results obtained using the polynomial chaos reduced model.

3. Results

This model is used to compute the *IOP* distribution in four different cases of clinical interest: (i) ocular normotensive healthy subjects (ONT); (ii) ocular hypertensive subjects (OHT); (iii) ONT subjects treated with IOP-lowering medications (ONTm); and (iv) OHT subjects treated with IOP-lowering medications (OHTm). The IOP probability density function and first and total Sobol indices are reported in Fig. 1 for the four cases. Mean values, standard deviations, and skewness of the IOP distribution in the four cases are reported in Table 2. Model simulations and results are described below.

3.1. ONT subjects

The mean values of *cBP*, *L*, $\Delta\pi_s$, C_0, k_1 and *EVP* are set equal to their control state values and are summarized in Table 1. Variations in *cBP* are deduced from variations in mean arterial pressure (*MAP*). Specifically, we write $cBP = \alpha\,MAP$, where $\alpha = 0.296$ is chosen as to obtain *cBP = 27.5* mmHg when *MAP = 93* mmHg; we assumed a normal distribution for *MAP* of *93 ± 7.6* mmHg.[25] Variations in *L*, $\Delta\pi_s$, C_0, k_1 and *EVP* are assumed to follow a uniform distribution with a variation of ± *15%*.

   Simulation outcomes: The *IOP* probability density function for ONT subjects (Fig. 1a) fits a right-skewed Gaussian curve with a frequency peak of % at mmHg and a skewness of *0.2*, which is in a very good agreement with the results from a population-based study on approximately subjects[26] (green curve in Fig. 1a). The results for the Sobol indices (Fig. 1b) suggest that *IOP* is strongly influenced by *cBP* and $\Delta\pi_s$ and mildly influenced by the levels of *L*, C_0 and *EVP*. The influence of k_1 on *IOP* appears to be minimal.

Table 2. Mean values, standard deviations and skewness of the distribution of intraocular pressure (IOP) resulting from the sensitivity analysis of the mathematical model in equation (8) for four cases of clinical interest.

	IOP [mmHg] (mean ± standard deviation)	Skewness of IOP distribution
Ocular normotensive (ONT)	15.13 ± 1.58	0.2
Ocular hypertensive (OHT)	20.12 ± 2.35	0.09
Ocular normotensive treated with IOP-lowering medications (ONTm)	12.58 ± 1.32	0.17
Ocular hypertensive treated with IOP-lowering medications (OHTm)	15.81 ± 2.03	0.08
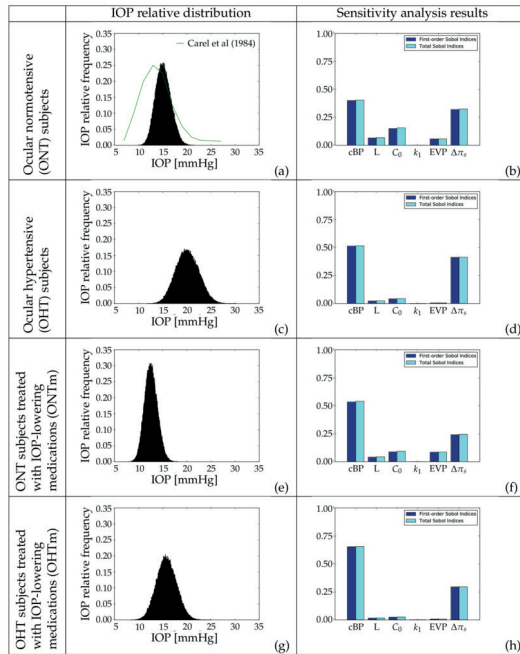
Fig. 1. Probability density function of intraocular pressure (IOP) and Sobol indices resulting from the sensitivity analysis performed on the mathematical model of equation (8) when variations in ciliary capillary blood pressure (cBP), total inflow facility (L), blood/AH osmotic pressure difference ($\Delta\pi_s$), trabecular outflow facility (C_0), uveoscleral outflow facility (k_1) and episcleral venous pressure (EVP) are considered.

3.2. OHT subjects

OHT condition is simulated by decreasing the mean value of the trabecular meshwork outflow facility as suggested by several clinical observations.[27,28] Thus, here we set $C_0 = 0.3\ \underline{C_0}$, leaving the mean values of the other parameters at control state values.

Simulation outcomes: probability density function in the OHT case (Fig. 1c) fits a Gaussian curve, but with a frequency peak of *15*% at *20.12* mmHg and with a more symmetric profile than ONT Gaussian curve (skewness = 0.09). The Sobol indices values for OHT subjects (Fig. 1d) show a stronger dependence of *IOP* on *cBP* and $\Delta\pi_s$ and a weaker dependence of *IOP* on *L*, C_0 and *EVP* than for ONT subjects. The influence of k_1 on *IOP* remains minimal.

3.3. ONT subjects treated with IOP-lowering medications (*ONTm*)

We model the effect of IOP-lowering medications by reducing the active ionic secretion by *25*%, which sets the mean value of the blood/AH osmotic pressure difference to $\Delta\pi_s = 0.75 \, \Delta\pi_s$; the mean values of the other parameters remained at control state. This modeling choice is justified by the fact that the sensitivity analyses in both the ONT and OHT cases have identified $\Delta\pi_s$ as an important determinant of *IOP* levels; in addition, clinical evidence and studies also support this notion.[1-3]

Simulation outcomes: The *IOP* probability density function in the ONTm case (Fig. 1e) fits a right-skewed Gaussian curve with a frequency peak of *30*% at *2.55* mmHg and a skewness of *0.08*. Thus, our simulations predict a reduction of *2.55* mmHg in the mean value of *IOP* when IOP-lowering medications are administered to ONT subjects. The results of Sobol indices (Fig. 1f) suggest that *IOP* is strongly influenced by *cBP* and $\Delta\pi_s$ and mildly influenced by the levels of *L*, C_0 and *EVP*. The influence of k_1 on *IOP* is again minimal.

3.4. OHT subjects treated with IOP-lowering medications (OHTm)

We simultaneously account for OHT conditions and IOP-lowering treatment by setting the mean values of C_0 and $\Delta\pi_s$ to $C_0 = 0.3 \, C_0$ and $\Delta\pi_s = 0.75 \, \Delta\pi_s$, leaving the mean values of the other parameters at control state values.

Simulation outcomes: IOP probability density function in the OHTm case (Fig. 1g) fits a Gaussian curve with a frequency peak of *20 %* at *15.81* mmHg and has a more symmetric profile than the curve in the ONTm case (skewness = *0.08*). Thus, our simulations predict a reduction of *4.31* mmHg in the mean value of *IOP* when IOP-lowering medications are administered to OHT subjects. The results on Sobol indices (Fig. 1h) are similar to those obtained in the ONTm case, but with a weaker contribution from *L*, C_0 and *EVP*.

Our results demonstrate that first-order and total Sobol indices do not present noticeable differences in any of the four simulated scenarios, suggesting that higher order interactions among the selected factors are minimal.

4. Discussion and conclusions

The model reproduced conditions of normal ocular tension, with blood pressure and *IOP* values within physiological ranges, and was subsequently used to simulate the effect of IOP-lowering medications in different conditions of clinical interest. The proposed model suggests that the outcomes of IOP-lowering treatments depend on the initial *IOP* level of the patient and on its individual clinical condition. Specifical-ly, the model predicts mean *IOP* reductions of *2.55* mmHg and *4.31* mmHg when the pre-treatment *IOP* mean values are *15.13* mmHg and *18.4* mmHg, respectively. These predictions are in good agreement with Rulo *et al.*[8] who reported mean *IOP* reductions of *15.3* mmHg and *18.4* mmHg for pre-treatment mean values of mmHg

and mmHg, respectively. However, it is important to remark that the study by Rulo *et al.* utilized Latanoprost, a prostaglandin analog that increases AH drainage, whereas we modeled IOP-lowering medications by decreasing AH production. Other studies reported *IOP* reductions ranging from *3* mmHg to *4.4* mmHg in response to brinzolamide,[20] from *4.5* mmHg to *6.1* mmHg in response to dorzolamide,[30] and from *2.4* mmHg to *4.5* mmHg in response to Latanoprost.[7] The mean IOP reductions reported in these studies[31] are close or slightly higher than those predicted by our model; this might be due to the fact that these studies started from higher pre-treatment IOP levels (ranging from *23.8* mmHg to *28.9* mmHg) than those considered in our simulations.

Our analysis also suggests that IOP-lowering effects are more pronounced when AH production is affected rather than AH drainage. The effects of lowering IOP are also more apparent when trabecular outflow is increased instead of the uveoscleral outflow. Another interesting finding of our analysis is that a patient's blood pressure strongly influences the outcomes of IOP-lowering treatments, which may explain why the effect of some drugs differ between day-time and night-time and/or amongst individuals.[5-8] A further investigation that incorporates a theoretical model coupling AH production and drainage with ocular blood flow may lead to a better understanding of this delicate, yet important, relationship.[3,32,33]

In conclusion, this study suggests that the inclusion of uncertainty in the AH flow parameters of our model is a promising approach that can aid patient-specific assessment of glaucoma management. Future developments of the model will include the coupling between AH flow and blood flow,[3,33] the simulation of IOP time-fluctuations[2,3] and the influence of specific biomechanical factors, such as axial length, scleral thickness and rigidity on these fluctuations.[34]

Acknowledgments

References

1.   Moses R Intraocular pressure. In: Moses R. (Ed.), Adler's Physiology of the Eye: Clinical Application, pp. 223-245. St. Louis: C.V. Mosby Co. 1987.
2.   Kiel J Physiology of the intraocular pressure; In: Feher, J. (Ed.), Pathophysiology of the Eye: Glaucoma, vol. 4, pp. 109-144. Budapest: Akademiai Kiado 1998.

3. Kiel J, Hollingsworth M, Rao R, Chen M, Reitsamer H. Ciliary blood flow and aqueous humor produc-tion. Prog Retin Eye Res 2011;30(1):1-17.
4. Weinreb RN, Araie M, Susanna Jr R, Goldberg I, Migdal C, Liebmann J (Eds.), Medical Treatment of Glaucoma. World Glaucoma Association Consensus Series 7. Kugler Amsterdam: Publications 2010.
5. Watson P, Stjernschantz J. A six-month, randomized, double-masked study comparing latanoprost with timolol in open-angle glaucoma and ocular hypertension. The Latanoprost Study Group. Oph-thalmology 1996;103(1):126-137.
6. Orzalesi N, Rossetti L, Bottoli A, Fogagnolo P. Comparison of the effects of latanoprost, travoprost, and bimatoprost on circadian intraocular pressure in patients with glaucoma or ocular hyperten-sion. Ophthalmology 2006;113(2):239-246.
7. Bayer A, Henderer JD, Kwak T, et al. Clinical predictors of latanoprost treatment effect. J Glaucoma 2005;14(4):260-263.
8. Rulo AH, Greve EL, Geijssen HC, Hoyng PF. Reduction of intraocular pressure with treatment of latano-prost once daily in patients with normal-pressure glaucoma. Ophthalmology 1996;103(8):1276-1282.
9. Netland P, Landry T, Sullivan E, et al. Travoprost compared with latanoprost and timolol in patients with open-angle glaucoma or ocular hypertension. Am J Ophthalmol 2001;132(4):472-484.
10. Tamada Y, Taniguchi T, Murase H, Yamamoto T, Kitazawa Y. Intraocular pressure-lowering efficacy of latanoprost in patients with normal-tension glaucoma or primary open-angle glaucoma. J Ocul Pharmacol Ther 2001;17(1):19-25.
11. Gaudana R, Ananthula H, Parenky A, Mitra A. Ocular drug delivery. AAPS J. 2010;12(3):348-360.
12. Larsson, L. The Effect of Latanoprost on Circadian Intraocular Pressure. Surv Ophthalmol 2002;47(Suppl 1):S90-96.
13. Fan S, Agrawal A, Gulati V, Neely DG, Toris CB. Daytime and nighttime effects of brimonidine on IOP and aqueous humor dynamics in participants with ocular hypertension. J Glaucoma 2014;23(5):276-281.
14. Liu JH, Medeiros FA, Slight JR, Weinreb RN. Diurnal and nocturnal effects of brimonidine monother-apy on intraocular pressure. Ophthalmology 2010;117(11):2075-2079.
15. Iskedjian M, Walker JH, Desjardins O, et al. Effect of selected antihypertensives, antidiabetics, statins and diuretics on adjunctive medical treatment of glaucoma: a population based study. Curr Med Res Opin 2009;25(8):1879-1888.
16. Guidoboni G, Harris A, Arciero J, et al. Mathematical modeling approaches in the study of glaucoma disparities among people of African and European descents. J Coupled Syst Multiscale Dyn 2013;1(1):1-21.
17. Geffen N, Guidoboni G, Armarnik S, Amireskandari A, Harris A. Glaucoma suspect book. The frontier. In: Jimenez-Roman J, Costa V (Eds.), Rational Management of the glaucoma suspect patient. The frontier. Doyma: Elsevier Masson 2015.
18. Brubaker R. The effect of intraocular pressure on conventional outflow resistance in the enucleated human eye. Invest Ophthalmol 1975;14(4):286-292.
19. Lyubimov G, Moiseeva I, Stein A. Dynamics of the intraocular fluid: Mathematical model and its main consequences. Fluid Dynamics 2007;42,684-694.
20. Siggers J, Ethier C. Fluid mechanics of the eye. Annu Rev Fluid Mech 2012;44:347-372.
21. Johnson KA, Goody RS. The Original Michaelis Constant: Translation of the 1913 Michaelis-Menten Paper. Biochemistry 2011;50(39),8264-8269. DOI: 10.1021/bi201284u
22. Sobol I. Sensitivity analysis for nonlinear mathematical models. Math Model Comput Exp 1993;1:407-414.
23. Saporta G. Probabilités, analyse des données et statistique. Editions Technip 2006.
24. Sudret B. Global sensitivity analysis using polynomial chaos expansions. Reliab Eng Syst Safe 2008;93:964-979.
25. Sesso HD, Stampfer MJ, Rosner B, et al. Systolic and diastolic blood pressure, pulse pressure, and mean arterial pressure as predictors of cardiovascular disease risk in Men. Hypertension 2000;36(5):801-807.

26. Carel RS, Korczyn AD, Rock M, Goya I. Association between ocular pressure and certain health param-eters. Ophthalmology 1984;91(4):311-314.
27. Kwon YH, Fingert JH, Kuehn MH, Alward WL. Primary open-angle glaucoma. N Engl J Med 2009;360(11):1113-1124.
28. Stamer WD, Acott TS. Current understanding of conventional outflow dysfunction in glaucoma. Curr Opin Ophthalmol 2012;23(2):135-143.
29. Silver LH. Dose-response evaluation of the ocular hypotensive effect of brinzolamide ophthalmic suspension (Azopt). Brinzolamide Dose-Response Study Group. Surv Ophthalmol 2000;44(Suppl 2):S147-153.
30. Lippa EA, Carlson L-E, Ehinger B, et al. Dose response and duration of action of dorzolamide, a topical carbonic anhydrase inhibitor. Arch Ophthalmol 1992;110(4):495-499.
31. van der Valk R, Webers CA, Schouten JS, et al. Intraocular pressure-lowering effects of all commonly used glaucoma drugs: a meta-analysis of randomized clinical trials. Ophthalmology 2005;112(7):1177-1185.
32. Guidoboni G, Harris A, Cassani S, et al. Intraocular pressure, blood pressure, and retinal blood flow autoregulation: a mathematical model to clarify their relationship and clinical relevance. Invest Ophthalmol Vis Sci 2014;55(7):4105-4118.
33. Sacco R, Cassani S, Guidoboni G, et al. Modeling the coupled dynamics of ocular blood flow and production and drainage of aqueous humor. In: Nithiarasu P, Budyn E (Eds.), Proceedings of the 4th International Conference on Computational and Mathematical Biomedical Engineering - CMBE2015, June 29-July 1, 2015, Cachan (France), pp. 608-611.Swansea: CMBE 2015.
34. Morris HJ, Tang J, Cruz Perez B, et al. Correlation between biomechanical responses of posteri-or sclera and IOP elevations during micro intraocular volume change. Invest Ophthalmol Vis Sci 2013;54(12):7215-7222. doi: 10.1167/iovs.13-12441.

Baseline characteristics predictive of structural and functional progression in open-angle glaucoma patients with different demographic characteristics

Katherine Hutchins[1], Alon Harris[1], Alice Chandra Verticchio Vercellin[1,2], Nicholas Moore[1], David Camp[1], George Eckert[3], Brent Siesky[1]

[1]Department of Ophthalmology, Indiana University School of Medicine, Indianapolis, USA; [2]University Eye Clinic, IRCCS Policlinico San Matteo, Pavia, Italy; [3]Department of Biostatistics, Indiana University School of Medicine, Indianapolis, USA

Abstract

Purpose: The aim of this study was to examine ocular blood flow parameters that may predict structural and functional disease progression in open-angle glaucoma (OAG) patients of different diabetic status, gender, ethnicity, and body mass index (BMI).
Methods: One hundred twelve patients with OAG were assessed for systemic blood pressure (BP), ocular perfusion pressure (OPP), retrobulbar blood flow, capillary blood flow, and optic nerve head morphology at baseline and every six months for a five-year period. Structural progression was monitored with optical coherence tomography and Heidelberg retinal tomography-III. Functional disease progression was monitored with automated perimetry using Humphrey visual fields. Factors associated with OAG structural and functional progression were analyzed using Cox proportional hazards models.
Results: The following were associated with shorter time to structural progression: In diabetic patients, larger area of avascular space; in males, lower central retinal artery peak systolic velocity and end diastolic velocity; in patients of African

Correspondence: Alon Harris, MS, FARVO, PhD Director of Clinical Research, Lois Letzer Professor of Ophthalmology, Professor of Cellular and Integrative Physiology, Department of Ophthalmology, Indiana University School of Medicine, 1160 West Michigan Street Indianapolis, IN 46202, USA. Email: alharris@indiana.edu

descent, higher systolic BP and OPP; in obese patients, lower ophthalmic artery end diastolic velocity. The following were associated with shorter time to functional progression: In diabetic patients, cup area, cup volume, cup/disc area ratio, linear cup/disc ratio, mean cup depth, cup shape; in males, systolic BP, diastolic BP, mean arterial pressure, systolic PP, diastolic PP, OPP, mean PP; in overweight patients, higher ophthalmic artery and central retinal artery resistive indices; in obese patients, lower central retinal artery resistive index.

Conclusions: Structural and functional OAG disease progression may be influenced differently in patients based on diabetic status, gender, ethnicity, and BMI. Mathematical modeling of risk variables that takes into account demographic characteristics may assist in better identifying OAG progression risk.

Key words: body mass index, demographic, diabetes, ethnicity, gender, glaucoma, blood flow

1. Introduction

Open-angle glaucoma (OAG) is a multifactorial optic neuropathy that remains the second leading cause of blindness worldwide.[1] Elevated intraocular pressure (IOP) is recognized as a main risk factor for OAG progression and is the primary modifiable risk factor focused on for management.[2] However, despite aggressive treatment, a high percentage of patients with normal IOP continue to experience visual field loss.[3] Over the past few decades, studies have investigated other risk factors for OAG that may contribute to disease progression. Additional risk factors identified include exfoliation, bilateral disease, advanced age, disc hemorrhages, thinner central corneas, lower systolic perfusion pressure, lower systolic blood pressure (BP), cardiovascular disease, history of migraine, female gender, vertical and horizontal cup-disc ratios, and pattern standard deviation, all of which have been linked to early predictors for the development of glaucoma.[3-6] Furthermore, findings indicate that ocular blood flow may contribute to OAG progression, but the exact nature of the relationship remains elusive.[7] In addition, African descent is a known risk factor for the development and progression of OAG, and more than six times as many people of African descent develop OAG.[8,9] The purpose of this analysis was to examine the relationship between baseline measurements that may predict structural and functional disease progression in OAG patients of different diabetic status, gender, ethnicity, and body mass index (BMI).

2. Methods

One hundred twelve patients with OAG were assessed for systemic BP, ocular

perfusion pressure (OPP), retrobulbar blood flow as measured by color Doppler imaging, capillary blood flow as measured by Heidelberg retinal flowmetry, and optic nerve head morphology as measured by Heidelberg retinal tomography III (HRT III) and optical coherence tomography (OCT) at baseline and every six months for a five-year period. The following subgroups were considered: Diabetic status, gender, ethnicity (African descent and European descent), and BMI (normal weight: BMI < 25, overweight: BMI 25 to 30, obese: BMI > 30). Structural progression was monitored with OCT and HRT III and was defined as two consecutive visits with retinal nerve fiber layer thickness decrease ≥ 8% and/or horizontal or vertical cup/disc ratio increase ≥ 0.2 compared to baseline. Functional disease progression was monitored with 24-2 Swedish interactive thresholding algorithm visual field exam using Humphrey automated perimetry and was defined as two consecutive visits with mean deviation decrease ≥ 2 and/or advanced glaucoma intervention study increase ≥ 2 compared to baseline. Analysis of covariance (ANCOVA) was used to test for statistical difference between groups from baseline to five-year follow-up. Time to structural and functional progression was analyzed using Cox proportional hazards models.

3. Results

In patients with diabetes mellitus (DM), a higher number of superior zero pixels (indicating increasing avascular area) was associated with shorter time to structural progression (p = 0.0352) (Table 1). The baseline optic nerve head parameters were associated with shorter time to functional progression in diabetic patients

Table 1. A summary of the factors associated with shorter time to structural progression from each demographic.

Factors in DM patients	
Increased superior zero pixels	p = 0.0352
Factors in male patients	
Lower CRA peak systolic velocity	p = 0.0113
Lower CRA end diastolic velocity	p = 0.0020
Factors in ED patients	
Higher systolic blood pressure	p = 0.0217
Higher systolic perfusion pressure	p = 0.0306
Factors in obese patients	
Lower OA end diastolic velocity	p = 0.0289

CRA: central retinal artery; OA: ophthalmic artery

compared to patients without DM (cup area: p = 0.0254; cup volume: p = 0.0089; cup/disc area ratio: p = 0.0382; linear cup/disc ratio p = 0.0437; mean cup depth: p = 0.0013; cup shape: p = 0.0160) (Table 2).

The following factors in males were associated with shorter time to structural progression compared to females: Lower central retinal artery (CRA) peak systolic velocity (PSV) (p = 0.0113) and lower CRA end diastolic velocity (EDV) (p = 0.0020) (Table 1). In males only, higher systemic BP and OPP were associated with shorter time to functional progression, leading to a significant gender difference (systolic BP: p = 0.0178; diastolic BP: p = 0.0230; mean arterial pressure: p = 0.0156; systolic PP: p = 0.0060; diastolic PP: p = 0.0066; OPP: p = 0.0061; mean PP: p = 0.0035) (Table 2).

The following were associated with shorter time to structural progression in patients of European descent as compared to African descent: Higher systolic BP (p = 0.0217) and higher systolic PP (p = 0.0306) (Table 1). No significant associations were found regarding the influence of ethnicity on functional disease progression.

A lower ophthalmic artery (OA) end diastolic velocity (EDV) was associated with shorter time to structural progression in obese patients (p = 0.0289) (Table 1). This was not observed in the cohorts of normal weight or overweight patients. In addition, higher ophthalmic artery (OA) resistivity index (RI) and central retinal artery (CRA) RI were predictive of functional progression in overweight patients (OA RI: p = 0.0483; CRA RI: p = 0.0148), but lower CRA RI was predictive of functional progression in obese patients (CRA RI: p = 0.0439). Baseline inferior mean capillary blood flow was associated with shorter time to functional progression in obese patients, leading to a significant difference between groups (p = 0.0317) (Table 2).

4. Discussion

4.1. Diabetes
The role of diabetes in glaucoma currently remains unclear. Some studies have established a positive relationship between the presence of diabetes and glaucoma progression.[10,11] Alternatively, others found no evidence or show evidence of a relationship between DM and IOP rather than DM and glaucoma.[12-15] Previous findings reported in the Indianapolis Glaucoma Progression Study found changes in retinal capillary blood flow to be correlated with optic nerve head changes in DM patients[16] and that DM patients showed impaired vascular regulation.[17] Our data demonstrated a shorter time to both structural and functional progression in OAG patients with DM based on certain optic nerve head and retinal capillary blood flow findings measured at baseline.

4.2. Gender
Discrepancies exist regarding the influence of gender on glaucoma progression as

Table 2. A summary of the factors associated with shorter time to functional progression from each demographic.

Factors in DM patients	
Cup area	p = 0.0254
Cup volume	p = 0.0089
Cup/disc area ratio	p = 0.0382
Linear cup/disc ratio	p = 0.0437
Mean cup depth	p = 0.0013
Cup shape	p = 0.0160
Factors in males	
Systolic blood pressure	p = 0.0178
Diastolic blood pressure	p = 0.0230
Mean arterial pressure	p = 0.0156
Systolic perfusion pressure	p = 0.0060
Diastolic perfusion pressure	p = 0.0066
Ocular perfusion pressure	p = 0.0061
Mean perfusion pressure	p = 0.0035
Factors in overweight patients	
Higher OA resistive index	p = 0.0483
Higher CRA resistive index	p = 0.0148
Factors in obese patients	
Lower CRA resistive index	p = 0.0439
Baseline inferior mean capillary blood flow	p = 0.0317

OA: ophthalmic artery; CRA: central retinal artery

well.[18,19] The Indianapolis Glaucoma Progression Study previously showed a positive association between retinal microcirculation and OPP in females but a negative association between these two factors in males.[20] The current study revealed that in males, lower retrobulbar blood flow velocity and higher systemic BP and OPP correlated with shorter time to structural and functional disease progression. These findings suggest that vascular involvement may be more strongly implicated in male patients in terms of risk for experiencing functional vision loss.

4.3. Ethnicity
OAG disproportionately affects individuals of African descent compared with

persons of European descent. Ocular structural differences have been found between patients of African and European descent, and systemic vascular diseases such as hypertension, cardiovascular disease, stroke, and DM also disproportionately affect individuals of African descent.[21,22] The Indianapolis Glaucoma Progression Study previously demonstrated that in persons of African descent, changes in retrobulbar blood flow velocities and vascular resistivity indices were correlated to retinal nerve fiber layer thickness.[23] Changes in retinal blood flow were correlated with glaucomatous morphological changes in optic nerve head in patients of African descent.[24] The present study found that higher systolic BP and OPP were associated with shorter time to structural progression in patients of European descent, while no significant differences were found between patients of African and European descent regarding functional disease progression.

4.4. Body Mass Index

The majority of studies have shown a positive association between increased BMI and glaucoma risk.[25-30] However, one study indicated that cerebral spinal fluid pressure showed a positive linear relationship with BMI, suggesting that higher BMI could reduce glaucoma risk.[31] The Singapore Malay Eye Study found that decreased BMI was associated with decreased optic rim area and increased cup/disc ratio, suggesting an inverse relationship.[32] Results from the current study revealed that in obese patients, lower OA EDV and lower CRA RI were associated with shorter time to structural and functional progression, respectively. In overweight patients, increased OA RI and CRA RI were predictive of functional progression, suggesting a stronger vascular influence in patients with higher BMI.

5. Conclusion

This study demonstrated that structural and functional disease progression may be influenced by differing demographic factors. Important considerations may include diabetic status, gender, ethnicity, and BMI. These findings suggest the establishment of mathematical modeling to allow for inclusion of demographic characteristics may increase specificity of risk assessment. Such models have previously been used to describe mechanical responses to changes in glaucoma risk factors such as IOP, scleral tension, and cerebral spinal fluid pressure.[33] Current models also aim to determine the methods by which ocular blood flow is regulated and the relative importance of these mechanisms.[33] Incorporating demographic differences may provide a more complete understanding of glaucoma progression and allow a more individualized, evidence based approach to disease management.

Contributors: All authors made a substantial contribution to the study design and acquisition and interpretation of the data. Each author participated in drafting or

revising the manuscript and approved submission of this version for publication.

Acknowledgments

References

1.   Cook C, Foster P. Epidemiology of glaucoma: What's new? Can J Ophthalmol 2012;47(3):223-226.
2.   Grewe R. The history of glaucoma. Klin Monbl Augenheilkd 1986;188(2):167-169.
3.   Leske CM, Heijl A, Hyman L, et al. Predictors of long-term progression in the early manifest glaucoma trial. Ophthalmology 2007;114(11):1965-1972.
4.   Suzuki Y, Shirato S, Adachi M, Hamada C. Risk factors for the progression of treated primary open-angle glaucoma: a multivariate life-table analysis. Graefes Arch Clin Exp Ophthalmol 1999;237(6):463-467.
5.   Drance S, Anderson DR, Schulzer M, Collaborative Normal-Tension Glaucoma Study G. Risk factors for progression of visual field abnormalities in normal-tension glaucoma. Am J Ophthalmol 2001;131(6):699-708.
6.   Gordon MO, Beiser JA, Brandt JD, et al. The Ocular Hypertension Treatment Study: baseline factors that predict the onset of primary open-angle glaucoma. Arch Ophthalmol 2002;120(6):714-720.
7.   Harris A, Siesky B, Wirostko B. Cerebral blood flow in glaucoma patients. J Glaucoma 2013;22(5):S46-S48.
8.   Friedman DS, Wolfs RC, O'Colmain BJ, et al. Prevalence of open-angle glaucoma among adults in the United States. Arch Ophthalmol 2004;122:532-538.
9.   Hyman L, Wu SY, Connell AM, et al. Prevalence and causes of visual impairment in the Barbados Eye Study. Ophthalmology 2001;108:1751-1756.
10.   Mitchell P, Smith W, Chey T, Healey PR. Open-angle glaucoma and diabetes: the Blue Mountains eye study, Australia. Ophthalmology 1997;104:712-718.
11.   Chopra V, Varma R, Francis BA, Wu J, Torres M, Azen SP. Type 2 diabetes mellitus and the risk of open-angle glaucoma: the Los Angeles Latino Eye Study. Ophthalmology 2008;115:227-232.
12.   Tielsch JM, Katz J, Quigley HA, Javitt JC, Sommer A. Diabetes, intraocular pressure, and primary open-angle glaucoma in the Baltimore Eye Survey. Ophthalmology 1995;102:48-53.

13. De Voogd S, Ikram MK, Wolfs RC, et al. Is diabetes mellitus a risk factor for open-angle glaucoma? The Rotterdam Study. Ophthalmology 2006;113(10):1827-1831.
14. Xu L, Xie XW, Wang YX, Jonas JB. Ocular and systemic factors associated with diabetes mellitus in the adult population in rural and urban China. The Beijing Eye Study. Eye (Lond) 2009;23(3):676-682.
15. Tan GS, Wong TY, Fong CW, Aung T. Diabetes, metabolic abnormalities, and glaucoma. Singapore Malay Eye Study. Arch Ophthalmol 2009;127(10):1354-1361.
16. Lee H, Harris A, Siesky B, et al. The influence of retinal blood flow on open-angle glaucoma in patients with and without diabetes. Eur J Ophthalmol 2014;24(4):542-549.
17. Shoshani Y, Harris A, Shoja MM, et al. Impaired ocular blood flow regulation in patients with open-angle glaucoma and diabetes. Clin Experiment Ophthalmol 2012;40(7):697-705.
18. Yanagida K, Iwase T, Yamamoto K, et al. Sex-related differences in ocular blood flow of healthy subjects using laser speckle flowgraphy. Invest Ophthalmol Vis Sci 2015;56(8):4880-4890.
19. Marianovic I, Marianovic M, Gvozdenovic R, Risovic D. Retrobulbar hemodynamic parameters in men and women with open-angle glaucoma. Vojnosanit Pregl 2014;71(12):1128-1131.
20. Tobe LA, Harris A, Trinidad J, et al. Should men and women be managed differently in glaucoma? Ophthalmol Ther 2012;1(1):1.
21. Huck A, Harris A, Siesky B, et al. Vascular considerations in glaucoma patients of African and European descent. Acta Ophthalmol 2014;92(5):e336-e340.
22. Girkin CA, Sample PA, Liebmann JM, et al. African Descent and Glaucoma Evaluation Study (ADAGES): II. Ancestry differences in optic disc, retinal nerve fiber layer, and macular structure in healthy subjects. Arch Ophthalmol 2010;128(5):541-550.
23. Schroeder A, Harris A, Siesky BA, et al. Retinal nerve fiber layer thickness is correlated to retrobulbar blood flow in glaucoma patients of African descent. Annual Meeting of the Association for Research in Vision and Ophthalmology; 2013. Program 442, Abstract D0182.
24. Tobe LA, Harris A, Siesky BA, et al. Changes in retinal blood flow are strongly correlated to changes in optic nerve head morphology in patients of African descent. Annual Meeting of the Association for Research in Vision and Ophthalmology; 2013. Program 4443, Abstract D0183.
25. Ngo S, Harris A, Siesky BA, et al. Blood pressure, ocular perfusion pressure, and body mass index in glaucoma patients. Eur J Ophthalmol 2013;23(5):664-669.
26. Geloneck MM, Crowell EL, Wilson EB, et al. Correlation between intraocular pressure and body mass index in the seated and supine positions. J Glaucoma 2015;24(2):130-134.
27. Wang YX, Xu L, Zhang XH, et al. Five-year change in intraocular pressure associated with changes in arterial blood pressure and body mass index. The Beijing eye study. PLoS One 2013;8(10):e77180.
28. Karadag R, Arslanyilmaz Z, Aydin B, Hepsen IF. Effects of body mass index on intraocular pressure and ocular pulse amplitude. Int J Ophthalmol 2012;5(5):605-608.
29. Wygnanski-Jaffe T, Bieran I, Tekes-Manova D, et al. Metabolic syndrome: a risk factor for high intraocular pressure in the Israeli population. Int J Ophthalmol 2015;8(2):403-406.
30. Yoshida M, Ishikawa M, Karita K, et al. Association of blood pressure and body mass index with intraocular pressure in middle-aged and older Japanese residents: a cross-sectional and longitudinal study. Acta Med Okayama 2014;68(1):27-34.
31. Berdahl JP, Fleischman D, Zaydlarova J, et al. Body Mass Index Has a Linear Relationship with Cerebrospinal Fluid Pressure. Invest Ophthalmol Vis Sci 2012;53(3):1422-1427.
32. Zheng Y, Cheung CY, Wong TY, Mitchell P, Aung T. Influence of height, weight, and body mass index on optic disc parameters. Invest Ophthalmol Vis Sci 2010;51(6):2998-3002.
33. Harris A, Guidoboni G, Arciero JC, et al. Ocular hemodynamics and glaucoma: the role of mathematical modeling. Eur J Ophthalmol 2013;23(2):139-146.

Electro-fluid dynamics of aqueous humor production: simulations and new directions

Aurelio Giancarlo Mauri[1], Lorenzo Sala[2], Paolo Airoldi[1], Giovanni Novielli[3], Riccardo Sacco[1], Simone Cassani[4], Giovanna Guidoboni[4,2], Brent Siesky[5], Alon Harris[5]

[1]Dipartimento di Matematica, Politecnico di Milano, Milano, Italy, *[2]Institut de Recherche Mathématique Avancée CNRS and Université de Strasbourg 7, Strasbourg Cedex, France*, *[3]ST Microelectronics, Agrate Brianza (MB) Italy*, *[4]Indiana University and Purdue University at Indianapolis, Department of Mathematical Sciences, IN, USA*, *[5]Eugene and Marilyn Glick Eye Institute, Indiana University School of Medicine, IN, USA*

Abstract

Purpose: to theoretically investigate the role of bicarbonate ion (HCO_3^-) on the non-pigmented transepithelial potential difference V_m, the sodium potassium pump (Na/K) and the active secretion of aqueous humor.

Methods: a three-dimensional mathematical model is proposed to isolate the roles of HCO_3^- and Na^+, which are difficult to investigate experimentally. The model combines the velocity-extended Poisson-Nernst-Planck equations to describe ion electrodiffusion and the Stokes equations to describe aqueous humor flow into the basolateral space adjacent to the nonpigmented ephitelial cells.

Results: Computations show that V_m is close to baseline experimental measurements (on monkeys) in the range $[-2.7, -2.3]\mathrm{mV}$ only if HCO_3^- is included in the simulation. The model is also capable of reproducing the flow of Na^+ exiting the cell and the flow of K^+ entering the cell, in accordance with the physiology of the Na/K pump. The simulated Na/K ratio is 1.53, which is in very good agreement with the theoretical value of 1.5.

Conclusion: Model simulations suggest that HCO_3^- inhibition may prevent physiologically correct baseline values of the nonpigmented transepithelial potential difference and Na/K ATPase function. This may provide useful indication in the design of medications that decrease the active secretion of aqueous humor, and supports the

Correspondence: Aurelio Giancarlo Mauri, Dipartimento di Matematica, Politecnico di Milano, Piazza Leonardo da Vinci 32, 20133 Milano, Italy.
E-mail: aureliogiancarlo.mauri@polimi.it

advantage of using mathematical models as a noninvasive complement of animal models.

Keywords: aqueous humor production, electrochemical transport, mathematical modeling, numerical simulation, sodium-potassium pump

Abbreviations/Nomenclature: HCO_3^- : bicarbonate; Na^+: sodium; K^+: potassium; Cl^-: chloride; ATPase: adenosine triphosphatase; IOP: intraocular pressure; AH: aqueous humor; VE-PNP: velocity-extended Poisson-Nernst-Planck; NPE: nonpigmented epithelial cell; PDE: partial differential equation.

1. Introduction

Elevated intraocular pressure (IOP) is a recognized risk factor for glaucoma. Evidences show that the steady-state value of IOP is determined by the balance between production and drainage of aqueous humor (AH), and that sodium (Na^+) and bicarbonate (HCO_3^-) secretion into the basolateral space between nonpigmented epithelial cells (NPEs) contribute to AH production (see[1] and references cited therein). A possible strategy to reduce IOP via topical medications is to reduce AH production via beta-antagonists, alpha-agonists and carbonic anhydrase inhibitors[2,3]. The connection between HCO_3^- , Na^+ and topical medications in the regulation of AH production is still controversial and difficult to study experimentally. Thus, the development and use of a mathematical model appears to be a promising approach to help unravel such a connection through simulation and comparison of different predicted scenarios.

   In the present work, we propose a mathematical model capable of describing the relationship between nonpigmented epithelial transmembrane ion flow and AH production. The velocity-extended Poisson-Nernst-Planck (VE-PNP) equations are used to describe ion electrodiffusion through a moving electrolyte medium, whereas the Stokes equations are used to describe the motion of the incompressible electrolyte fluid. The illustration and discussion of the theoretical properties and algorithms to numerically solve the coupled VE-PNP/Stokes system can be found in[4–9]. Here, the model is implemented within the three-dimensional object-oriented software platform MP-FEMOS (Multi-Physics Finite Element Modeling Oriented Simulator[9–13]).

   The proposed model is validated against baseline values of the nonpigmented transepithelial potential difference V_m. Then, the model is used to predict ion current flow under different working conditions characterized by the absence or presence of bicarbonate ions in the electrolyte fluid. Model simulations suggest that HCO_3^- inhibition may prevent to attain physiologically correct baseline values of V_m and Na/K ATPase function.

2. Methods

AH production within the ciliary body is driven by three main mechanisms: (a) transport of aqueous components by the ciliary circulation; (b) ultrafiltration and diffusion of clear fluid across the capillary-stroma barrier, and (c) osmotic efflux of clear fluid into the posterior chamber[3]. In this paper, we focus on the osmotic efflux, which is due to the active secretion of ions into the basolateral space between nonpigmented epithelial cells. Interestingly, ion accumulation in the basolateral space generates a transepithelial potential difference V_m measured experimentally in various animal species, as reported in Table 1.

Table 1. Reference data for the transepithelial potential difference V_m for several animal species.

$V_m \,[\mathrm{mV}]$	animal species	reference
3.80 ± 0.26	ox	14
5.53 ± 0.41	ox	15
3.83 ± 0.16	rabbit	15
-3.7 ± 0.3	toad	16
-1.2 ± 0.1	rabbit	17
-1.35 ± 0.08	dog	18
-2.5 ± 0.2	monkey	19
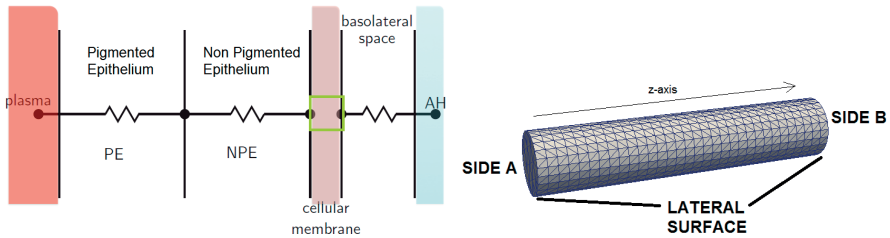
Fig. 1. Left panel: electrical scheme of the ciliary body system. PE: pigmented epithelial cellular layer. The various compartments are connected through resistances. Black bullets identify circuit nodes whose associated electrical variable is an electric voltage. The yellow box identifies the nonpigmented epithelial membrane region treated by the model. *Right panel:* geometry of a transmembrane channel in the yellow region. Side A represents the intracellular NPE region, Side B represents the extracellular region in the basolateral space. The thickness of the channel is $5\mathrm{nm}$.

The resistive path between ciliary capillaries and posterior chamber is schematized in Fig. 1 (left panel). Based on the ionic concentrations reported in[19] for the various segments in the path, it appears that the voltage drop between capillaries and

NPE is 5 orders of magnitude smaller than the values in Tab. 1 so that, as a conse-
quence, most of the transepithelial voltage drop occurs across the membrane of the
NPE. Thus, in this work we focus on the NPE membrane, as indicated by the yellow
square in Fig. 1 (left panel), and we consider a cylindrical ion channel whose inlet (SIDE
A) and outlet (SIDE B) sections denote the intracellular NPE side and the basolateral
space side, respectively, as depicted in Fig. 1 (right panel). We remark that the differ-
ence in potential between SIDE A and SIDE B corresponds to V_m. In particular, here we
consider a particular type of ion channel, namely a sodium/potassium pump, since it
has been proposed by many authors as important player in AH production[1,3,20].

   As mentioned in Section 1, we describe the electro-fluid dynamics within an ion
channel in the NPE membrane by combining two main mathematical blocks:

- Velocity-Extended Poisson-Nernst-Planck (VE-PNP) equations to treat ionic
  transport into the basolateral space;

- Stokes equations to treat water movement down the resultant osmotic pres-
  sure gradient into the posterior chamber.

The VE-PNP equations express the conservation of each ionic charge moving across
the ion channel and of the associated electrical current[4]. The Stokes equations ex-
press the conservation of mass and momentum of the electrolyte charged fluid flow-
ing across the channel and transporting the ions at low Reynolds number[4,5,7,8]. The
partial differential equations (PDEs) constituting the VE-PNP and the Stokes model
blocks are illustrated in detail in Appendix A. The two blocks are mutually coupled
through the volume force density due to the electric pressure exerted by the ions on
each infinitesimal fluid element[21]. The solution of the VE-PNP/Stokes coupled sys-
tem yields as output the spatio-temporal number density n_i of the i-th ion species,
$i = 1, \ldots, M$, the electric potential φ, the electrolyte fluid velocity $\mathbf{u}$ and the fluid
pressure p. Let t denote the time variable, $t_0 = 0$ the starting simulation time and
T the total simulation time. The numerical approximation of the VE-PNP/Stokes cou-
pled system is based on the following three steps:

1. We partition the time observational window $[t_0, t_0 + T]$ into $N_T \geq 1$ time in-
   tervals $\tau_k = [t_k, t_{k+1}]$, $k = 0, \ldots, N_T - 1$, of uniform width $\Delta t = T/N_T$;

2. For each $k = 0, \ldots, N_T - 1$, we advance in time using the Backward Euler
   time discretization method and we solve the PNP nonlinear block using a fixed
   point algorithm for a given velocity $\mathbf{u}^k$. This step returns the VE-PNP solution
   pair $(n_i^{k+1}, \varphi^{k+1})$, $i = 1, \ldots, M$, at the next time level;

3. We use n_i^{k+1}, $i = 1, \ldots, M$, and φ^{k+1} to compute the electric pressure exerted
   by the ions on the fluid and we solve the Stokes linear block. This step returns
   the Stokes solution pair $(\mathbf{u}^{k+1}, p^{k+1})$ at the next time level.

Numerical experiments for the validation of the model and the solution map schemat-
ically illustrated above are reported and discussed in[9] and[22] in the study of several
nanoscale ionic channels of biophysical interest.

3. Results and discussion

In this section we use the model illustrated in Section 2 to investigate the role of the NPE transmembranal sodium-potassium pump on the osmotic efflux of AH into the basolateral space. Boundary conditions on the surface of the cylindrical domain of Fig. 1 (right panel) are enforced in such a way that: *(i)* the K^+ ions enter the NPE at the intracellular side (A); *(ii)* the Na^+ ions enter the basolateral space at the aqueous side (B), with the ratio Na^+/K^+ = 3:2 as in physiological Na/K ATPase; *(iii)* the electrostatic potential φ is grounded at side A; and *(iv)* the electric field flux is zero at side B. The values of all model parameters and of the initial and boundary conditions for the VE-PNP system are summarized in Table 2. The longitudinal dimension of the simulated ion channel is $5\mathrm{nm}$ whereas the radius of the channel is $0.4\mathrm{nm}$. The computer sim-ulations with the MP-FEMOS software platform run on a (rather coarse) grid made of 2000 tetrahedral elements and 600 vertices, with about 3000 degrees of freedom for the VE-PNP system and more than 10000 degrees of freedom for the Stokes system. Two distinct sets of ions are considered in the description of ion electrodiffusion, the first set including the species K^+, Na^+ and Cl^- ($M = 3$), the second set including also the HCO_3^- ion ($M = 4$). The baseline ion concentrations are set according to the values reported in[19].
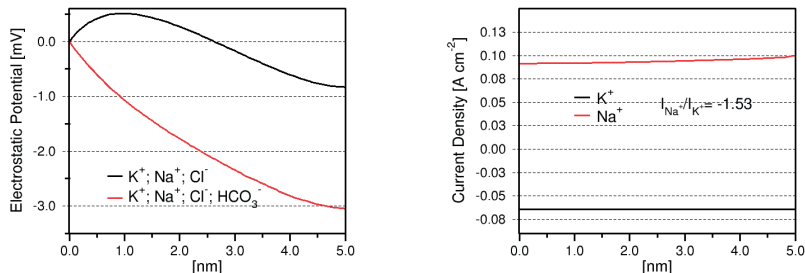
Fig. 2. Left panel: spatial distribution of φ in the NPEC channel. Black curve: HCO_3^- is inhibited. Red curve: HCO_3^- is included. *Right panel:* spatial distributions of K^+ (black) and Na^+ (red) steady-state current densities.

Fig. 2 (left panel) illustrates the results of model validation against physiological ref-erence data by plotting the steady-state spatial distribution of the electric potential (in mV). The computed nonpigmented transepithelial potential difference, $V_{m,c}$, is equal to the value of φ at side B. The negative value of $V_{m,c}$ indicates local net anion accumulation. We notice that $V_{m,c}$ is close to experimental baseline measurement (for monkeys) in the range $[-2.7, 2.3]\mathrm{mV}$[19] (cf. Table 1, last row) only if bicarbonate is included in the simulation (red curve). Fig. 2 (right panel) illustrates model predic-tions showing the spatial distributions of the Na^+ and K^+ steady-state current den-

sities (in $\mathrm{A\ cm^{-2}}$). The positive value of the Na$^+$ current indicates that Na$^+$ ions exit the NPE whereas the negative value of the K$^+$ current indicates that K$^+$ ions enter the NPE, in accordance with the physiology of the Na/K pump. The ratio between the (module) of the two currents is 1.53 in very good agreement with the theoretical value of 1.5.

4. Conclusions and future perspectives

In the present article we have carried out the theoretical study of the osmotic efflux of aqueous humor into the posterior chamber of the eye due to the active secretion of ions into the basolateral space between nonpigmented epithelial cells. The research is motivated by the fact that it is rather difficult in experimental investigations to isolate the role of a single electrolyte in regulating aqueous humor production. To this purpose, we have devised a mathematical model localized at the nonpigmented transepithelial cellular scale with the aim of describing the ionic flux of sodium, potassium, chloride and bicarbonate across a single membrane ion channel to the basolateral space which is believed to lead ultimately to a net H$_2$O efflux into the posterior eye chamber. The model is constituted by a system of partial differential equations representing balance laws for ionic charge, fluid mass, ionic momentum density, fluid momentum, mobile charge and electric field at each spatial position in the channel and at each time level. Simulation results tested against experimental measurements in monkeys suggest that bicarbonate inhibition may prevent to attain physiologically correct baseline values of the transepithelial membrane potential. Simulations accounting the presence of bicarbonate also predict the possibility of reproducing a physiologically correct Na/K ATPase function. These results may provide useful indication in the design of IOP lowering medications to decrease aqueous humor production on an effective patient-specific basis, and support the advantage of using mathematical modelling as a noninvasive complement of the animal model. Future effort will be devoted to investigating the role of permanent surface charge and of protein conformation[23] on the modulation of the electrophysiological response of the transepithelial membrane channel.

Acknowledgements

Table 2. Model parameters, boundary and initial conditions for the VE-PNP model. All values are taken as in[22].

Parameter	value	units
z_{K^+}	$+1$	[-]
z_{Na^+}	$+1$	[-]
z_{Cl^-}	-1	[-]
$z_{HCO_3^-}$	-1	[-]
μ_{K^+}	$1.957 \cdot 10^{-5}$	$cm^2 V^{-1} s^{-1}$
μ_{Na^+}	$1.334 \cdot 10^{-5}$	$cm^2 V^{-1} s^{-1}$
μ_{Cl^-}	$2.033 \cdot 10^{-5}$	$cm^2 V^{-1} s^{-1}$
$\mu_{HCO_3^-}$	$1.185 \cdot 10^{-5}$	$cm^2 V^{-1} s^{-1}$
$\overline{f}_{K^+}\big|_{\text{SIDE A}}$	$2 \cdot 10^{19}$	$cm^{-2} s^{-1}$
$\overline{n}_{Na^+}\big|_{\text{SIDE A}}$	$7.82 \cdot 10^{19}$	cm^{-3}
$\overline{n}_{Cl^-}\big|_{\text{SIDE A}}$	$6.44 \cdot 10^{19}$	cm^{-3}
$\overline{n}_{HCO_3^-}\big|_{\text{SIDE A}}$	$1.81 \cdot 10^{19}$	cm^{-3}
$\overline{n}_{K^+}\big|_{\text{SIDE B}}$	$2.41 \cdot 10^{18}$	cm^{-3}
$\overline{f}_{Na^+}\big|_{\text{SIDE B}}$	$3 \cdot 10^{19}$	$cm^{-2} s^{-1}$
$\overline{n}_{Cl^-}\big|_{\text{SIDE B}}$	$7.89 \cdot 10^{19}$	cm^{-3}
$\overline{n}_{HCO_3^-}\big|_{\text{SIDE B}}$	$1.2 \cdot 10^{19}$	cm^{-3}
$n_{K^+}^0$	$2.41 \cdot 10^{18}$	cm^{-3}
$n_{Na^+}^0$	$8.19 \cdot 10^{19}$	cm^{-3}
$n_{Cl^-}^0$	$7.17 \cdot 10^{19}$	cm^{-3}
$n_{HCO_3^-}^0$	$1.51 \cdot 10^{19}$	cm^{-3}
T	300	K
ϵ_f	$708.32 \cdot 10^{-10}$	$F\, cm^{-1}$
$\overline{\varphi}\big|_{\text{SIDE A}}$	0	V
σ_{fixed}	0	$C\, cm^{-2}$
μ_f	10^{-2}	$g\, cm^{-1}\, s^{-1}$
ρ_f	1	$g\, cm^{-3}$
$\mathbf{g}$	$\mathbf{0}$	$cm\, s^{-1}$
$\mathbf{u}^0$	$\mathbf{0}$	$cm\, s^{-1}$
$\overline{p}\big|_{\text{SIDE A}}$	0	$g\, cm^{-1}\, s^{-2}$
$\overline{p}\big|_{\text{SIDE B}}$	0	$g\, cm^{-1}\, s^{-2}$

A. Mathematical Model

In Sect. A.1 we introduce the mathematical description of the problem geometry. In Sect. A.2 we describe the PNP equations for ion flow and in Sect. A.3 we describe the Stokes equations for the intrachannel electrolyte fluid.

A.1 Geometry

Let $\mathbf{x}$ and t denote the spatial and temporal coordinates, respectively. The simulation domain $\Omega \subset \mathbb{R}^3$ (the ion channel) is shown in Fig. 1 (right panel). The channel is filled with an incompressible, viscous and Newtonian fluid moving with velocity $\mathbf{u} = \mathbf{u}(\mathbf{x}, t)$, in which $M \geq 1$ chemical species are dissolved. Each chemical has effective charge z_i, $i = 1, ..., M$, and concentration (number density) $n_i = n_i(\mathbf{x}, t)$ [cm^{-3}]. Cations have $z_i > 0$, anions have $z_i < 0$. We denote by $\partial\Omega$ the boundary of the domain Ω and by $\mathbf{n}$ the unit outward normal vector on $\partial\Omega$. With each dependent variable U, we associate a partition of the domain boundary $\partial\Omega$ into the union of (generally different) subsets. We indicate by Γ_D^U the subset of $\partial\Omega$ where a Dirichlet condition and by Γ_N^U the subset where a Neumann condition is applied, in such a way that $\Gamma_D^U \cup \Gamma_N^U = \partial\Omega$ and $\Gamma_D^U \cap \Gamma_N^U = \varnothing$.

A.2 The Velocity-Extended Poisson-Nernst-Planck equation system

The Velocity-Extended Poisson-Nernst-Planck system to describe the electrodiffusion of M ion species n_i, $i = 1, \ldots, M$, throughout a fluid in motion with velocity $\mathbf{u}$ consists of the following PDEs:

$$\frac{\partial n_i}{\partial t} + \operatorname{div} \mathbf{f}_i = 0, \tag{1a}$$

$$\mathbf{f_i} = \frac{z_i}{|z_i|}\mu_i n_i \mathbf{E} - D_i \nabla n_i + n_i \mathbf{u}, \tag{1b}$$

$$\operatorname{div} \mathbf{D} = q \sum_{i=1}^{M} z_i n_i, \tag{1c}$$

$$\mathbf{D} = \epsilon_f \mathbf{E} = -\epsilon_f \nabla\varphi. \tag{1d}$$

We refer to[4,24–26] for a detailed derivation of (1), to[5,7] for the study of existence of its solution and to[11,27] for recent applications to ion channel simulations. In (1), the symbol $\mathbf{f}_i$ denotes the ion particle flux [cm^{-2}s^{-1}], μ_i and D_i are the ion electrical mobility and diffusivity and T is system temperature. The third term in the right-hand side of the linear momentum balance equation (1b) expresses the coupling between the motion of the ion species and the moving electrolyte fluid. In the Poisson equation (1c), $\mathbf{D}$ is the electric displacement, $\mathbf{E}$ and φ are the electric field [Vcm^{-1}] and electric potential [V], respectively, whereas $q = 1.602 \cdot 10^{-19}$[C] and ϵ_f denote the electron charge and the electrolyte fluid dielectric permittivity, respectively. The diffusion coefficient

D_i and the mobility μ_i are proportional through the Einstein relation

$$D_i = \mu_i \frac{k_B T}{q|z_i|}, \tag{2}$$

where $k_B = 1.38 \cdot 10^{-16} [\mathrm{cm}^2\,\mathrm{g}\,\mathrm{s}^{-2}\,\mathrm{K}^{-1}]$ is Boltzmann's constant and T is system temperature. Initial conditions for ion concentrations are $\forall i = 1, ..., M$:

$$n_i(\mathbf{x}, 0) = n_i^0(\mathbf{x}) \qquad \text{in } \Omega, \tag{3a}$$

where the functions n_i^0 are positive given data. The boundary conditions for the VE-PNP system are $\forall i = 1, ..., M$:

$$\varphi = \overline{\varphi} \qquad\qquad \text{on } \Gamma_D^\varphi, \tag{4a}$$
$$\mathbf{D} \cdot \mathbf{n} = \sigma_{\text{fixed}} \qquad\qquad \text{on } \Gamma_N^\varphi, \tag{4b}$$
$$n_i = \overline{n}_i \qquad\qquad \text{on } \Gamma_D^{n_i}, \tag{4c}$$
$$\mathbf{f_i} \cdot \mathbf{n} = \overline{f}_i \qquad\qquad \text{on } \Gamma_N^{n_i}, \tag{4d}$$

where $\overline{\varphi}$ is the electrostatic potential of the side Γ_D^φ, $\sigma_{\text{fixed}}\,[\mathrm{C}\,\mathrm{cm}^{-2}]$ is a fixed surface charge density on side Γ_N^φ due to the lipid membrane bilayer and $\overline{n}_i$ is a given concentration of the chemical species i on side $\Gamma_D^{n_i}$. Conditions (4a) and (4c) enforce a given voltage and a given concentration on the associated side, respectively, whereas (4b) and (4d) enforce nonhomogeneous Neumann conditions on each associated side.

A.3 The Stokes equation system

The Stokes system describing the slow motion of an incompressible viscous fluid with a constant density $\rho_f\,[\mathrm{g}\,\mathrm{cm}^{-3}]$ consists of the following PDEs:

$$\operatorname{div} \mathbf{u} = 0, \tag{5a}$$

$$\rho_f \frac{\partial \mathbf{u}}{\partial t} = \operatorname{div} \underline{\underline{\sigma}}(\mathbf{u}, p) + q \sum_{i=1}^{M} z_i n_i \mathbf{E}, \tag{5b}$$

$$\underline{\underline{\sigma}}(\mathbf{u}, p) = 2\mu_f \underline{\underline{\epsilon}}(\mathbf{u}) - p\underline{\underline{\delta}}, \tag{5c}$$

$$\underline{\underline{\epsilon}}(\mathbf{u}) = \underline{\underline{\nabla}}_s \mathbf{u} = \frac{1}{2}(\nabla \mathbf{u} + (\nabla \mathbf{u})^T). \tag{5d}$$

We refer to[28] for a complete mathematical and numerical treatment of the Stokes and Navier-Stokes equations for incompressible and compressible fluids. In (5), $\mathbf{u}$ is the fluid velocity $[\mathrm{cm}\,\mathrm{s}^{-1}]$, p the fluid pressure [Pa], μ_f the fluid shear viscosity $[\mathrm{g}\,\mathrm{m}^{-1}\,\mathrm{s}^{-1}]$, $\underline{\underline{\sigma}}$ the stress tensor $[\mathrm{g}\,\mathrm{cm}^{-1}\,\mathrm{s}^{-2}]$ and $\underline{\underline{\epsilon}}$ the strain rate tensor $[\mathrm{s}^{-1}]$. The symbol $\underline{\underline{\delta}}$ is the second-order identity tensor of dimension 3 and the second-order tensor $\underline{\underline{\nabla}}_s \mathbf{u}$ is the symmetric part of the gradient of $\mathbf{u}$. Notice that in accordance

with the assumption of slow fluid motion, the quadratic convective term in the inertial forces has been neglected in the momentum balance equation (5b). The second term in the right-hand side of the momentum balance equation (5b) physically corresponds to the electric pressure exerted by the ionic charge on the electrolyte fluid, and mathematically represents the coupling between electrodiffusive ion transport and electrolyte fluid motion. The initial condition for electrolyte fluid velocity is

$$\mathbf{u}(\mathbf{x}, 0) = \mathbf{u}^0(\mathbf{x}) \qquad \text{in } \Omega, \qquad (6a)$$

where the function $\mathbf{u}^0$ is a given datum, usually set equal to zero. The boundary conditions for the Stokes system are:

$$\mathbf{u} = \mathbf{g} \qquad \text{on } \Gamma_D^{\mathbf{u}}, \qquad (7a)$$

$$\underline{\underline{\sigma}}(\mathbf{u}, p)\mathbf{n} = \mathbf{h} \qquad \text{on } \Gamma_N^{\mathbf{u}}, \qquad (7b)$$

where $\mathbf{g}$ is the imposed velocity on the side $\Gamma_D^{\mathbf{u}}$ and $\mathbf{h} = -\overline{p}\mathbf{n}$ is the value of the traction on $\Gamma_N^{\mathbf{u}}$. Relation (7a) is the wall adherence condition (typically $\mathbf{g} = \mathbf{0}$) and (7b) is the application of the action-reaction principle at the boundary.

References

1. Kiel JW. Physiology of the intraocular pressure. Pathophysiology of the Eye. Ed. by J Feher. Glaucoma (4): Akademiai Kiadò, Budapest, 1998; 79–107.
2. Gupta S, Niranjan D, Agrawal S, Srivastava S, Saxena R. Recent advances in pharmacotherapy of glaucoma. Indian Journal of Pharmacology, 2008;40(5): 197–208.
3. Kiel JW, Hollingsworth M, Rao R, Chen M, Reitsamer HA. Ciliary blood flow and aqueous humor production. Progress in Retinal and Eye Research, 2011;30(1): 1 –17.
4. Rubinstein I. Electrodiffusion of Ions. SIAM, 1990;
5. Jerome JW. Analytical approaches to charge transport in a moving medium. Transport Theory and Statistical Physics, 2002;31, 333–366.
6. Longaretti M, Chini B, Jerome JW, Sacco R. Computational models in nano-bio-electronics: simulation of ionic transport in voltage operated channels. Journal of Nanoscience and Nanotechnology, 2007;8(7): 1–9.
7. Jerome JW, Sacco R. Global weak solutions for an incompressible charged fluid with multi-scale couplings: Initial-boundary value problem. Nonlinear Analysis, 2009;71, e2487–e2497.
8. Schmuck M. Analysis of the Navier-Stokes-Nernst-Planck-Poisson system. Mathematical Models and Methods in Applied Sciences, 2009;19(6): 993–1015.
9. Airoldi P, Mauri AG, Sacco R, Jerome JW. Three-dimensional numerical simulation of ion nanochannels. Journal of Coupled Systems and Multiscale Dynamics, 2015-04-01T00:00:00;3(1): 57–65.
10. Novielli G, Ghetti A, Varesi E, Mauri A, Sacco R. Atomic migration in phase change materials. 2013 IEEE International Electron Devices Meeting (IEDM) Washington, DC, USA. 2013; 22.3.1–22.3.4. doi: 10.1109/IEDM.2013.6724683.
11. Mauri AG, Sacco R, Verri M. Electro-thermo-chemical computational models for 3D heterogeneous semiconductor device simulation. Applied Mathematical Modelling, 2015;39(14): 4057 –4074.
12. Benvenuti A, Ghetti A, Mauri A, Liu H, Mouli C. Current and future prospects of non-volatile memory modeling. 2014 IEEE International Electron Devices Meeting (SISPAD) Yokohama, Japan. 2014; 249–252.

13. Mauri AG, Bortolossi A, Novielli G, Sacco R. 3D finite element modeling and simulation of industrial semiconductor devices including impact ionization. Journal of Mathematics in Industry, 2015;5(1): doi:10.1186/s13362-015-0015-z.

14. Cole DF. Electrical potential across the isolated ciliary body observed in vitro. Br J Ophthalmol, 1961;45(10): 641–653.

15. Cole DF. Electrical potential across the isolated ciliary body of ox and rabbit. Br J Ophthalmol, 1962;46(10): 577–591.

16. Watanabe T, Saito Y. Characteristics of ion transport across the isolated ciliary epithelium of the toad as studied by electrical measurements. Exp Eye Res, 1978;27(2): 215–226.

17. Krupin T, Reinach PS, Candia OA, Podos SM. Transepithelial electrical measurements on the isolated rabbit iris-ciliary body. Exp Eye Res, 1984;38(2): 115–123.

18. Iizuka S, Kishida K, Tsuboi S, Emi K, Manabe R. Electrical characteristics of the isolated dog ciliary body. Curr Eye Res, 1984;3(3): 417–421.

19. Chu TC, Candia OA, Podos SM. Electrical parameters of the isolated monkey ciliary epithelium and effects of pharmacological agents. Invest Ophthalmol Vis Sci, 1987;28(10): 1644–1648.

20. Moses R. Intraocular pressure. Adler's Physiology of the Eye: Clinical Application. Ed. by R Moses, W Hart. C. V. Mosby Co., St Louis, 1987; 223–245.

21. Stratton J, Antennas I, Society P. Electromagnetic Theory. An IEEE Press classic reissue. Wiley, 2007;

22. Sacco R, Airoldi P, Mauri A, Jerome JW. Three-Dimensional Simulation of Biological Ion Channels Under Mechanical, Thermal and Fluid Forces. ArXiv e-prints, 2015; arXiv: 1509 . 07301. Available from: http://adsabs.harvard.edu/abs/2015arXiv150907301S.

23. Malasics A, Gillespie D, Nonner W, Henderson D, Eisenberg B, Boda D. Protein structure and ionic selectivity in calcium channels: Selectivity filter size, not shape, matters. Biochimica et Biophysica Acta (BBA) - Biomembranes, 2009;1788(12): 2471 –2480.

24. Mori Y, Liu C, Eisenberg RS. A model of electrodiffusion and osmotic water flow and its energetic structure. Physica D: Nonlinear Phenomena, 2011;240(22): 1835–1852.

25. Ray N, Muntean A, Knabner P. Rigorous homogenization of a Stokes–Nernst–Planck–Poisson system. J. Math. Anal. Appl. 2012;390, 374–393.

26. Ray N, Noorden T van, Frank F, Knabner P. Multiscale Modeling of Colloid and Fluid Dynamics in Porous Media Including an Evolving Microstructure. Transport in Porous Media, 2012;95(3): 669–696.

27. Jerome JW, Chini B, Longaretti M, Sacco R. Computational modeling and simulation of complex systems in bio-electronics. Journal of Computational Electronics, 2008;7(1): 10–13.

28. Quarteroni A, Valli A. Numerical Approximation of Partial Differential Equations. Springer-Verlag, 1997;

Computer-aided identification of novel ophthalmic artery waveform parameters in healthy subjects and glaucoma patients

Lucia Carichino[1], Giovanna Guidoboni[1,2,3], Alice Chandra Verticchio Vercellin[4], Giovanni Milano[4], Carlo Alberto Cutolo[5], Carmine Tinelli[6], Annalisa De Silvestri[6], Sergey Lapin[7,8], Joshua C. Gross[3], Brent Siesky[3], Alon Harris[3]

[1]Department of Mathematical Sciences, Indiana University Purdue University Indianapolis, Indianapolis, IN, USA; [2]Institut de Recherche Mathématique Avancée UMR 7501, Université de Strasbourg, Strasbourg, France; [3]Eugene and Marilyn Glick Eye Institute, Indiana University School of Medicine, Indianapolis, IN, USA; [4]University Eye Clinic, Foundation IRCCS, Policlinico San Matteo, Pavia, Italy; [5]University Eye Clinic, DiNOGMI, University of Genoa, Genoa, Italy; [6]Clinical Epidemiology and Biometric Unit, Foundation IRCCS, Policlinico San Matteo, Pavia, Italy; [7]Washington State University, Pullman, WA, USA; [8]Kazan Federal University, Kazan, Russian Federation

Abstract

Purpose: Arterial waveform parameters (WPs) are commonly used to monitor and diagnose systemic diseases. Color Doppler Imaging (CDI) is a consolidated technique to measure blood velocity profile in some of the major ocular vessels. This study proposes a computer-aided manipulation process of ophthalmic artery (OA) CDI images to classify and quantify WPs that might be significant in the assessment of glaucoma.
Methods: Fifty CDI images acquired by four different operators on nine healthy individuals and 38 CDI images of 38 open-angle glaucoma (OAG) patients were considered. An ad-hoc semi-automated image processing code was implemented to detect the digitalized OA velocity waveform and to extract the WPs. Concordance correlation coefficient (CCC), two-sample t-test and Pearson's correlation coefficient were used to test for similarities, differences and associations among variables.

Correspondence: Lucia Carichino, 402 N. Blackford St, LD 270, 46202 Indianapolis, USA.
E-mail: lcarichi@iupui.edu

Results: The OA-CDI images manipulation proposed showed a higher concordance between measured peak systolic velocity (PSV) data and extracted PSV data (0.80≤CCC≤0.98) than on end diastolic velocity (EDV) (0.45≤CCC≤0.63) and resistive index (RI) (0.30≤CCC≤0.58) data. In OAG patients, EDV, RI, subendocardial viability ratio (SEVR), period (T), area ratio (f) and normalized distance between ascending and descending limb (DAD/T) were found statistically correlated to at least one of the following factors: gender, age, ocular medications and year of diagnosis. When compared to healthy individuals, OAG patients OA-CDI profiles showed statistically higher values of f (p < 0.001) and DAD/T (p = 0.002) (p-values corrected by age and gender).
Conclusion: The proposed computer-aided manipulation of OA-CDI images allowed to identify DAD/T as a novel WP that vary significantly among healthy individuals and OAG patients, and among female and male OAG patients. Future studies on longitudinal OAG data are suggested to investigate the potential of DAD/T to predict severity and progression of the disease.

Key words: color Doppler imaging, glaucoma, image processing, ophthalmic artery, velocity, waveform parameters

1. Introduction

Ophthalmic disease encompasses many risk factors and physiological pathways, including those of the ocular vasculature. For instance, vascular deficits have been identified in open-angle glaucoma (OAG),[1-4] diabetes,[5,6] and age-related macular degeneration (AMD),[7-10] among other diseases. Additionally, vascular deficits are more prone in certain groups such as those of African descent.[11] Geometric and hemodynamic features of the ocular vasculature can be visualized and measured using various techniques, such as fundus imaging, optical coherence tomography (OCT), Heidelberg retinal flowmetry (HRF), confocal scanning laser flowmetry, cannon laser blood flowmeter, retinal angiography, and Color Doppler imaging (CDI). In this article, we focus on CDI and the computer-aided extraction of arterial waveform parameters (WPs).

CDI is a consolidated technique to measure blood velocity profile in some of the major ocular vessels, including the ophthalmic artery (OA), the central retinal artery (CRA), the posterior ciliary arteries (PCAs), as well as the central retinal vein (CRV). CDI measurements are noninvasive, collected data is not affected by poor ocular media, and absolute velocity measurements can be confirmed.[12] CDI studies have shown significant blood velocity derangements in the OA, CRA, and PCAs in association with diabetic retinopathy,[13] glaucoma,[14-17] and they have also been utilized to estimate the intracranial pressure (ICP) noninvasively.[18]

For decades, CDI has demonstrated its effectiveness and reliability in measuring

different vascular beds in the eye and throughout the body.[12] For example, CDI is commonly used in the fields of radiology,[19,20] cardiology,[21-24] and obstetrics.[25,26] Interestingly, since the arterial waveform changes as we move along the arterial tree, various WPs have been proposed in the scientific literature. Typical WPs utilized in ophthalmology are peak systolic velocity (PSV), end diastolic velocity (EDV) and resistive index (RI).[27] Galassi *et al*. demonstrated that CDI EDV and RI of the ophthalmic artery are correlated with the risk of visual field progression in patients with OAG.[28] Recently, several WPs commonly used in renal and hepatic arteries to predict transplant failures and detect stenosis might provide new insights in the characterization of the OA velocity waveform in glaucoma patients.[29] In the present study, we further advance the analysis of CDI measurements by proposing a computer-aided manipulation process of ophthalmic artery CDI images that enables the extraction of a novel set of WPs that might help better characterize the disease status in glaucoma.

2. Methods

In this study CDI images obtained form healthy individuals and glaucoma patients are considered. The CDI images of healthy individuals were collected at the University Eye Clinic, Foundation IRCCS, Policlinico San Matteo, Pavia, Italy, and the CDI images of glaucoma patients were collected at the Eugene and Marilyn Glick Eye Institute, Indiana University School of Medicine, Indianapolis, IN, USA. In Pavia, the Siemens Antares Stellar Plus™, probe VFX 9-4 MHz vascular linear array, was used to obtain 50 CDI images acquired by 4 different operators on 9 healthy individuals. In Indianapolis, the Philips HDI 5000 SonoCT Ultrasound System with the microvascular small parts clinical option (Philips Medical Systems, Bothell, Washington, USA), 7.5 MHz linear probe, was used to obtain CDI images of 38 glaucoma patients within the Indianapolis Glaucoma Progression Study. The baseline characteristics of the study group are described in Table 1. The PSV, EDV and RI raw data are obtained directly from the ultrasound machine as an average of the values measured over at least three cardiac cycles.

An ad-hoc semi-automated image processing code was implemented in MATLAB to analyze the CDI images, detect the digitalized OA velocity waveforms and extract the WPs (Fig. 1). The image processing consists of several steps:

1. The CDI image in red-green-blue (RGB) color scale is converted into grayscale format;
2. The resulting grayscale image is analyzed to extract the time scale, velocity scale, cardiac cycle period and height of PSV (all of them measured in terms of image pixels);
3. The original grayscale image is cropped, using the previously extracted

Table 1. Baseline characteristics of the healthy individuals and glaucoma patients included in the study.

	Healthy	Glaucoma
Number of patients	9	38
Females	5	19
Males	4	19
Age	24 ± 2	70 ± 13
Years of glaucoma diagnosis at the time of the visit	-	17 ± 10
Intraocular pressure [mmHg]	14 ± 3	16 ± 4
Heart rate (HR) [bpm]	-	67 ± 12
Systolic blood pressure (SBP) [mmHg]	117 ± 7	138 ± 21
Diastolic blood pressure (DBP) [mmHg]	70 ± 8	84 ± 11
Mean arterial pressure (MAP) [mmHg]	86 ± 7	102 ± 13
Systolic ocular perfusion pressure (SOPP) [mmHg]	103 ± 8	77 ± 15
Diastolic ocular perfusion pressure (DOPP) [mmHg]	56 ± 8	41 ± 8
Mean ocular perfusion pressure (MOPP) [mmHg]	43 ± 5	53 ± 10
Ocular medications	-	25 (66%)
Systemic medications	-	22 (58%)
Peak systolic velocity (PSV) raw [cm/s]	40 ± 7	26 ± 10
End diastolic velocity (EDV) raw [cm/s]	8 ± 2	6 ± 3
Resistive index (RI) raw	0.80 ± 0.05	0.78 ± 0.7
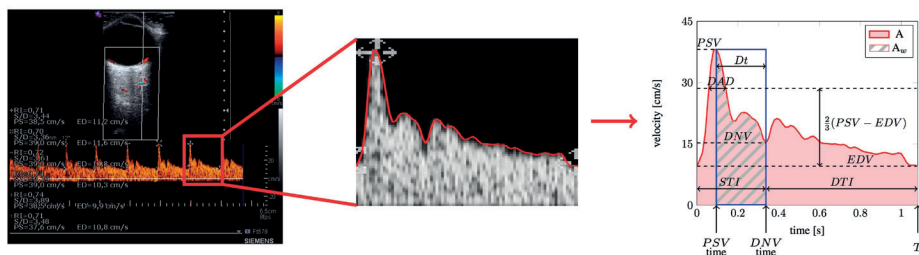
Fig. 1. A summary of the semi-automated image manipulation process used to extract the ophthalmic artery waveform parameters. Starting from the CDI image (left), the digitalized OA velocity waveform is detected (center) and the corresponding waveform parameters are extracted (right).

          pixels values, to contain only one cardiac cycle;
4.   The Sobel method[30,31] is used to detect waveform edges;
5.   The waveform edges are smoothed via local regression using weighted linear least squares and a first degree polynomial model;
6.   The resulting waveform profile is then scaled from pixel units to physical units.

Once the OA waveform digitalized profile is constructed, the following WPs are extracted (Fig. 1): peak systolic velocity (PSV), dicrotic notch velocity (DNV), end diastolic velocity (EDV), resistive index RI = (PSV-EDV)/PSV, period of a cardiac cycle (T), first systolic ascending time (PSV time), difference between PSV time and DNV time (Dt), subendocardial viability ratio (SEVR) between the diastolic time interval (DTI) and the systolic time interval (STI),[32] area under the wave (A), area ratio (f) defined as f = A_w/A_{box} = A_w/(PSV Dt), normalized distance between ascending and descending limb of the wave at two thirds of the difference between PSV and EDV (DAD/T).[33]

The Shapiro-Wilk test was used to test the normal distribution of quantitative variables: as all quantitative variables were normally distributed, the results expressed as the mean value and standard deviation (SD) were reported. Qualitative variables are summarized as counts and percentages. An analysis of concordance is performed to compare the raw values of PSV, EDV and RI with the corresponding values extracted from the digitalized OA profile using the image manipulation process detailed previously. The concordance correlation coefficient (CCC) determines how far the data deviate from the line of perfect concordance, combining measures of precision and accuracy.[34] CCC ranges in values from 0 to 1. A CCC value of 0 indicates that most of the error originates from differences in measurements between operators. As CCC values approach 1, the measurement differences between the different operators are becoming negligible and more consistent. Inter-observer agreement was classified as poor (0.00 to 0.20), fair (0.21 to 0.40), moderate (0.41 to 0.60), good (0.61 to 0.80), excellent (0.81 to 1.00).[35] CCCs are reported together with theirs 95% Confidence Interval (95% CI). To investigate the WPs differences among OAG patients with respect to gender and ocular medications, and between healthy subjects and OAG patients, a two-sample t-test for independent data is used. Moreover, the differences between healthy subjects and OAG patients are adjusted for age and gender fitting multivariable linear regression models. The Pearson's correlation coefficient (r) is computed to explore the associations among WPs and age, year of diagnosis and clinical measurements in OAG patients. A p-value (p) less then 0.05 was considered statistically significant. All tests were two-sided. The data analysis was performed with the STATA statistical package (release 14.0, 2015, Stata Corporation, College Station, Texas, USA).

3. Results

When considering all individuals included in the study, *i.e.*, healthy individuals and glaucoma patients, the analysis showed an excellent concordance on PSV (CCC = 0.85; 95%CI 0.77-0.93), a good concordance on EDV (CCC = 0.63; 95%CI: 0.49-0.78) and a fair concordance on RI (CCC = 0.33; 95% CI: 0.14-0.52). When considering only glaucoma patients, the analysis showed a good concordance on PSV (CCC = 0.80; 95%CI: 0.69-0.91), a good concordance on EDV (CCC = 0.62; 95% CI: 0.46-0.78) and a fair concordance on RI (CCC = 0.30; 95%CI: 0.09-0.52). When considering only healthy individuals, the analysis showed an excellent concordance on PSV (CCC = 0.99; 95%CI: 0.97-1.00), a moderate concordance on EDV (CCC=0.45; 95%CI: 0.15-0.74) and a moderate concordance on RI (CCC = 0.58; 95%CI: 0.31-0.85).

When compared to male glaucoma patients, female glaucoma patients showed statistically higher values of the ratio DAD/T (p = 0.002), and statistically lower values of SEVR (p = 0.031). No statistical difference was found in the remaining WPs when comparing glaucoma patients of different gender. Glaucoma patients taking ocular medications showed significantly higher values of T (p = 0.005) and SEVR (p = 0.002) when compared to glaucoma patients not taking ocular medications. No statistical difference was found in the remaining WPs when comparing glaucoma patients taking ocular medications with glaucoma patients not taking ocular medications.

Glaucoma patients' age is positively correlated with RI (r = 0.52; p < 0.001) and negatively correlated with EDV (r = -0.35; p = 0.030). No statistical correlation was found among the remaining WPs and glaucoma patients' age. The years of glaucoma diagnosis at the time of the visit is negatively correlated with T (r = -0.41; p = 0.015) and SEVR (r = -0.36; p = 0.038). No statistical correlation was found among the remaining WPs and glaucoma patients' years of diagnosis at the time of the visit. Among the set of clinical measurements of heart rate (HR), systolic blood pressure (SBP), diastolic blood pressure (DBP), mean arterial pressure (MAP), intraocular pressure (IOP), systolic ocular perfusion pressure (SOPP), diastolic ocular perfusion pressure (DOPP) and mean ocular perfusion pressure (MOPP), HR is the only parameter that showed statistical correlations with some of the WPs in glaucoma patients: HR is negatively correlated with T (r = -0.65), PSV time (r = -0.41), SEVR (r = -0.39), f (r = -0.35).

When compared to healthy individual, glaucoma patients showed significantly higher values of f (p < 0.001) and DAD/T (p < 0.001), and statistically lower values of A (p = 0.041), Dt (p = 0.008), PSV (p = 0.004) and EDV (p = 0.033) (Fig. 2). If the comparison is adjusted by gender and age (fitting a multivariable linear regression model), then, glaucoma patients showed significantly higher values of f (p < 0.001) and DAD/T (p = 0.002), and significantly lower values of RI (p = 0.002) when compared with healthy individuals. No statistical difference was found in the other WPs when comparing glaucoma patients with healthy individuals.
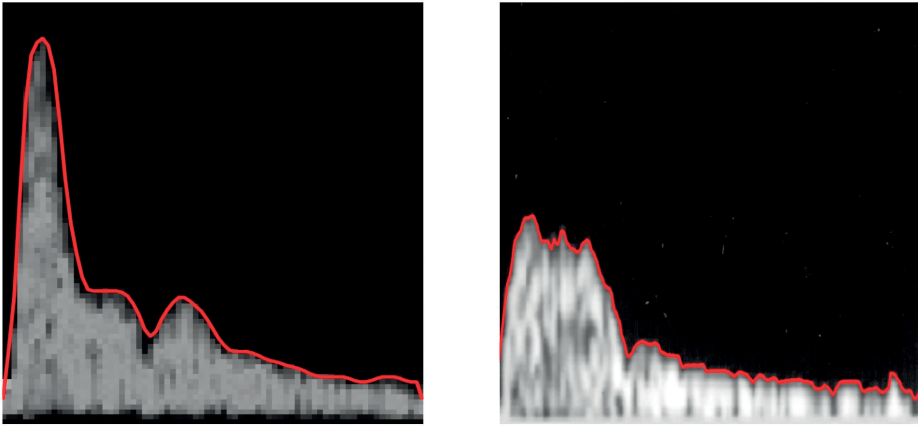
Fig. 2. Digitalized OA velocity profile of a healthy individual (left) and a glaucoma patient (right).

4. Discussion and conclusions

Over the past decades, CDI has gained popularity as a reliable tool to measure blood flow in a variety of vascular beds throughout the body. For instance, analysis of different WPs in cardiology has led to novel approaches in diagnosis and prognosis.[21-24] When measuring ocular blood flow, PSV, EDV, and RI have been traditionally used, and several studies have shown that OAG patients have reduced blood velocity with respect to these parameters when compared to healthy patients. However, novel approaches to analyzing CDI waveform parameters in ophthalmology have trailed behind the advancements of WP characterization in other fields of medicine. In this study, we investigated whether new approaches to analyzing WPs using computer-aided manipulation of OA-CDI images could distinguish between healthy subjects and OAG patients.

The OA-CDI images manipulation proposed here showed a higher concordance between PSV raw data and extracted PSV data than on EDV and RI data. Note that, the raw PSV, EDV and RI values were obtained averaging over at least three cardiac cycles; instead the corresponding parameters extracted via the OA-CDI manipulation process correspond to just one of those cardiac cycles. Moreover, CDI PSV measurements have been found to be more reproducible and accurate then EDV and RI measurements.[36-38]

There now is strong evidence that OAG patients have a vascular contribution to their disease. Several previous studies have suggested that OAG patients have reduced ocular blood flow velocities compared to healthy subjects. Most recently, Abegão Pinto *et al.* showed that when examining the ocular vasculature of 614 subjects using CDI, OAG patients had lower PSV and EDV when compared to healthy

subjects.[39] In our study we found that OAG patients had a statistically significant higher DAD/T than did healthy subjects. This is interesting because when Oliva and Roztocil[33] examined patients with obliterating atherosclerosis by Doppler ultrasound and then analyzed the waveform to identify P/L, which is identical to DAD/T here, they found that P/L identified the severity of the disease and the presence or absence of progression based on the variability coefficients. We also found that OAG patients had a statistically significant higher area ratio f than did healthy individuals. Of note, f represents another method to measure the shape of the wave in the systolic portion of the cardiac cycle similar to that proposed by Oliva and Roztocil. The correlation between DAD/T, vascular status, and OAG could prove to enhance the screening of OAG, and potentially serve as a marker for progression.

It has long been debated whether men or women are at higher risk of OAG. Recently, Kapetanakis *et al*. found that men were more likely to have OAG.[40] However, Vajaranant *et al*. found that older women were more at risk for OAG.[41] Additionally, it is thought that post-menopausal women could be at a higher risk of OAG due to the loss of estrogen and its protective vascular effects.[42] In our study we found a statistically significant increase in DAD/T in females when comparing male and female patients with OAG whose average age was 70 ± 13. This is significant because by examining ultrasonography waveforms in a non-traditional way, it may be possible to differentiate between female and male patients at higher risk and predict severity for OAG.

It is well-known that age is a risk factor for OAG,[43] and its been proposed that while age alone may not give rise to disease, its advancement generates vulnerable vascular beds that increase susceptibility to further insults.[44] In our study, we found that age correlated positively with RI and negatively with EDV. To date, there have been only a few reports specifically detailing ocular blood flow parameters as they correlate with age.[45-47] These findings suggest that, similar to other vascular beds,[48] the OA is susceptible to the atherosclerotic effects of aging.

Although the correlation with DAD/T, glaucoma, and gender shows very promising results, there were, however, several limitations to the study design. The difference in mean age between healthy and OAG patients was 46 years. Due to the role of age on general health and disease process, future studies comparing age-matched healthy and OAG patients might provide closer evaluation between healthy subjects and OAG. The total number of enrolled subjects was 47, with nine healthy subjects. In future studies, analysis of a larger population with equal numbers of healthy subjects and OAG patients would provide greater insight into the potential role of DAD/T. Some of the OAG patients were taking potentially vasoactive OAG medications throughout the study, and however, since they were not prescribed a uniform treatment regimen, we did not expect a uniform bias. Future studies with more steady treatment protocols could mitigate bias among vasoactive OAG medications taken by participants.

In summary, our computed-aided analysis of OA velocity waveforms obtained

via CDI were able to distinguish WP values between healthy subjects and OAG patients, as well as between gender among OAG patients. In future studies, analysis of DAD/T should be examined in relationship to longitudinal data of OAG patients to investigate the potential to predict severity and progression of the disease is suggested.

Acknowledgements

References

1. Costa VP, Harris A, Anderson D, et al. Ocular perfusion pressure in glaucoma. Acta Ophthalmol 2014;92(4):e252-266.
2. Cherecheanu AP, Garhofer G, Schmidl D, Werkmeister R, Schmetterer L. Ocular perfusion pressure and ocular blood flow in glaucoma. Curr Opin Pharmacol 2013;13(1):36-42.
3. Yanagi M, Kawasaki R, Wang JJ, et al. Vascular risk factors in glaucoma: a review. Clin Exper Ophthalmol 2011;39(3):252-258.
4. Schmidl D, Garhofer G, Schmetterer L. The complex interaction between ocular perfusion pressure and ocular blood flow - relevance for glaucoma. Exper Eye Res 2011;93(2):141-155.
5. Gerber AL, Harris A, Siesky B, et al. Vascular Dysfunction in Diabetes and Glaucoma: A Complex Relationship Reviewed. J Glaucoma 2015;24(6):474-479.
6. Lee E, Harris A, Siesky B, et al. The influence of retinal blood flow on open-angle glaucoma in patients with and without diabetes. Eur J Ophthalmol 2014;24(4):542-549.
7. Harris A, Chung HS, Ciulla TA, Kagemann L. Progress in measurement of ocular blood flow and relevance to our understanding of glaucoma and age-related macular degeneration. Progr Ret Eye Res 1999;18(5):669-687.

8.   Pemp B, Schmetterer L. Ocular blood flow in diabetes and age-related macular degeneration. Can J Ophthalmol/J Can Ophtalmol 2008;43(3):295-301.

9.   Ciulla TA, Harris A, Martin BJ. Ocular perfusion and age-related macular degeneration. Acta Ophthalmol Scand 2001;79(2):108-115.

10. Ehrlich R, Harris A, Kheradiya NS, et al. Age-related macular degeneration and the aging eye. Clin Interv Aging 2008;3(3):473-482.

11. Siesky B, Harris A, Racette L, et al. Differences in ocular blood flow in glaucoma between patients of African and European descent. J Glaucoma 2015;24(2):117-121.

12. Harris A, Jonescu-Cuypers CP, Kagemann L, et al. Atlas of Ocular Blood Flow. Vascular Anatomy, Pathophysiology, and Metabolism. Philadelphia, PA: Elsevier 2010.

13. Meng N, Liu J, Zhang Y, et al. Color Doppler Imaging Analysis of Retrobulbar Blood Flow Velocities in Diabetic Patients Without or With Retinopathy: A Meta-analysis. J Ultrasound Med 2014;33(8):1381-1389.

14. Srikanth K, Kumar MA, Selvasundari S, Prakash ML. Colour Doppler Imaging of Ophthalmic Artery and Central Retinal Artery in Glaucoma Patients with and without Diabetes Mellitus. J Clin Diagn Res 2014;8(4):VC01-VC02.

15. Suprasanna K, Shetty CM, Charudutt S, Kadavigere R. Doppler evaluation of ocular vessels in patients with primary open angle glaucoma. J Clin Ultrasound 2014;42(8):486-491.

16. Abegao Pinto L, Vandewalle E, Willekens K, Marques-Neves C, Stalmans I. Ocular pulse amplitude and Doppler waveform analysis in glaucoma patients. Acta Ophthalmol 2014;92(4):e280-285.

17. Jimenez-Aragon F, Garcia-Martin E, Larrosa-Lopez R, et al. Role of color Doppler imaging in early diagnosis and prediction of progression in glaucoma. BioMed Res Internat 2013;2013:871689.

18. Querfurth HW, Arms SW, Lichy CM, Irwin WT, Steiner T. Prediction of intracranial pressure from non-invasive transocular venous and arterial hemodynamic measurements: a pilot study. Neurocrit Care 2004;1(2):183-194.

19. Leoniuk J, Lukasiewicz A, Szorc M, et al. Doppler ultrasound detection of preclinical changes in foot arteries in early stage of type 2 diabetes. Polish J Radiol 2014;79:283-289.

20. Tahmasebpour HR, Buckley AR, Cooperberg PL, Fix CH. Sonographic examination of the carotid arteries. Radiographics 2005;25(6):1561-1575.

21. Correale M, Totaro A, Ieva R, et al. Tissue Doppler imaging in coronary artery diseases and heart failure. Curr Cardiol Rev 2012;8(1):43-53.

22. Kadappu KK, Thomas L. Tissue Doppler imaging in echocardiography: value and limitations. Heart Lung Circ 2015;24(3):224-233.

23. Choi J, Heo R, Hong GR, et al. Differential effect of 3-dimensional color Doppler echocardiography for the quantification of mitral regurgitation according to the severity and characteristics. Circ Cardiovasc Imaging 2014;7(3):535-544.

24. Wunderlich NC, Beigel R, Siegel RJ. Management of mitral stenosis using 2D and 3D echo-Doppler imaging. JACC Cardiovasc Imaging 2013;6(11):1191-205.

25. He J, Yan G. Research on Ovary Blood Flow Before and After Uterine Artery Embolization with the Application of Color Doppler Blood Imaging. J Reprod Med 2015;60(11-12):513-520.

26. Saini AP, Ural S, Pauliks LB. Quantitation of fetal heart function with tissue Doppler velocity imaging-reference values for color tissue Doppler velocities and comparison with pulsed wave tissue Doppler velocities. Artificial Organs 2014;38(1):87-91.

27. Pourcelot L. Applications cliniques de l'examen Doppler transcutane. Velocimetrie Ultrasonore Doppler 1974;34:780-785.

28. Galassi F, Sodi A, Ucci F, et al. Ocular hemodynamics and glaucoma prognosis: a color Doppler imaging study. Arch Ophthalmol 2003;121(12):1711-1715.

29. Abegao Pinto L, Vandewalle E, De Clerck E, Marques-Neves C, Stalmans I. Ophthalmic artery Doppler waveform changes associated with increased damage in glaucoma patients. Invest Ophthalmol Vis Sci 2012;53(4):2448-2453.

30. Parker JR. Algorithms for image processing and computer vision. New York: Wiley Computer Pub 1997.

31. Lim JS. Two-dimensional signal and image processing. Englewood Cliffs, N.J.: Prentice Hall 1990.
32. Savage MT, Ferro CJ, Pinder SJ, Tomson CR. Reproducibility of derived central arterial waveforms in patients with chronic renal failure. Clin Sci 2002;103(1):59-65.
33. Oliva I, Roztocil K. Toe pulse wave analysis in obliterating atherosclerosis. Angiol 1983;34(9):610-619.
34. Lin LI. A concordance correlation coefficient to evaluate reproducibility. Biometrics 1989;45(1):255-268.
35. Altman DG. Practical statistics for medical research. 1st ed. London, New York: Chapman and Hall 1991.
36. Founti P, Harris A, Papadopoulou D, et al. Agreement among three examiners of colour Doppler imaging retrobulbar blood flow velocity measurements. Acta Ophthalmol 2011;89(8):e631-634.
37. Harris A, Williamson TH, Martin B, Shoemaker JA, Sergott RC, Spaeth GL, et al. Test/Retest reproducibility of color Doppler imaging assessment of blood flow velocity in orbital vessels. J Glaucoma 1995;4(4):281-286.
38. Quaranta L, Harris A, Donato F, et al. Color Doppler imaging of ophthalmic artery blood flow velocity: a study of repeatability and agreement. Ophthalmology 1997;104(4):653-658.
39. Abegao Pinto L, Willekens K, Van Keer K, et al. Ocular blood flow in glaucoma - the Leuven Eye Study. Acta Ophthalmol 2016.
40. Kapetanakis VV, Chan MP, Foster PJ, et al. Global variations and time trends in the prevalence of primary open angle glaucoma (POAG): a systematic review and meta-analysis. Brit J Ophthalmol 2016;100(1):86-93.
41. Vajaranant TS, Nayak S, Wilensky JT, Joslin CE. Gender and glaucoma: what we know and what we need to know. Curr Opin Ophthalmol 2010;21(2):91-99.
42. Schmidl D, Schmetterer L, Garhofer G, Popa-Cherecheanu A. Gender differences in ocular blood flow. Curr Eye Res 2015;40(2):201-212.
43. Akpek EK, Smith RA. Overview of age-related ocular conditions. Am J Managed Care 2013;19(5 Suppl):S67-75.
44. Ehrlich R, Kheradiya NS, Winston DM, et al. Age-related ocular vascular changes. Graefe's Arch Clin Exper Ophthalmol 2009;247(5):583-591.
45. Modrzejewska M, Siesky B, Amireskandari A, et al. Parameters characterizing age-dependent retrobulbar circulation in healthy subjects measured by color Doppler ultrasonography. Curr Eye Res 2015;40(7):729-736.
46. Michelson G, Harazny J, Schmieder RE, et al. Fourier analysis of the envelope of the ophthalmic artery blood flow velocity: age- and blood pressure related impact. Hypertension 2007;50(5):964-969.
47. Maruyoshi H, Kojima S, Kojima S, et al. Waveform of ophthalmic artery Doppler flow predicts the severity of systemic atherosclerosis. Circ J 2010;74(6):1251-1256.
48. Wang JC, Bennett M. Aging and atherosclerosis: mechanisms, functional consequences, and potential therapeutics for cellular senescence. Circ Res 2012;111(2):245-259.

Theoretical predictions of metabolic flow regulation in the retina

Simone Cassani[1], Julia Arciero[1], Giovanna Guidoboni[1,2], Brent Siesky[3], Alon Harris[3]

[1]Department of Mathematical Sciences, Indiana University Purdue University Indianapolis, Indianapolis, IN, USA; [2]Institute de Recherche Mathématique Avancée UMR 7501, Université de Strasbourg, Strasbourg, France; [3]Eugene and Marilyn Glick Eye Institute, Indiana University School of Medicine, Indianapolis, IN, USA

Abstract

Purpose: This study uses a theoretical model to investigate the response of retinal blood flow to changes in tissue oxygen demand. The study is motivated by the need for a better understanding of metabolic flow regulation mechanisms in health and disease.
Methods: A mathematical model is used to calculate retinal blood flow for different levels of tissue oxygen demand in the presence or absence of regulatory mechanisms. The model combines a compartmental view of the retinal vasculature and a Krogh cylinder description for oxygen delivery to retinal tissue.
Results: The model predicts asymmetric behavior in response to changes in tissue oxygen demand. When all regulatory mechanisms are active, the model predicts a 6% decrease in perfusion when tissue oxygen demand is decreased by 50% and a 23% increase in perfusion when tissue oxygen demand is increased by 50%. In the absence of metabolic and carbon dioxide responses, the model predicts a constant level of blood flow that does not respond to changes in oxygen demand, suggesting the importance of these two response mechanisms. The model is not able to replicate the increase in oxygen venous saturation that has been observed in some flicker stimulation studies.
Conclusions: The increase in blood flow predicted by the model due to an increase in oxygen demand is not in the same proportion as the change in blood flow observed with the same decrease in oxygen demand, suggesting that vascular regulatory

Correspondence: Simone Cassani, 402 N. Blackford, LD 270, 46202, Indianapolis, IN, USA.
E-mail: scassani@iupui.edu.

mechanisms may respond differently to different levels of oxygen demand. These results might be useful for interpreting clinical and experimental findings in health and disease.

1. Introduction

Impaired retinal perfusion is associated with many ocular and systemic diseases such as glaucoma, age-related macular degeneration, and diabetes. Under healthy conditions, the retina is able to adjust perfusion in response to alterations in tissue oxygen demand (metabolic flow regulation) or blood pressure (autoregulation). This change in perfusion is achieved through vascular responses to mechanisms including myogenic, shear-dependent, metabolic, and carbon dioxide responses. It is hypothesized that in disease states some of these mechanisms are impaired, compromising the oxygenation of the retina. Mathematical modeling has been used previously[1,2] to investigate the roles of these mechanisms in achieving autoregulation. Here, these mathematical models are used to investigate the response of retinal blood flow to changes in tissue oxygen demand.

There is inconsistency in the scientific literature regarding the vascular response to changes in oxygen demand, as observed in flicker stimulation studies and light-dark adaptation studies. In particular:

- Flicker stimulation causes an increase in retinal oxygen demand, triggering an increase in blood flow;[6] changes in vessel diameter appear to depend on the frequency and/or exposure time of the flicker stimulation.[5,6,7,11,14]
- Retinal oxygen consumption differs with light, dark, and flicker stimulation.[12,16,18]
- Venous oxygen saturation is observed to increase in cases of flicker stimulation and dark as compared to adaptations to light in humans.[11,12]
- Changes in metabolism in the retina are not the same in the inner and outer retina, likely due to differences in vascularization.[12,16]
- Adaptation studies to light-dark and flicker stimulation differ by species, as shown in Table 1.

In this study, the response of the retinal vasculature to changes in oxygen demand is modeled using a compartmental model of the retinal vasculature and a Krogh cylinder model for oxygen delivery to retinal tissue.[2] The model results are consistent with some clinical observations[6] but do not replicate the behavior observed in other studies, suggesting the need for an improved description of retinal geometry and oxygen delivery.

2. Methods

In this study, the retinal vasculature is modeled as a series of lumped compartments, representing the central retinal artery (CRA), large arterioles (LA), small arterioles (SA), capillaries (C), small venules (SV), large venules (LV) and the central retinal vein (CRV) (Fig. 1). Analogous to an electric circuit in which the potential difference drives the electric current, the pressure difference between the inlet and outlet nodes of the model ($\Delta P = P_{in} - P_{out}$) drives the blood flow (Q) through the system according to Ohm's Law: $Q = \Delta P/R$, where R represents the total vascular resistance to blood flow offered by the retinal vasculature.

The variable resistances, indicated by an arrow in Figure 1, modulate the level of blood flow in the system accounting for passive (pressure-related) and active (vascular regulation-related) changes in the diameter of the representative vessel. The balance between internal pressure and intraocular pressure (IOP) leads to passive changes of resistances $R_{1,IOP}$ and $R_{5,IOP}$. The balance between internal pressure and the mechanical stress exerted by the lamina cribrosa (LC), resulting
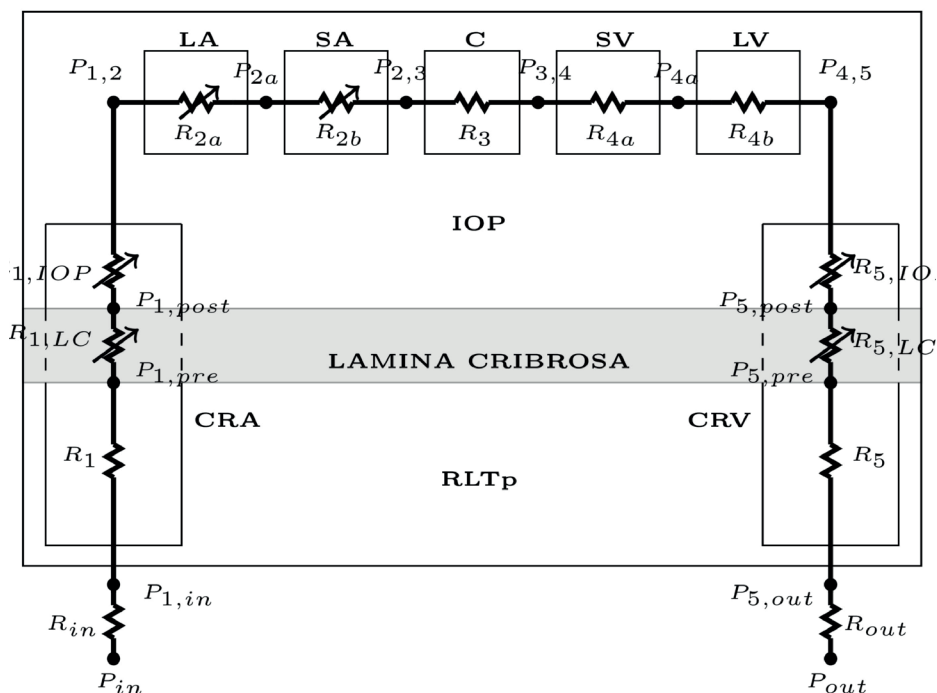
Fig. 1. Retinal vasculature represented by the following compartments: the central retinal artery (CRA), large arterioles (LA), small arterioles (SA), capillaries (C), small venules (SV), large venules (LV), and the central retinal vein (CRV).

from the combined effect of IOP, retrolaminar tissue pressure (RLTp) and scleral tension,[2,9,10] leads to passive changes of resistances $R_{1,LC}$ and $R_{5,LC}$. The changes in the variable resistances of the CRA and CRV follow the Law of Laplace.[2,10] Active changes in resistances R_{2a} and R_{2b} are achieved via four regulatory mechanisms that respond to changes in (a) systemic pressure (myogenic response); (b) arteriolar shear stress (shear stress response); (c) ATP concentration (metabolic response); and (d) carbon dioxide concentration (carbon dioxide response).

A dynamic (ODE) representation of the vessel response to diameter and vascular smooth muscle tone is used to approach the steady state conditions in the LA and SA; the resulting values of vascular resistance are computed using Poiseuille's law. The conservation of blood flow in the network leads to a nonlinear system of equations which is solved to obtain the pressure distribution at the nodes of the network and the level of blood flow as oxygen demand (M_0) is varied.[2] The value of blood oxygen saturation in the system is predicted using a Krogh cylinder model in which the CRA, LA, SA and C compartments are assumed to deliver oxygen to a surrounding cylinder of tissue. A more detailed description of the model, including equations and parameter values, can be found in Cassani *et al.*[2]

3. Results

Table 1 provides a summary of the observed effects of flicker stimulation and light-dark studies on retinal blood flow, blood oxygen saturation, and vessel diameter in multiple species (humans, rats, cats, and bullfrogs). These studies do not translate the degree of flicker stimulation or exposure to light into a quantifiable level of oxygen demand in the retina. In addition, the observed hemodynamic changes are not the same across species or for similar flicker stimulation frequencies or light exposure time. Because of these aspects, these data provide mathematical modelers with a unique challenge of capturing the various responses according to the geometric and mechanistic assumptions built into their models.

Figure 2 provides a first attempt of using a mathematical model to predict the change in perfusion when tissue oxygen demand is varied between 1 and 5 cm^3 O_2/100 cm^3/min. The effects of different response mechanisms (myogenic, shear, metabolic, and carbon dioxide) are evaluated by running multiple model simulations with some of the mechanisms active and some inactive. The model predicts asymmetric behavior in response to changes in tissue oxygen demand. For example, when all mechanisms are active, the model predicts a 6% decrease in perfusion when tissue oxygen demand is decreased by 50% and a 23% increase in perfusion when tissue oxygen demand is increased by 50%. If both the metabolic and carbon dioxide responses are impaired (light blue line), the model predicts a constant level of blood flow that does not respond to changes in oxygen demand, suggesting the importance of these two response mechanisms.

Table 1. Summary of vascular response to flicker stimulation and light-dark adaptation studies.

Study	Species	Results	Source
Flicker light stimulation	humans	Retinal arterial and venous blood flow increases during flicker stimulation. Major retinal arterial and venous diameter increases during flicker stimulation.	[6]
Flicker light stimulation	humans	Retinal venous oxygen saturation is higher during flicker stimulation than in light adaptation. Major retinal arterial and venous diameter increase during flicker stimulation.	[11]
Flicker light stimulation	rats	Retinal venous oxygen saturation is lower during flicker stimulation than in light adaptation.	[17]
Light-dark adaptation	humans	Retinal arterial and venous oxygen saturation is higher during dark than in light adaptation (in humans). Oxygen consumption in the outer retina is higher in dark than light adaptation (in cats). Oxygen consumption in the inner retina is similar in dark and light adaptation (in cats).	[12]
Light-dark adaptation	cats	Outer retina tissue oxygen partial pressure is lower in dark than light adaptation (in cats). Inner retina tissue oxygen partial pressure is higher in dark than light adaptation (in cats). Retinal oxygen consumption is higher in dark than in light adaptation (in bullfrogs).	[18]
Light-dark adaptation and flicker light stimulation	rats	Oxygen consumption in the outer retina is higher in dark than in light adaptation. Inner retina activity is lower in dark than in light adaptation. Retinal blood flow is higher in light adaptation and during flicker stimulation than in dark adaptation.	[16]
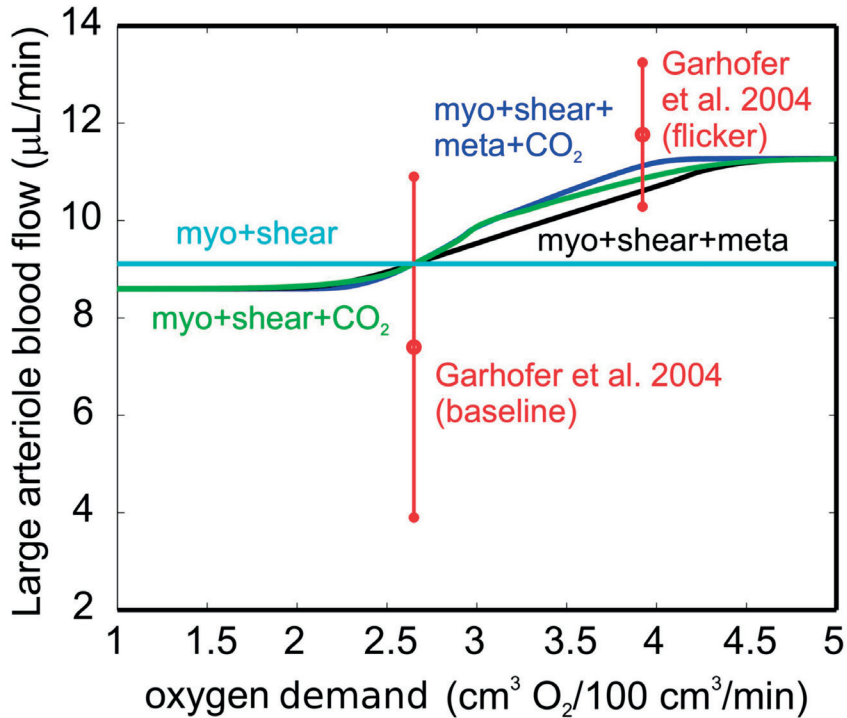
Fig. 2. Large arteriole blood flow vs. oxygen demand. The model predictions for different autoregulation mechanisms are compared with clinical data[6] at baseline and during flicker stimulation.

The predictions of blood flow through a large arteriole are also compared with data from a study on flicker stimulation in healthy individuals[6] in Figure 2. The clinical study measures: (i) the average value of blood flow in one large retinal arteriole of 7.4 ± 3.5 *μl/min* in light adapted conditions; and (ii) a 59% increase in blood flow with flicker stimulation. In the model, a baseline value for oxygen demand is chosen to be $M_0 = 2.65$ cm³ O_2/100 cm³/min in order to yield the experimentally observed value of venous blood oxygen saturation of 60%.[11] The M_0 value corresponding to flicker stimulation is obtained from a study showing that flicker stimulation induces a 48% increase in oxygen demand.[17] Using these clinical data points, Figure 2 shows that the model predictions are in good agreement with clinical data.

The model predicted value of oxygen saturation in the large venules is also compared with data from a clinical study on flicker stimulation.[11] The clinical study measures an increase in venous saturation from $60\% \pm 5.7\%$ to $64\% \pm 5.9\%$ with flicker stimulation, while the model predictions show a decrease in venous saturation with flicker stimulation from 60% to 52%.

Discussion

The increase in blood flow predicted by the model due to an increase in oxygen demand is not in the same proportion as the change in blood flow observed with the same decrease in oxygen demand, suggesting that vascular regulatory mechanisms may respond differently to different levels of oxygen demand. In addition, the model is used to quantify the relevance of the different regulatory mechanisms, suggesting that metabolic and carbon dioxide responses play a major role in achieving vascular regulation. While the model is able to quantify the average retinal response to changes in oxygen demand, it cannot differentiate between the contributions of the inner and the outer retina. In the current model, variations in the tissue oxygen demand M_0 have a global effect on the retina; the separate contributions of the inner and outer retina, which would yield local changes in metabolic activity, are not included. This could explain the difference between the model-predicted levels of oxygen saturation and the saturation levels observed in flicker stimulation and light-dark adaptation studies cited in this work. In addition, modeling the SV and LV as Starling resistors[10] would alter the venous resistance in response to changes in the transmural pressure difference and thereby alter the levels of retinal blood flow and oxygen saturation predicted in the system. Overall, the preliminary results of this model give important insight into metabolic flow regulation; however, the inability to capture all of the *in vivo* observations listed in Table 1[11,12,16,18] suggests a need for more realistic descriptions of the retinal geometry and oxygen delivery to explain the response of blood flow to changes in retinal oxygen demand.

To represent the retinal geometry more accurately, the model can be adapted to account for the multiple layers (vascular and avascular) of the retina, as depicted in Figure 3. In this updated geometry, oxygen will be assumed to diffuse from retinal capillaries and the choroid into the various retinal tissue layers.
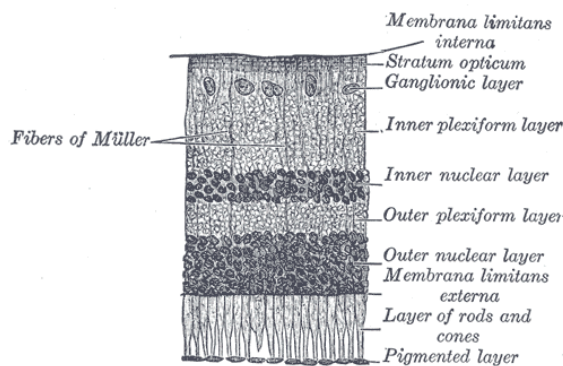
Fig. 3. Tissue layers of the retina, Henry Vandyke Carter [Public domain], via Wikimedia Commons from Gray.[8]

Previous works have been developed to predict the hemodynamics in the retina[10,13] or oxygen distribution in the multiple layers of the retina.[4,15,18] Causin *et al.*[3] modeled retinal flow and oxygenation in a realistic geometry but did not include the effect of vascular regulation. Extending the current study to combine more realistic descriptions of retinal geometry, oxygen delivery, and vascular regulation should improve the predictive ability of this mathematical model to describe the experimental observations summarized in Table 1. The development of such a model will involve non−trivial mathematical challenges related to mass conservation and approximation techniques but will ultimately yield a model that can better explain the retinal response to different metabolic conditions.

Acknowledgments

References

1. Arciero J, Harris A, Siesky B, et al. Theoretical analysis of vascular regulatory mechanisms contributing to retinal blood flow autoregulation mechanisms contributing to retinal autoregulation. Invest Ophthalmol Vis Sci 2013;54(8):5584-5593.
2. Cassani S, Harris A, Siesky B, Arciero J. Theoretical analysis of the relationship between changes in retinal blood flow and ocular perfusion pressure. J Coupled Syst Multiscale Dyn 2015;3(1):38-46.
3. Causin P, Guidoboni G, Malgaroli F, Sacco R, Harris A. Blood flow mechanics and oxygen transport and delivery in the retinal microcirculation: multiscale mathematical modeling and numerical simulation. Biomech Model Mechanobiol 2016;15(3):525-542
4. Cringle SJ, Yu D-Y. A multi-layer model of retinal oxygen supply and consumption helps explain the muted rise in inner retinal po 2 during systemic hyperoxia. Comp Biochem Physiol A Mol Integr Physiol 2002;132(1):61-66.
5. Dorner GT, Garhöfer G, Huemer KH, et al. Hyperglycemia affects flicker-induced vasodilation in the retina of healthy subjects. Vis Res 2003;43(13):1495-1500.
6. Garhöfer G, Zawinka C, Resch H, et al. Diffuse luminance flicker increases blood flow in major retinal arteries and veins. Vis Res 2004;44(8):833-838.
7. Garhöfer G, Zawinka C, Resch H, et al. Reduced response of retinal vessel diameters to flicker stimulation in patients with diabetes. Br J Ophthalmol 2004;88(7):887-891.
8. Gray H. Anatomy of the human body. Philadelphia: Lea & Febiger, 1918.
9. Guidoboni G, Harris A, Carichino L, Arieli Y, Siesky BA. Effect of intraocular pressure on the hemodynamics of the central retinal artery: a mathematical model. Math Biosci Eng 2014;11(3):523-546.
10. Guidoboni G, Harris A, Cassani S, et al. Intraocular pressure, blood pressure, and retinal blood flow autoregulation: A mathematical model to clarify their relationship and clinical relevance effects of IOP, BP, and AR on retinal hemodynamics. Invest Ophthalmol Vis Sci 2014;55(7):4105-4118.

11. Hammer M, Vilser W, Riemer T, et al. Retinal venous oxygen saturation increases by flicker light stim-ulation. Invest Ophthalmol Vis Sci 2011;52(1):274-277.
12. Hardarson SH, Basit S, Jonsdottir TA, et al. Oxygen saturation in human retinal vessels is higher in dark than in light. Invest Ophthalmol Vis Sci 2009;50(5):2308-2311.
13. Liu D, Wood NB, Witt N, et al. Computational analysis of oxygen transport in the retinal arterial network. Curr Eye Res 2009;34(11):945-956.
14. Mandecka A, Dawczynski J, Blum M, et al. Influence of flickering light on the retinal vessels in diabetic patients. Diabetes Care 2007;30(12):3048-3052.
15. Roos MW. Theoretical estimation of retinal oxygenation during retinal artery occlusion. Physiol Mea-surements 2004;25(6):1523.
16. Shih YYI, Wang L, De La Garza BH, et al. Quantitative retinal and choroidal blood flow during light, dark adaptation and flicker light stimulation in rats using fluorescent microspheres. Curr Eye Res 2013;38(2):292-298.
17. Teng P, Wanek J, Blair NP, Shahidi M. Response of inner retinal oxygen extraction fraction to light flicker under normoxia and hypoxia in rat. Invest Ophthalmol Vis Sci 2014;55(9):6055-6058.
18. Norbert D Wangsa-Wirawan ND, Linsenmeier RA. Retinal oxygen: fundamental and clinical aspects. Arch Ophthalmol 2003;121(4):547-557.

Integrated electrophysiological evaluation in early normal-tension glaucoma

Dario Messenio[1], Giuseppe Marano[2], Elia Biganzoli[2,3]

[1]Eye Clinic, Department of Clinical Science, Luigi Sacco Hospital, University of Milan, Milan, Italy; [2]Unit of Medical Statistics and Biometry, Fondazione IRCCS Istituto Nazionale dei Tumori, Milan, Italy; [3]Department of Clinical Sciences and Community Health, University of Milan, Italy

Abstract

Purpose: To evaluate the variations of intraocular pressure (IOP), morphometric optic nerve head characteristic, perimetric indices and electrophysiological parameters (pattern electroretinogram and visual evoked potentials) before and after topical IOP lowering in patients with early normal-tension glaucoma.
Methods: we evaluated 38 eyes of 20 patients with IOP < 21 mmHg, initial glaucomatous optic neuropathy (valued with HRT: retinal nerve fiber layer thickness (RNFL) and linear cup/disk ratio (linear C/D ratio)), minimal visual field defects (Octopus 101: G2 program), best correct visual acuity more than 15/20 and pathological electrophysiological parameters (valued with pattern electroretinogram (PERG) and visual evoked potentials (VEPs)), free of systemic or other ocular diseases. All parameters were evaluated at the beginning of the study (T_0) and after 12 months of therapy (T_{12}). A randomized normal control group (27 eyes of 14 subjects) with apparent larger disc cupping underwent all exams at initial of study (T_0) and after 12 months (T_{12}).
Results: Among electrophysiological parameters, at the beginning of the study NTG P100 VEPs latency is slightly increased and P100 amplitude is reduced compared to normal subjects. There are not significant variations after 12 months. P50 PERG latency in NTG is quite similar respect normal and do not modify after therapy. P50N95 complex PERG amplitude in NTG is reduced compared to normal subjects and slightly increases after 12 months (1.8 vs 1.5 ; 2.4 vs 1.9 micronvolts, with different

Correspondence: Dario Messenio, via Domenichino 49, 20149 Milano, Italy.
E-mail: dmessenio@virgilio.it

checkboard spatial frequency). Cortical retinal time (CRT) is slightly delayed in NTG and does not modify. Among visual field indices, MD and CLV is slightly higher in NTG and do not significantly modify after therapy. Among morphometric optic nerve head characteristics, linear C/D and RNFL thickness are quite similar in NTG and do not modify. IOP is quite similar between NTG and control group and modifies in NTG after therapy.

Conclusion: In a viewpoint of an integrated diagnostic, electrophysiological tests (VEPs and PERG) could provide a more sensitive measure of retinal ganglion cell integrity and help to distinguish between early normal-pressure glaucoma patients with no or minimal visual field alterations and normal subjects with apparent larger disc cupping.

Key words: early normal-tension glaucoma, initial glaucomatous optic neuropathy, minimal visual defects, pattern electroretinogram, visual evoked potentials

1. A short guide to read electrophysiological parameters

1.1. Pattern electroretinogram (PERG)
PERG represents an objective and direct measure of RGC function. It is a retinal bio-potential evoked by a temporally modulated patterned stimulus (checkerboard or grating) of constant mean luminance. The waveform of the PERG depends on the temporal frequency of the stimulus. At low temporal frequencies (< 6 reversal per second, equivalent to 3 Hz) transient PERGs are obtained: PERG waveform in normal subjects usually consists of a small initial negative component with a peak time of 35 msec (N35), followed at 45-60 msec by a much larger positive component (P50), and a large negative component at about 95 msec (N95). In glaucoma analysis, P50N95 complex amplitude (in micronvolt) and P50 implicit time (in ms) are measured; this is done with different spatial frequency: either with checkboard subtending 30' of arc of visual angle or 15' (smaller).

1.2. Visual evoked potentials (VEPs)
VEPs characterize the state of the whole visual pathway. Also the waveform of the VEPs evoked by contrast reversal of pattern stimuli depends on the temporal frequency of the stimulus. The considerations are the same of these of PERG. At low temporal frequencies (< 6 reversal per second (rps) equivalent to 3 Hz), transient VEPs are obtained: VEPs waveforms consist of a initial negative component with a peak time of approximately 75 msec (N75), followed by a larger positive component (P100) at 100-110 msec and by a large negative component at 90-130 msec (N135). P100 latency (in msec) and amplitude (in micronvolt) are measured; this is done with different spatial frequency: either with checkboard subtending 30' of arc of visual angle or 15' (smaller).

2. Introduction

Glaucoma is a multifactorial optic neuropathy characterized by progressive loss of retinal ganglion cells, changes in optic disk morphology and visual field defects. IOP is recognized as the most important risk factor for the development and/or progression of glaucomatous damage.[1] A particular type of open-angle glaucoma, normal-tension glaucoma (NTG), has typical glaucomatous optic neuropathy evolution with diurnal IOP below 21 mmHg without treatment.[2,3] IOP reduction does not necessarily slow or halt disease progression.[4]

Pattern electroretinogram (PERG) is a useful tool for detection of open-angle glaucoma, but is not a routine diagnostic exam. It is a direct indicator of retinal ganglion cell function.[5] PERG reflects diffuse RCG damage but not focal,[6] so one should not necessarily find correlations between alterations of PERG and visual field.[7] Up of 30% of retinal ganglion cells loss is associated with statistically significant changes in visual field sensitivity:[8] visual field is not impaired in ocular hypertension (OHT) or in early manifest glaucoma and therefore it is important to early diagnosis, before visual field defects are evident. PERG is altered in glaucoma and in many cases of OHT,[9] even if in some case with OHT PERG may be normal.[10] Several authors in human studies found PERG as a *predictive value* to identify those patients with elevated IOP who develop a glaucoma before visual field changes occur.[11,12]

PERG has higher sensibility to detect glaucomatous changes[12,13] and it is abnormal in most patients with manifest disease.[13,14] In some cases, PERG changes can precede detectable field losses because PERG is particularly sensitive to early damage.[15]

PERG reflects the total amount of electrophysiological activity of RGC, *i.e.*, represents an objective and direct measure of RGC function. Analysing structure-function relationship in experimental and human studies, same authors suggest a hypothesis that may there be a stage of reversible dysfunction, that may be long, before RGCs dying.[16] This dysfunction is potentially reversible and may be restored after IOP reduction[17], not only in OHT or high-tension glaucoma,[18] but also in NTG.[17]

Visual evoked potentials (VEPs) characterize the state of the whole visual pathway. In glaucomatous patients, there is a delay of P100 latency and/or P100 amplitude reduction.[13] Moreover, cortical-retinal time (CRT), index of neural conduction in post-retinal visual pathways, derived by simultaneous recordings of VEPs and PERGs, *i.e.*, latency difference between P50 PERG and P100 VEPs, is unchanged in OHT, but increases as the diseases progresses and is correlated with reduction of PERG amplitude. Some of the earlier works have demonstrated a poor sensitivity of the VEP to detection of glaucomatous patients.[19] Increased pattern VEP latency is significantly correlated with both the severity and location of visual field defects (particularly MD index) and the degree of cupping and pallor of the optic disc.[13,20,21]

In this study, we evaluate functional (visual field indices; electrophysiological (VEPs and PERG) parameters) and morphometric optic nerve head characteristic, before and after topical IOP lowering in patients with early normal-tension glaucoma.

3. Methods

The study was approved by the Hospital Medical Ethics Committee, and informed consent was obtained from the subjects after explanation of the nature and possible consequences of the study. Health control subjects and patients with early stages of glaucoma were recruited from the eye clinics at Sacco Hospital of Milan (Italy).

3.1. Patients with suspect normal-tension glaucoma
Twenty subjects (38 eyes) with early normal-tension glaucoma were recruited. All patients underwent a complete clinical examination, Goldmann applanation tonometry, optic nerve head assessment, scanning laser tomography (Heidelberg Retina Tomograph – HRT), perimetry (Octopus 101: G2 program), VEPs and PERG recording at the beginning of the study (T_0) and after 12 months (T_{12}).
    The inclusion criteria were: visual acuity more than 15/20 with best correction; untreated IOP on a diurnal pressure curve lower than 21 mmHg without treatment; initial glaucomatous optic neuropathy valued with HRT considering these inclusion criteria: one sector measurement labelled 'borderline' or 'outside of normal' at Moorfield Regression Analysis and two indices: RNFL less than 200, and linear C/D ratio more than 600; alteration of electrophysiological parameters: P50N95 PERG amplitude decreased or/and VEPs VEPs wave amplitude decreased; we consider as pathological if the values differ by less than two standard deviations from the correct normative value for age; visual field indices: MD and CLV, considering values 'borderline' or '1st Stage' of 'Glaucoma Staging System 2' perimetric staging. Exclusion criteria were: history of refractive surgery, high myopia, other ocular or systemic diseases, patients already in therapy or with other ocular or systemic diseases.

3.2. Healthy subjects
An age-matched control group of 14 healthy subjects (27 eyes) with the same morphometric optic nerve head characteristics (RNFL thickness less 200, and linear C/D ratio more than 600) but normal PERG, PEVs, and visual field indices; no ophthalmic diseases and no family history of glaucoma. Control group underwent a complete clinical examination at the beginning of the study (T_0) and after 12 months (T_{12}).
    We analysed these two groups at the start of the study (T_0) and after 12 months (T_{12}). Glaucomatous patients underwent hypotonizing therapy with prostaglandins eye drops one drop a day, otherwise none therapy was done in control group.

3.2.1.Electroretinography

Electrophysiological tests (VEPs and PERG) were recorded monocularly and simultaneously.

3.2.2. Statistics

The main aim of the statistical analysis is to quantify the diagnostic features of patients with early NTG and healthy subjects. Data were obtained from a sample of 38 eyes of patients (n = 20) with early NTG, and 27 eyes of healthy subjects (n = 14). The investigated variables are: latency and amplitude of P50N95 complex PERG wave and P100 VEP wave, with 30-minute and 15-minute checkerboard pattern stimulus; MD; CLV; RNFL thickness; linear C/D ratio; IOP; pachymetry. All the variables were recorded at T_0 and T_{12}, except pachymetry (only at T_0). CRT is defined as the difference between P100 VEPs wave and P50 PERG wave latencies.

The average values of the variables above were estimated, along with the following average differences: differences between eyes of NTG patients and healthy subjects, at T_0 and at T_{12}; differences between T_{12} and T_0 for each of the two groups. To such end, mixed effects ANOVA methods were used.[22] In each ANOVA model: (1) each variable is included as response variable; (2) time of measurement (start of study; 12 months later), group (NTG; healthy) is included as categorical predictor, with both simple effects and interaction effect; (3) to account for the correlation between measurements at distinct times (for each eye), and for the correlation between measurements of fellow eyes, two random effects, corresponding to subjects and eyes, respectively, are included. The results are reported in terms of estimated averages with respective 95% confidence intervals, corrected with the Bonferroni rule. The analysis was performed using the software R 3.2.2, with the addition of the packages nlme and multcomp.

4. Results

Of the twenty patients with early NTG, 10 are female (50.0%); the mean age is 67.6 years, with a standard deviation of 7.6 years. Of the fourteen healthy subjects, 11 are female (78.6%); the mean age is 59.2 years, with a standard deviation of 13.1 years.

As reported in Table 1, positive average differences between eyes of NTG patients and healthy subjects emerge for VEP latencies. For P100/15 latencies, the differences are: 12.9 msec (95% Confidence interval: (5.5, 20.2) msec) at T_0, and 10.5 msec (95% C.I.: (3.2, 17.8) msec) at T_{12}. For P100/30' latencies the differences are smaller: 8.9 msec (95% C.I.: (2.6, 15.1) msec) at T_0, and 8.8 msec (95% C.I.: (2.5, 15.0) msec). For amplitude measurements, negative differences between NTG and healthy subjects emerge at T_0 and T_{12}, both for P100 VEP wave and P50N95 complex PERG amplitudes. For CRT, there are positive differences, both at T_0 and at T_{12}.

An average increase in the period between T_0 and T_{12} of P50 PERG amplitudes

D. Messenio, G. Marano and E. Biganzoli

Table 1. Estimated average values and differences of electrophysiological parameters.

		Estimated average values		Estimated average differences	
		NTG Est (95% C.I.)	Healthy Est (95% C.I.)	NTG vs Healthy : Est (95% corr. C.I.)	T_{12} vs T_0: Est (95% corr. C.I.)
L100/15' :	at T_0 at T_{12}	124.1 (120.4, 127.8) 122.3 (118.7, 126.0)	111.2 (106.8, 115.6) 111.9 (107.5, 116.3)	at T_0: 12.9 (5.5, 20.2) at T_{12}: 10.5 (3.2, 17.8)	NTG: -1.7 (-4.0, 0.5) Healthy: 0.6 (-0.4, 1.7)
L100/30' :	at T_0 at T_{12}	114.3 (111.2, 117.5) 114.8 (111.6, 117.9)	105.4 (101.7, 109.2) 106.0 (102.2, 109.8)	at T_0: 8.9 (2.6, 5.1) at T_{12}: 8.8 (2.5, 15.0)	LNG : 0.5 (-1.5, 2.5) Healthy : 0.6 (-1.8, 3.0)
A100/15':	at T_0 at T_{12}	8.2 (6.5, 9.9) 9.0 (7.3, 10.8)	14.6 (12.6, 16.7) 14.5 (12.5, 16.6)	at T_0: -6.4 (-9.8, -3.0) at T_{12}: -5.5 (-8.9, -2.1)	NTG : 0.9 (-0.1, 1.8) Healthy : -0.1 (-1.2, 1.1)
A100/30':	at T_0 at T_{12}	8.2 (6.5, 10.0) 8.4 (6.7, 10.1)	13.6 (11.6, 15.7) 14.5 (12.4, 16.5)	at T_0: -5.4 (-8.9, -2.0) at T_{12}: -6.1 (-9.5, -2.6)	NTG : 0.2 (-0.8, 1.2) Healthy : 0.8 (-0.3, 2.0)
L50/15' :	at T_0 at T_{12}	62.1 (59.7, 64.4) 60.7 (58.3, 63.0)	60.1 (57.4, 62.9) 58.0 (55.2, 60.8)	at T_0: 1.9 (-2.7, 6.5) at T_{12}: 2.7 (-1.9, 7.3)	NTG : -1.4 (-5.3, 2.5) Healthy : -2.1 (-6.7, 2.5)
L50/30' :	at T_0 at T_{12}	57.8 (55.7, 59.9) 56.4 (54.2, 58.5)	56.5 (54.0, 59.1) 55.8 (53.3, 58.4)	at T_0: 1.2 (-3.0, 5.5) at T_{12}: 0.5 (-3.7, 4.7)	NTG -1.4 (-4.6, 1.8) Healthy : -0.7 (-4.5, 3.1)
A50/15' :	at T_0 at T_{12}	1.5 (1.2, 1.7) 1.8 (1.6, 2.1)	2.4 (2.1, 2.6) 2.5 (2.2, 2.8)	at T_0: -0.9 (-1.4, -0.4) at T_{12}: -0.7 (-1.1, -0.2)	NTG : 0.3 (0.1, 0.6) Healthy : 0.1 (-0.2, 0.5)
A50/30' :	at T_0 at T_{12}	1.9 (1.6, 2.2) 2.4 (2.1, 2.6)	2.7 (2.4, 3.0) 2.9 (2.6, 3.3)	at T_0: -0.8 (-1.3, -0.3) at T_{12}: -0.6 (-1.1, 0.0)	NTG : 0.5 (0.2, 0.8) Healthy : 0.3 (-0.1, 0.6)
CRT/15' :	at T_0 at T_{12}	61.8 (58.2, 65.4) 61.5 (57.9, 65.1)	51.1 (46.8, 55.4) 53.9 (49.6, 58.2)	at T_0: 10.7 (3.5, 17.9) at T_{12}: 7.6 (0.4, 14.8)	NTG : -0.3 (-4.6, 3.9) Healthy : 2.8 (-2.3, 7.9)
CRT/30' :	at T_0 at T_{12}	61.8 (58.2, 65.4) 61.5 (57.9, 65.1)	51.1 (46.8, 55.4) 53.9 (49.6, 58.2)	at T_0: 7.6 (0.6, 14.6) at T_{12}: 8.2 (1.2, 15.2)	NTG : 1.9 (-2.0, 5.8) HEalthy : 1.3 (-3.3, 5.8)

NTG: eyes of patients with early normal-tension glaucoma; Healthy: eyes of healthy subjects. Electrophysiological parameters: L100 and L50: latency of P100 VEP and P50 PERG waves respectively; A100 and A50: amplitude of P100 VEP and P50N95 complex PERG waves. The text: /15' and /30' indicate measurements taken with 15-minutes and 30-minutes checkerboard pattern stimulus, respectively.

emerges only for the NTG group. The estimates are: 0.3 µV (95% C.I.: (0.1, 0.6) µV) for the P50/15' amplitude and 0.5 µV (95% C.I.: (0.2, 0.8) µV) for the P50/30' amplitude. No relevant difference emerges for the remainder electrophysiological measurements.

Concerning the visual field indices (Table 2): for mean defect (MD), a positive average difference between NTG and healthy subjects groups emerges at T_0: 1.7 dB (95% C.I.: (0.5, 3.0) dB). Also, a positive difference between the groups is evidenced for CLV at T_{12}: 2.8 dB (95% C.I.: (0.6, 4.9) dB). For IOP, at T_0 the difference between NTG and healthy subjects is not relevant. Then, a reduction of IOP between T_0 and T_{12} emerges in the NTG group only: -5.2 mmHg (95% C.I.: (-5.9, -4.4) mmHg). In

Table 2. Estimated average values and differences of visual field indices

	NTG Est (95% C.I.)	Healthy Est (95% C.I.)	NTG vs Healthy : Est (95% corr. C.I.)	T_{12} vs T_0: Est (95% corr. C.I.)
MD : at T_0 at T_{12}	3.3 (2.7, 3.9) 3.2 (2.6, 3.9)	1.5 (0.8, 2.3) 2.2 (1.4, 2.9)	at T_0: 1.7 (0.5, 3.0) at T_{12}: 1.1 (-0.2, 2.3)	NTG : -0.1 (-0.6, 0.5) Healthy : 0.6 (0.0, 1.2)
CLV : at T_0 at T_{12}	3.9 (2.8, 5.0) 4.8 (3.8, 5.9)	2.0 (0.7, 3.3) 2.1 (0.8, 3.3)	at T_0: 1.9 (-0.2, 4.0) at T_{12}: 2.8 (0.6, 4.9)	NTG : 0.9 (-0.1, 1.9) Healthy : 0.1 (-1.1, 1.3)
Lin.C\D : at T_0 at T_{12}	641.1 (601.7, 680.5) 640.9 (601.5, 680.4)	703.8 (656.8, 750.8) 702.9 (655.9, 749.9)	at T_0: -62.7 (-140.9, 15.5) at T_{12}: -62.0 (-140.2, 16.2)	NTG : -0.2 (-21.2, 20.8) Healthy : -0.9 (-25.8, 24.1)
RNFL : at T_0 at T_{12}	188.2 (167.9, 208.4) 181.7 (161.4, 202.0)	202.8 (178.7, 227.0) 198.8 (174.6, 222.9)	at T_0: -14.7 (-54.9, 25.5) at T_{12}: -17.1 (-57.3, 23.1)	NTG : -6.5 (-19.2, 6.3) Healthy : -4.1 (-19.2, 11.0)
IOP : at T_0 at T_{12}	17.5 (16.5, 18.5) 12.3 (11.3, 13.3)	15.7 (14.5, 16.9) 15.5 (14.3, 16.7)	at T_0: 1.8 (-0.2, 3.7) at T_{12}: -3.2 (-5.2, -1.3)	NTG : -5.2 (-5.9, -4.4) Healthy : -0.2 (-1.1, 0.7)
PAC : at T_0	572.5 (555.2, 589.9)	549.6 (528.8, 570.3)	at T_0: 23.0 (-4.0, 50.0)	-

NTG: eyes of patients with early normal-tension glaucoma; Healthy: eyes of healthy subjects. Visual field indices: MD: mean defect; CLV = correct loss variance. Morphometric parameters: RNFL: RNFL thickness; lin.C/D = linear C/D. IOP: intraocular pressure. PAC: pachimetry.

agreement with this result, at T_{12} a negative difference between NTG and healthy subjects is found: -5.2 mmHg (95% C.I.: (-5.9, -4.4) mmHg). No sensible difference is found for the remainder variables.

5. Discussion

The most important problem for the correct therapy of glaucoma is the early diagnosis. Precocious diagnosis is more difficult in normal-tension glaucoma because IOP values are apparently normal,[23] even if larger disks seem to be more susceptible to IOP-related stress. Eyes with NTG have a significantly thinner lamina cribrosa and so undergoes significant displacement due to IOP, according to mathematical finite element modelling.[3,24]

Among diagnostic exams, electrophysiological tests, as VEPs and PERG, can be used to quantify retinal ganglion cells function. Some authors[17,18,25] indicate that the abnormal PERG recorded in eyes with early stages of glaucoma may often improve after IOP reduction. According to these authors, retinal ganglion cells undergo a prolonged period of dysfunction and degeneration before cell loss; PERG (particularly P50N95 complex amplitude) can evaluate this dysfunction, that may be

restored after IOP reduction, not only in OHT but also in glaucoma patients, and in NTG glaucoma. To have a substantial improvement, the PERG must be abnormal: no significant changes occurred in acetazolamide-treated normal subjects, despite an IOP reduction of approximately 30%.[26] In NTG it improves also after smaller IOP reductions because NTG eyes have a lower functional threshold.[16] Finally, PERG improvement is very little in patients with advanced glaucoma because the number of ganglion cell loss is higher and therefore the functional recovery is small.[26]

In NTG there is only an electrophysiological study: Lestak found remarkable P100 VEPs amplitude reduction, while PERG was almost unaffected.[27]

In our study on early NTG patients, P100 VEPs amplitude is reduced, according to Lestak,[27] and P100 latency is slightly delayed. After therapy, these PEV parameters do not significantly modify: this is understandable because it is unlikely that a topical therapy may have some effect on the functionality (strictly neurological) of the visual pathways. P50N95 complex PERG amplitude at the beginning of study (T_0) is reduced compared to the control group and slightly arise after IOP lowering: these results suggest that there could be a correlation between IOP and PERG changes.

IOP reduces significantly even if the baseline IOP is slightly higher than 15.5 mmHg and this confirms that those patients have NTG, as explained above. The reduction of IOP is correlated to the effective presence of a glaucoma: hyponizing normal eyes don't modify P50N95 complex PERG amplitude at all[15]. So an increase of amplitude of P50N95 complex PERG following to a decrease of IOP is suggestive of a dysfunction in a suspect or early glaucoma (in this study, NTG), dysfunction that could be (partially) restored after hyponizing.[16]

Morphometric optic nerve head characteristics don't modify after therapy, and also visual field indices. This indicates that the papillary morphometric nerve head parameters and the classic functional (perimetric) are not sensitive to detect improvements secondary to hypotonic therapy.

A limitation of this study could be to not have included patients with the disease even at more advanced stages. In fact, considering multiple levels of NTG progression would enable to check more exhaustively the extent of functional recovery in later stages.

6. Conclusion

Our pilot study is the first study trying to individuate and differentiate with electrophysiological tests normal patient with apparent larger disc cupping and early NTG ones with still quite normal visual field or minimal visual field defect.[23] This diagnostic approach may provide an important information to avoid starting useless therapy, or, on the contrary, to start precociously hypotonizing therapy in NTG before visual field occurs.

References

1.   Heijl A, Leske MC, Bengtsson B, Hyman L, Hussein M. Reduction of intraocular pressure and glaucoma progression: results from the early manifest glaucoma trial. Arch Ophthalmol 2002;120(10):1268-1279.
2.   Krupin T. Special considerations in low-tension glaucoma. Can J Ophthalmol 2007;42(3):414-417.
3.   Hayamizu F, Yamazaki Y, Nakagami T, Mizuki K. Optic disc size and progression of visual field damage in patients with normal-tension glaucoma. Clin Opthalmol 2013;7:807-813.
4.   Anderson DR, Drance SM, Schulzer M. Collaborative normal-tension glaucoma study group. Factors that predict the benefit of lowering intraocular pressure in normal-tension glaucoma. Am J Ophthalmol 2003;136(5):820-829.
5.   Maffei L, Fiorentini A. Electroretinographic responses to alternating gratings before and after section of the optic nerve. Science 1981;211(4485):953-955.
6.   Bach M, Hoffmann MB. Update on the Pattern Electroretinogram in Glaucoma. Optom Vis Sci 2008;85(6):386-395.
7.   Bach M, Sulimma F, Gerling J. Little correlation of the pattern electroretinogram (PERG) and visual filed measures in early glaucoma. Doc Ophthalmol 1997-1998;94(3):253-263.
8.   Quigley HA, Addicks EM, Green WR. Optic nerve damage in human glaucoma. III Quantitative correlation of nerve fiber loss and visual field defect in glaucoma, ischemic neuropathy, papilledema and toxic neuropathy. Arch Ophthalmol 1982;100(1):135-146.
9.   Price MJ, Drance SM, Price M, Schulzer M, Douglas GR, Tansley B. The pattern electroretinogram and visual-evoked potential in glaucoma. Greafes Arch Clin Exp Ophthalmol 1988:226:542-547.
10. Bielik M, Zwas F, Shin DH, Tsai CS. PERG and spectral sensitivity in ocular Hypertensive and chronic open-angle glaucoma patients. Graefes Arch Clin Exp Ophthalmol 1991;229(5):401-405.
11. Gonzalvo Ibanes FJ, Fernandez Tirado FJ, Almarcegui Lafita C, et al. Predictive value of the pattern-electroretinogram in glaucoma. Arch Soc Esp Oftalmol 2001;76(8):485-491.
12. Bach M, Unsoeld AS, Philippin H, et al. Pattern ERG as an early indicator in ocular hypertension: a long-term prospective study. Invest Ophthalmol Vis Sci 2006;47(11):4881-4887.
13. Parisi V, Miglior S, Manni G, Centofanti M, Bucci M. Clinical ability of pattern electroretinograms and visual evoked potentials in detecting visual dysfunction in ocular hypertension and glaucoma. Ophthalmology 2006;113(2):216-228.
14. Bayer AU, Maag KP, Erb C. Detection of optic neuropathy in glaucomatous eyes with normal standard visual fields using a test battery of short-wavelength automated perimetry and pattern electro-retinography. Opthalmology 2002;109(7):1350-1361.
15. Hood DC, Xu L, Thienprasiddhi P, et al. The pattern electroretinogram in glaucoma patients with confirmed visual field deficit. Invest Opthalmol Vis Sci 2005;46(7):2411-2418.
16. Ventura LM, Porciatti DS. Restoration of retinal ganglion cell function in early glaucoma after intraocular pressure reduction. A pilot study. Ophthalmology 2005;112(1):20-27.
17. North RV, Jones AL, Drasdo N, Wild JM, Morgan JE. Electrophysiological evidence of early functional damage in glaucoma and ocular hypertension. Inv Ophthalmol Vis Sci 2010;51(2):1216-1222.
18. Ventura LM, Porciatti V. Pattern electroretinogram in glaucoma. Curr Opin Ophthalmol 2006;17(2):196-202.
19. Mitchell KW, Howe JW, Spencer SR. Visual evoked potentials in the older population: age and gender effects. Clin Phys Physiol Meas 1987;8(4):317-324.
20. Towle VL, Moskowitz A, Sokol S, Schwartz B. The visual evoked potential in glaucoma and ocular hypertension: effects of check size, field size, and stimulation rate. Inv Ophthalmol Vis Sci 1983;24(2),175-183.
21. Kothari R, Bokariya P, Singh S, Singh R. Significance of Visual Evoked Potentials in the Assessment of Visual Field Defects in Primary Open-Angle Glaucoma: A Review. Neurosci J 2013;2013:418320.
22. Murdoch IE, Morris SS, & Cousens SN: People and eyes: statistical approaches in ophthalmology. Br J Ophthalmol 1998;82(8):971-973.

23. Jonas JB, Sturmer J, Papastathopoulos KI, Meier-Gibbsons F, Dichtl A. Optic disc size and optic nerve damage in normal pressure glaucoma. Br J Ophthalmol 1995;79(12):1102-1105.
24. Bellezza AJ, Hart RT, Burgoyne CF. The optic nerve head as a biomechanical structure: initial finite element modeling. Invest Ophthal Vis Sci 2000;41(10):2991-3000.
25. Ventura LM, Porciatti V, et al. Pattern electroretinogram abnormality and glaucoma. Ophtalmology 2005;112(1):10-19.
26. Tuulonen A, Lehtola J, Airaksinen PJ. Nerve fiber layer defects with normal visual field: do normal optic disc and normal visual field indicate absence of glaucomatous abnormality? Ophthalmology 1993;100(5):587-597.
27. Lestak J, Nutterova Elena, Pitrova Sarka, et al. High tension versus normal-tension glaucoma. A comparison of structural and functional examinations. J Clinic Experiment Ophthalmol 2012; S5:006. doi:10.4172/2155-9570.S5-006.

Role of ocular perfusion pressure in glaucoma: the issue of multicollinearity in statistical regression models

Alessandra Guglielmi[1], Giovanna Guidoboni[2], Alon Harris[3]

[1]Dipartimento di Matematica, Politecnico di Milano, Italy, *[2]Department of Mathematical Sciences, Indiana University Purdue University Indianapolis, Indianapolis, USA*, *[3]Eugene and Marilyn Glick Eye Institute, Indianapolis, IN, USA*

Abstract

Purpose: Intraocular pressure (IOP), mean arterial pressure (MAP), systolic blood pressure (SYS), diastolic blood pressure (DIA), ocular perfusion pressure (OPP) are important factors for clinical considerations in glaucoma. The existence of linear relationships among these factors, referred to as multicollinearity in statistics, makes it difficult to determine the contribution of each factor to the overall glaucoma risk. The aim of this work is to describe how to account for multicollinearity when applying statistical methods to quantify glaucoma risk.
Methods: Logistic regression models including multicollinear covariates are reviewed, and statistical techniques for the selection of non-redundant covariates are discussed. A meaningful statistical model including IOP, OPP and SYS as non-redundant covariates is obtained from a clinical dataset including 84 glaucoma patients and 73 healthy subjects, and is used to predict the probability that new individuals joining the study may have glaucoma, based on the values of their covariates.
Results: Logistic models with satisfactory goodness-of-fit to the clinical dataset include age, gender, heart rate and either one of the following triplets as covariates: (*i*)(SYS, DIA, OPP); (*ii*) (IOP, SYS, OPP); (*iii*) (IOP, SYS, DIA); or (*iv*) (IOP, SYS, MAP). Choosing triplet (*ii*), higher disease probabilities are predicted for higher IOP levels. Similar predictions in terms of disease probability can be obtained for different combinations of OPP, SYS and IOP.

Correspondence: Alessandra Guglielmi, Politecnico di Milano, Piazza Leonardo da Vinci 32, 20133 Milano, Italy.
E-mail: alessandra.guglielmi@polimi.it

Conclusion: Multicollinearity does not allow to clearly estimate the single effect of an individual covariate on the overall glaucoma risk. Instead, statistically assessing the combined effects of IOP, OPP, and blood pressure provide useful predictions of disease probability.

Keywords: glaucoma, generalized linear models, logistic regression, multicollinearity, statistical methods, disease probability

1. Introduction

It is well known that elevated intraocular pressure (IOP) is a recognized risk factor for glaucoma. Several other glaucoma risk factors have been suggested, among which low blood pressure deserves particular mention. In order to combine the effects of elevated IOP and low blood pressure, a synthetic index called ocular perfusion pressure (OPP) has been proposed. The index is defined as $\mathrm{OPP} = (2/3)\mathrm{MAP} - \mathrm{IOP}$, where the mean arterial pressure (MAP) is defined as a linear convex combination of the systolic pressure (SYS) and diastolic pressure (DIA), namely $\mathrm{MAP} = (1/3)\mathrm{SYS} + (2/3)\mathrm{DIA}$. Thus, low values of the index OPP may be due to low MAP, elevated IOP or a combination of the two. Whether and to what extent IOP, OPP, MAP, SYS and DIA should be considered as risk factors for glaucoma is still a matter of debate in glaucoma research[1–3]. The present article considers this question from the statistical viewpoint and provides directions to its answer. The existence of formulas relating IOP, OPP, MAP, SYS and DIA is indicative of an issue that in statistics is known as *multicollinearity*, occurring when one or more covariates are defined as a function of the remaining variables. In this paper, we consider this issue from the theoretical viewpoint and provide examples from a real clinical dataset. Our analysis shows that it is the joint effect of all the covariates in the selected logistic model that determines the glaucoma risk, rather than the value of an individual covariate.

2. Methods

2.1 Description of the dataset

Our dataset contains $n = 157$ individuals, including 84 glaucoma patients and 73 healthy subjects. The data were collected within the Indianapolis Glaucoma Progression study and other clinical studies at *Eugene and Marilyn Glick Eye Institute*, Indianapolis (USA), directed by Prof. Alon Harris. The final goal of our statistical analysis is to identify a meaningful set of covariates, i.e. clinical parameters, that provide a good estimate of the probability that a new individual joining the study is a healthy subject or is suffering from glaucoma.

   Let us introduce a *glaucoma indicator* for each individual in the dataset. Let $i = 1, \ldots, n$, with $n = 157$, be the index identifying each individual in the dataset, and let

y_i be the glaucoma indicator for the i-th individual, with $y_i = 1$ if the i-th individual suffers from glaucoma and $y_i = 0$ otherwise. The set of covariates considered for this analysis are: age in years (Age), Gender (1 if female, 0 if male), heart rate (HR), IOP, SYS, DIA, MAP and OPP. Empirical means of these variables and standard deviations for continuous covariates are reported in Table 1. There are 88 women and 69 men in the sample.

Table 1. Empirical means of all the covariates in the dataset; standard deviations for continuous variables are given between brackets.

Age	Gender	HR	IOP
59.95 (11.38)	88 F (69 M)	71.22 (12.60)	16.15 (4.00)

SYS	DIA	MAP	OPP
128.90 (18.32)	83.13 (11.21)	98.41 (12.46)	49.45 (9.39)

.

We recall that the following linear relationships exist among some covariates:

$$\text{MAP} = \frac{1}{3}\text{SYS} + \frac{2}{3}\text{DIA}, \quad \text{OPP} = \frac{2}{3}\text{MAP} - \text{IOP} = \frac{2}{9}\text{SYS} + \frac{4}{9}\text{DIA} - \text{IOP}, \quad (1)$$

meaning that MAP, SYS, DIA, OPP and IOP are *multicollinear covariates*. Lack of awareness of multicollinearity may yield erroneous interpretation of statistical results[4]. A nice concise, but non-technical, overview of statistical problems that may be encountered when covariates are multicollinear can be found in Tu et al[5].

2.2 Logistic regression models and multicollinearity

The use of linear regression models to investigate the effect of IOP, MAP and OPP has recently been questioned. In this section, we aim at clarifying the main points of this debate. Let us assume that the glaucoma indicator y_i for each individual is the realization of a random variable Y_i, and that the individuals are independent. Let us denote by π_i the probability that $Y_i = 1$ and let us assume that π_i can be described by a logistic regression model, so that we can write

$$P(Y_i = 1) := \pi_i, \quad \log(\frac{\pi_i}{1 - \pi_i}) = \beta_0 + \beta_1 x_{i1} + \cdots + \beta_p x_{ip}, \quad i = 1, \ldots, n, \quad (2)$$

where x_{ij} is the value assumed by the j-th covariate in the i-th individual. For example, the model discussed in Khawaja et al[6] considers two covariates, i.e. $p = 2$, with $x_{i1} = $IOP and $x_{i2} = $OPP for each patient i. In (2), the coefficients β_j represent the effect of the j-th covariate on the response (glaucoma indicator). Note that all the parameters β_j, for $j = 0, 1, \ldots, p$, are unknown and they are usually estimated from the dataset $\{(y_i, x_{i1}, , x_{i2}, \ldots, , x_{ip}), i = 1, \ldots, n\}$ via standard statistical techniques, such as maximum likelihood estimate (MLE). The estimated values of the parameters are denoted by $\hat{\beta}_0, \hat{\beta}_1, \ldots, \hat{\beta}_p$. Since individuals are randomly sampled from a larger population (i.e. from the world population), and a vector of covariate values identifies subpopulations of individuals, from (2), it follows that each exponential e^{β_j}, for

$j = 1, \ldots, p$, represents the conditional odds ratio of two subpopulations of individuals, one having the value of the j-th covariate fixed at some value $x^* + 1$, and the other having the value of the same j-th covariate equal to x^* namely

$$e^{\beta_j} = \frac{\text{odds if the covariate } x_{ij} \text{ is incremented by 1}}{\text{odds if the covariate } x_{ij} \text{ is not incremented}}, \tag{3}$$

while keeping all other covariates fixed (i.e. adjusting for the other covariates). It is common practice to drop the index i from the notation and simply write

$$x_j := x_{ij}, \quad Y := Y_i, \quad y := y_i \, .$$

Thus, in mathematical terms, we can rewrite (3) as

$$e^{\beta_j} = \frac{P(Y = 1 | x_j = x + 1, x_l = x_l^*) \, / \, (1 - P(Y = 1 | x_j = x + 1, x_l = x_l^*))}{P(Y = 1 | x_j = x, x_l = x_l^*) \, / \, (1 - P(Y = 1 | x_j = x, x_l = x_l^*))} \tag{4}$$

where x_l^* are fixed values, with $l = 1, \ldots, p$ and $l \neq j$. Thus, β_j quantifies the change in the response variable Y (whose realization corresponds to the glaucoma indicator y) for a unit change in the covariate x_j when the rest of the covariates are fixed (or no other covariates are present). In this perspective, β_j is usually interpreted as the effect of x_j on the response (glaucoma indicator), while adjusting for the other covariates, and $\hat{\beta}_j$ is its estimated value.

This interpretation of β_j does not extend to the case of multicollinear covariates, which is indeed the case for IOP, MAP and OPP, as shown by the relationships in (1). Let us clarify this issue by means of a simple example. Let us suppose that the glaucoma indicator depends only on two covariates, say IOP and OPP. Thus, in this case $p = 2$, $x_1 =$ IOP and $x_2 =$ OPP. According to (2), dropping the index i, the logarithm of the odds of having glaucoma, i.e. $\log(\pi/(1 - \pi))$, is given by:

$$\log \frac{\pi}{1 - \pi} = \beta_0 + \beta_1 \times \text{IOP} + \beta_2 \times \text{OPP} \tag{5}$$

thereby suggesting that β_1 represents the effect of IOP (in the logit scale) on the glaucoma indicator for OPP fixed and that β_2 represents the effect of OPP on the glaucoma indicator for IOP fixed. However, IOP and OPP are related to each other via (1); thus, for IOP fixed, OPP can vary only if MAP varies, yielding:

$$\begin{aligned} \log \frac{\pi}{1 - \pi} &= \beta_0 + \beta_1 \times \text{IOP} + \beta_2 \times OPP \\ &= \beta_0 + \beta_1 \times \text{IOP} + \beta_2 \times \left(\frac{1}{3} \text{MAP} - \text{IOP} \right) \\ &= \beta_0 + \frac{\beta_2}{3} \times \text{MAP} + (\beta_1 - \beta_2) \times \text{IOP}. \end{aligned}$$

The last line suggests that the effect of IOP on the glaucoma indicator is represented by the difference $\beta_1 - \beta_2$ for MAP fixed, which is a different conclusion than that suggested by (5). The controversial aspect related to the interpretation of logistic regression parameters for multicollinear covariates in glaucoma has been discussed in recent works[2,6]. However, Khawaja et al[6] erroneously argue that the intrinsic relationship between IOP and OPP precludes any useful interpretation of OPP as glaucoma risk factor, whereas the issue is just that a different statistical approach should be used to properly account for the relationship between IOP and OPP when analizing clinical data, as discussed in the next section.

2.3 Accounting for multicollinearity in statistical analysis

Multicollinearity does not allow, in general, to interpret the regression parameters e^{β_j} and their estimates $e^{\hat{\beta}_j}$ as the effects of variations of single covariates, while keeping all the others fixed. However, when analyzing a dataset, the main statistical question should not be: "what is the meaning of the regression parameters in the logistic model?", rather "which covariates should be included in the logistic regression in order to obtain a statistical model capable of predicting the response with good accuracy?". The latter question does indeed make sense also in the case of multicollinear variables, as discussed in classical Statistics textbooks (see, for istance, Section 4.6 of the book by Agresti[4]).

For the specific example involving IOP and OPP discussed above, the statistical question should not be whether or not β_2 describes the effect of OPP on the glaucoma indicator for fixed IOP (the answer is obviously *no* since OPP and IOP are intrinsically related); rather, the *real statistical question* is whether OPP, IOP and blood pressure should all be considered as risk factors in glaucoma. On the ground of statistical tools, we prove that the answer to the last question is positive. In order to show this, we need to: identify redundant covariates for the determination of the glaucoma indicator *(Step1)*; obtain statistical models that include only non-redundant covariates and provide good estimates of the probability of having glaucoma for a new individual joining the study *(Step 2)*.

Step 1. The dependency of x_j on the other covariates can be quantified using the variance inflation factor (VIF). For the covariate x_j, this factor is defined as $\text{VIF}_j = 1/(1 - R_j^2)$, where R_j^2 denotes the value of the index $R^2 \in (0, 1)$ in a linear regression model where the value of x_j is determined by the other covariates (see, for istance, Section 4.6.5 of the book by Agresti[4]). If x_j is predicted very well by the other covariates in the linear model, then $R_j^2 \approx 1$ (the higher R^2, the best is the corresponding linear model in predicting the output); as a consequence, VIF_j in this case will be large. As a rule of thumb, the covariate x_j is considered to be redundant if $\text{VIF}_j > 10$. By applying this simple rule to the covariates in the dataset described in Section 2.1, we found that the VIF values were larger than 10 for IOP, SYS, DIA, MAP and OPP, as expected.

Step 2. The outcomes of Step 1 imply that logistic models for the glaucoma in-

dicator can include Age, Gender, HR, and only some covariates among IOP, SYS, DIA, MAP and OPP. Actually, we could select any three covariates among the five above, and would obtain a statistically significant model for any of these choices. The software R is able to select the covariates through a stepwise backward eliminating procedure that starts from a complex model fitted to the dateset and sequentially removes terms, such as the largest p-value in a test of significance, or the least deterioration in the Aikake Information Criterior (AIC), which is a statistical tool to measure goodness-of-fit[4]. For the dataset described in Section 2.1, the software R found that, using the stepwise backward eliminating procedure, the best model includes Age, Gender, HR, SYS, DIA and OPP as covariates. The AIC in this case is optimal, but the same optimal value of AIC is obtained when, in addition to Age, Gender, HR, we select either (IOP, SYS, OPP) or (IOP, SYS, DIA) or (IOP, SYS, MAP). For all these four models, the VIF values for the covariates included in the model are similar (and all smaller than 10). In conclusion, these four models are equivalent in terms of goodness-of-fit measures and measure of dependency among covariates. Therefore, we can choose any of these four models in order to predict the probability of having glaucoma for a new individual entering the study with given values of the selected covariates.

3. Results

The outcomes of Steps 1 and 2 confirm that it makes perfect sense to consider either (SYS, DIA, OPP), or (IOP, SYS, OPP), or (IOP, SYS, DIA), or (IOP, SYS, MAP) as sets of co-variates in order to predict glaucoma probability, despite the existence of functional relationships between them. In this section, we consider the model in equation (2) for $p = 6$ and covariates $x_{ij}, j = 1, \ldots, 6$, given by Age, Gender, HR, IOP, SYS and OPP, respectively, measured for all patients i in the dataset; as usual, independence among patients is assumed. The fitted coefficients are $\hat{\beta}_0 = -16.905$, $\hat{\beta}_1 = 0.107$, $\hat{\beta}_2 = -1.160$, $\hat{\beta}_3 = -0.036$, $\hat{\beta}_4 = 0.177$, $\hat{\beta}_5 = 0.120$, $\hat{\beta}_6 = -0.089$. We use this model to predict the probability of having glaucoma for a new female patient, aged 60 and with HR= 71, joining the study. Table 2 shows that, for given values of OPP, SYS, Age and Gender, different disease probabilities are predicted depending on the level of IOP. In particular, higher IOP levels correspond to higher probabilities of having glaucoma. On the other hand, similar predictions in terms of disease probability can be obtained for different combinations of OPP, SYS, IOP (within the ranges of values in our dataset), suggesting that these covariates should all be considered as important risk factors in glaucoma.

We remark that including diastolic blood pressure in the model would also be an option, as indicated by the cases (SYS, DIA, OPP) and (IOP, SYS, DIA) at the beginning of Section 3. However, we cannot simultaneously include all the covariates in the same statistical model because of the relationship among them, i.e. multicollinearity. It is important to emphasize that removing some of the covariates from the statistical model does not mean that the model does not account for that covariate; rather,

Table 2. Predicted disease probabilities for new female patients, aged 60, HR= 71. For OPP and SYS fixed, higher values of IOP correspond to higher probabilities of having glaucoma (left side of the Table). However, similar disease probabilities are obtained for different values of the covariates (right side of the Table).

OPP	SYS	IOP	Disease prob	Disease prob	OPP	SYS	IOP
43	129	12	0.678	0.673	52	134	13
43	129	16	0.811	0.809	34	132	10
43	129	20	0.897	0.899	20	115	20

variations in that covariate are accounted for through variations in the other collinear variables in the model.

4. Conclusions

The main question motivating our work is whether IOP, OPP and blood pressure should all be interpreted as risk factors in glaucoma. Based on the statistical techniques and analysis reported in this article, our answer is that it is the *joint effect* of IOP, OPP and blood pressure, or, more precisely, of all the covariates in the selected logistic model, that determines the probability of disease, rather than the value of an individual covariate. Importantly, the main statistical interest should be the prediction of disease probabilities for new patients entering the study, presenting specific values of the covariates included in the model, rather than the estimated individual effect of a single predictor.

References

1. Costa V, Harris A, Anderson D, Stodtmeister R, Cremasco F, Kergoat H, et al. Ocular perfusion pressure in glaucoma. Acta Ophthalmol, 2014;92(4): e252–66.
2. Khawaja AP, Crabb DP, Jansonius NM. Time to abandon over-simplified surrogates of ocular perfusion pressure in glaucoma research. Acta ophthalmologica, 2015;93(1): e85–e86.
3. Costa V, Anderson D, Harris A. Surrogates for ocular perfusion pressure are not perfect. Acta Ophthalmol, 2015;93(1): e86–7.
4. Agresti A. Foundations of Linear and Generalized Linear Models. John Wiley & Sons, 2015;
5. Tu YK, Kellett M, Clerehugh V, Gilthorpe M. Problems of correlations between explanatory variables in multiple regression analyses in the dental literature. British dental journal, 2005;199(7): 457–461.
6. Khawaja AP, Crabb DP, Jansonius NM. The Role of Ocular Perfusion Pressure in Glaucoma Cannot Be Studied With Multivariable Regression Analysis Applied to SurrogatesLetters. Investigative ophthalmology & visual science, 2013;54(7): 4619–4620.

Different IOP, different diseases?

Michele Iester, Elisa D'Alessandro

Anatomical-Clinical Laboratory for Functional Diagnosis and Treatment of Glaucoma and Neuro-ophthalmology, Eye Clinic, DINOGMI, University of Genoa, Genoa, Italy

Glaucoma is a chronic, progressive disease characterized by typical optic nerve head changes and visual field defects. These alterations are caused by an intraocular pressure (IOP) being too high for the wellbeing of the specific optic disc.[1] Typical clinical findings in glaucoma patients include thinning of the optic disc rim (Fig. 1), loss of retinal nerve fibers in the inferior sector with subsequent visual field defects in the superior sector.

Fig. 1. Early glaucomatous ONH. The inferior rim is thinner than normal one.

The IOP of the eye is determined by the balance between the amount of aqueous humor that the eye makes and the ease with which it leaves the eye. The Goldmann equation states: Po = (F/C) + Pv; Po is the IOP in millimeters of mercury (mmHg), F is the rate of aqueous formation, C is the facility of outflow, and Pv is the episcleral venous pressure.[2]

As instruments were being developed for more objective measurement of IOP, population surveys at that time found that only approximately two percent of the population had IOP levels above 21 mmHg.[3]

From the literature we know that the mean IOP in the general population varies between 16 and 17 mmHg with the upper 95% confidence interval being 21 mmHg.[4]

Correspondence: Michele Iester, MD, PhD, University Eye Clinic, Viale Benedetto XV, 5, 16132 Genoa, Italy. E-mail: iester@unige.it.

For many years, the cut-off value of 21 mmHg has helped physicians in classifying healthy subjects from glaucomatous patients and ocular hypertension. In the 1960's, Armaly organized in a collaborative investigation of 'ocular hypertensive patients' with intraocular pressure greater than 21 mmHg, but without optic nerve damage or visual loss, Armaly found that the majority of patients in his study did not develop visual field loss over a seven-year period.[5]

IOP value is also used to classified primary open-angle glaucoma (POAG) into having high-tension glaucoma (HTG) or normal-tension glaucoma (NTG). According to the European Glaucoma Society Guidelines, both groups present the same signs and symptoms: initial asymptomatic disease until visual field loss is advanced, typical changes in the optic nerve head, and subsequenttypical alterations of the visual field. NTG patients present these typical changes while presenting a normal IOP (*i.e.*, < 21 mmHg) in contrast to HTG patients who present an IOP of > 21 mmHg without treatment.[1] When evaluating IOP through applanation tonometry it is important to keep corneal thickness, elasticity and structure in mind as the tonometer assumes the central corneal thickness to be 520 µm with minimal variations.[6] However, if the cornea is thinner it is probable that the IOP be under-estimated, and if thicker, an overestimation is more likely. At present, no formula is available for calculating a correct IOP based on corneal thickness.[7]

In particular, for each 10 µm change in central corneal thickness (CCT), the change in the IOP reading could range from 0.1 to 0.7 mmHg.[8-10] Furthermore, the variability of Goldmann IOP measurements could depend on the thickness of the tear film, corneal astigmatism, the season, and the examiner's competence in IOP measure-ments. The CCT is not associated with refractive error, corneal curvature, anterior chamber depth, or axial length. It is an independent factor unrelated to other ocular parameters.[11,12] Furthermore, the CCT can vary between glaucoma populations. For example, the Japanese eyes have thinner corneas than the Chinese and Filipino eyes; white, Chinese, Hispanic, and Filipino eyes have comparable CCT values; and the corneas of African Americans are significantly thinner.[13]

Corneal hysteresis might also interfere with IOP measurements, although it is not clear what it measures; it appears as though this corneal variable describes the response of the cornea to rapid deformation. Congdon *et al.* suggest that the relationship between glaucoma and corneal features is more complex than simple anatomic thickness.[14]

Astigmatism, direction of gaze, and tear thickness are clinically important sources of error in Goldmann applanation tonometry. In a model comparing tonometers with the mean IOP value, the Goldmann tonometer was least affected by differences in CCT and the Tono-Pen was least affected by differences in hysteresis.[15]

With regard to NTG we can identify two main opinions regarding the disease. Many authors[16-24] define NTG as being a particular subtype of glaucoma presenting typical glaucomatous optic nerve head damage and visual field defects. These include inferior rim loss, paracentral scotoma, and peripapillary hemorrhages. On the other

hand, another group of authors believe NTG and HTG to be the same disease.[25-32]

In a recent study,[32] the aim of which was 'to determine whether the patterns of visual field damage between HTG and NTG are equivalent', Iester *et al.* did not find any difference in the pointwise analysis between the two nor any difference in paracentral areas as was described in other studies. Furthermore, Drance *et al.* were able to subdivide glaucoma patients based on the characteristics of the optic disc. More specifically, in a paper co-authored by Drance and Nicolela, four different subgroups were identified based on the appearance of the optic disc: focal ischemic, senile sclerotic, myopic and concentric enlargement.[33] For each group different, statistically significant risk factors were identified, for instance: focal ischemic patients were younger with a localized typical visual field damage, mainly female with migraine or Raynoud syndrome and lower IOP, on the other hand concentric enlargement patients were older with higher IOP and typical visual field defect.

Another study conducted by Drance and Schultzer analyzed different clinical risk factors in a population composed of both patients with NTG and HTG (risk factors included age, gender, mean IOP, anticardiolipin antibody, HDL, LDL, etc.).[34] Multi-variate analysis revealed two statistically different clusters of patients with NTG and HTG cases equally distributed. The two clusters showed different risk factors associated, therefore showing that IOP is fundamental but not the sole factor necessary in distinguishing NTG from HTG.[34]

When patients present with typical glaucomatous optic disc, visual field and high IOP diagnosis of HTG is very simple. On the other hand, in the presence of normal IOP, with the same clinical characteristics, diagnosis is not as easy. Diseases other than NTG must therefore be taken in consideration. These include optical nerve head coloboma, congenital optic nerve head pit and tilted optic nerve head and arteritic anterior ischemic optic neuropathy which in the chronic phase can have a large cupping outlining that ischemic disease can change the optic nerve hypoplasia (ONH) color after the acute moment, but with time the degeneration of ganglion cells and astroglia can cause a loss of tissue with an increase of cupping.

Before diagnosing NTG, it is important to assess other possible causes which may determine otherwise pseudo-glaucomatous alterations. One of the structures to evaluate is the visual pathway from the retina to the cortex.[35] In a study, conducted by Iqbal *et al.*,[36] the prevalence of intracranial compressive lesions in NTG and HTG were compared through the use of MRI. A statistically significant difference between the two was found with four of the NTG patients having clinically significant intra-cranial compressive lesions compared to none in the HTG group (p = 0.039). The identification of these lesions therefore excluded the diagnosis of NTG, even though the patients presented with typical optic disc and visual field anomalies, making evaluation of the visual pathway important in the normal work-up of these patients. In the latter paper, Iqbal et al. showed atypical chiasmatic lesions which could mimic typical glaucomatous optic disc lesions.[36]

A further evaluation which is needed is the assessment of the progression of

the disease, as glaucoma is, by definition, progressive. Therefore close follow-up is mandatory in these patients in order to identify an ongoing decline in the visual field or structure of the optic disc. It has been shown that at least three visual field tests per year for at least two years is necessary to assess the rate of progression of glaucomatous patients.[37] Other neuro-ophthalmological diseases can develop a visual field damage but usually the rate of progression is different: in the anterior ischemic optic neuropathy (AION) the progression, if it happens, is 'a poussée', or there is not a correlation between ONH damage and, in particular, cupping appearance and visual field lesions. In POAG, usually, the loss of ganglion cells in ONH or in the retinal nerve fiber imaging (RNFL) is well-localized and correlated to visual field defect.

No very specific or sensitive factor has been identified to predict optic nerve head cupping in glaucomatous patients or ONH change in non-glaucomatous patients.[35]

In conclusion, NTG and HTG seem to be very similar diseases with IOP being the main differentiating factor. Different types of glaucoma exist and are probably based on presence of different risk factors, however, differential diagnosis is fundamental when considering NTG.

Acknowledgment

References

1.   European Glaucoma Society. Terminology and Guidelines for Glaucoma. Ch. 2. Savona: Dogma 2003.
2.   American Academy of Ophthalmology. Basic and Clinical Science Course Section 10: Glaucoma. Singapore: American Academy of Ophthalmology 2008.
3.   Colton T, Ederer F. The distribution of intraocular pressures in the general population. Surv Ophthalmol 1980;25(3):123-129.
4.   Alimuddin M. Normal intra-ocular pressure. Br J Ophthalmol 1956;40(6):366-372.
5.   Armaly MF. On the distribution of applanation pressure and arcuate scotoma. In: Patterson G, Miller SJ, Patterson GD (eds.), Drug Mechanisms in Glaucoma. Boston, MA: Little, Brown 1966.
6.   Goldmann H, Schmidt T. Über Applanationstonometrie. Ophthalmologica 1957;134:221-242
7.   Iester M, Mete M, Figus M, Frezzotti P. Incorporating corneal pachymetry into the management of glaucoma. J Cataract Refract Surg 2009;35:1623-1628.
8.   Doughty MJ, Zaman ML. Human corneal thickness and its impact on intraocular pressure measures: a review and meta-analysis approach. Surv Ophthalmol 2000;44:367-408.
9.   Kniestedt C, Lin S, Choe J, et al. Clinical comparison of contour and applanation tonometry and their relationship to pachymetry. Arch Ophthalmol 2005;123:1532-1537.
10.   Tonnu P-A, Ho T, Newson T, et al. The influence of central corneal thickness and age on intraocular pressure measured by pneumotonometry, non-contact tonometry, the Tono-Pen XL, and Goldmann

applanation tonometry. Br J Ophthalmol 2005;89:851-854.

11. Chen M-J, Liu Y-T, Tsai C-C, et al. Relationship between central corneal thickness, refractive error, corneal curvature, anterior chamber depth and axial length. J Chin Med Assoc 2009;72:133-137.

12. Shimmyo M, Orloff PN. Cornea thickness and axial length. Am J Ophthalmol 2005;139:553-554.

13. Aghaian E, Choe JE, Lin S, Stamper RL. Central corneal thickness of Caucasians, Chinese, Hispanics, Filipinos, African Americans, and Japanese in a glaucoma clinic. Ophthalmology 2004;111:2211-2219.

14. Congdon NG, Broman AT, Bandeen-Roche K, Grover D, Quigley HA. Central corneal thickness and corneal hysteresis associated with glaucoma damage. Am J Ophthalmol 2006;141:868-875.

15. Broman AT, Congdon NG, Bandeen-Roche K, Quigley HA. Influence of corneal structure, corneal responsiveness, and other ocular parameters on tonometric measurement of intraocular pressure. J Glaucoma 2007;16:581-588.

16. Tuulonen A, Airaksinen PJ. Optic disc size in exfoliative, primary open angle, and low tension glaucoma. Arch Ophthalmol 1992;110:211-213.

17. Caprioli J, Spaeth GL. Comparison of the optic nerve head in high- and low-tension glaucoma. Arch Ophthalmol 1985;103:1145-1149.

18. Greve EL, Geijssen HC. The relation between excavation and visual field in glaucoma patients with high and with low intraocular pressure. Doc Ophthalmol Proc Ser 1983;35:35-42.

19. Anderton S, Hitchings RA. A comparative study of visual fields of patients with low tension glaucoma and those with chronic simple glaucoma. Doc Ophthalmol Proc Ser 1983;35:97-99.

20. Chauhan BC, Drance SM, Douglas GR, Johnson CA. Visual field damage in normal tension and high tension glaucoma. Am J Ophthalmol 1989;108:636-642.

21. Drance SM. The visual fields of low tension glaucoma and shock-induced optic neuropathy. Arch Ophthalmol 1977;95:1359-1361.

22. Fazio P, Krupin T, Feitl ME, Werner EB, Carrè DA. Optic disc topography in patients with low-tension and primary open angle glaucoma. Arch Ophthalmol 1990;108:705-708.

23. Yamagami J, Araie M, Shirato S. A comparative study of optic nerve head in low- and high-tension glaucomas. Graefe's Arch Clin Exp Ophthalmol 1992;230:446-450.

24. Samuelson TW, Spaeth GL. Focal and diffuse visual field defects: their relationship to intraocular pressure. Ophthalmic Surg 1993;24:519-525.

25. Motolko M, Drance SM, Douglas DR. The visual field defects of low-tension glaucoma. In Greve EL, Heijl A (eds.),Fifth International Visual Field Symposium, pp. 107-111. The Hague, Dr W Junk NV Publishers 1983.

26. Lewis RA, Hayreh SS, Phelps CD. Optic disc and visual field correlations in primary open-angle and low-tension glaucoma. Am J Ophthalmol 1983;96:148-152.

27. Motolko M, Drance SM, Douglas GR. Visual field defects in low tension glaucoma. Comparison of defects in low tension glaucoma and chronic open angle glaucoma. Arch Ophthalmol 1982;100:1074-1077.

28. King D, Drance SM, Douglas GR, Schulzer M, Wijsman K. Comparison of visual field defects in normal-tension glaucoma and high-tension glaucoma. Am J Ophthalmol 1986;101:204-207.

29. Miller KM, Quigley HA. Comparison of optic disc features in low-tension and typical open-angle glaucoma. Ophthalmic Surg 1987;18:882-889.

30. Iester M, Mikelberg FS. Optic nerve head morphologic characteristics in high-tension and normal-tension glaucoma. Arch Ophthalmol 1999;117:1010-1013.

31. Iester M, Swindale NV, Mikelberg FS. Sector-based analysis of optic nerve head shape parameters and visual field indices in healthy and glaucomatous eyes. J Glaucoma 1997;6:371-376.

32. Iester M, DeFeo F, Douglas GR. Visual field loss morphology in high- and normal-tension glaucoma. J Ophthalmol 2012;2012:327326. (Epub 2012 Feb 8)

33. Nicolela MT, Drance SM. Various glaucomatous optic nerve appearances: clinical correlations. Ophthalmology 1996;103:640-649.

34. Schulzer M, Drance SM, Carter CJ, Brooks DE, Douglas GR, Lau W. Biostatistical evidence for two distinct chronic open angle glaucoma populations.Br JOphthalmol 1990;74:196-200.

35. Greenfield DS, Siatkowski RM, Glaser JS, Schatz NJ, Parrish RK 2nd. The cupped disc. Who needs imaging? Ophthalmology 1998;105:1866-1874
36. Ahmed IIK, Feldman F, Kucharrczyk W, Trope GE. Neuroradiologic screening in normal-pressure glaucoma: study results and literature review. J Glaucoma 2002;11:279-286.
37. Chauhan BC, Garway-Heath DF, Goñi FJ, et al. Practical recommendations for measuring rates of visual field change in glaucoma. Br J Ophthalmol. 2008;92(4):569-573.

24-hour IOP fluctuation: myth or reality?

Luciano Quaranta[1], Ivano Riva[1], Francesco Oddone[2]

[1]Department of Medical and Surgical Specialties, Radiological Sciences and Public Health, University of Brescia, Brescia, Italy; [2]IRCCS Fondazione G.B. Bietti, Rome, Italy

Abstract

Existing literature is divided on the importance of short-term intraocular pressure fluctuation as an independent factor for glaucoma development and progression. In this paper we present evidences in favor of and against the value of 24-hour intraocular pressure fluctuation in the evaluation and prognosis of patients with glaucoma. Potential directions for future studies and the role of new instruments for continuous intraocular pressure monitoring will be presented.

Intraocular pressure (IOP) is an important factor in diagnosing and managing glaucoma. Studies suggest that IOP tends to fluctuate throughout the day and over longer intervals.[1-4] Although mean IOP is known to correlate with glaucoma progression,[5-8] actually no conclusive evidence can be drawn about IOP fluctuations.

The rationale for IOP measurements throughout the 24-hour cycle is that IOP exhibits time-dependent variation that can reach up to 6 mmHg over a 24-hour period in healthy eyes, even more in eyes with glaucoma.[9-12] Therefore, a single office-hour IOP measurement offers little information regarding the IOP profile of a patient. IOP variation could be associated with optic nerve injury because, at least in principle, the continuous and excessive fluctuation of parameters in any biological system may overwhelm the homeostatic mechanisms responsible for buffering stresses.

The traditional view is that IOP is generally higher in the morning. Konstas *et al.* found that although peak IOPs in up to 45% of untreated exfoliation glaucoma and 22.5% of untreated primary open-angle glaucoma (POAG) patients are outside office hours,[13] mean peak IOP in 24-hour curves is generally between 6 AM and 10

Correspondence: Luciano Quaranta, USVD "Centro per lo Studio del Glaucoma", Piazzale Spedali Civili, 1, 25123 Brescia, Italy. E-mail: luciano.quaranta@unibs.it

AM.[14-16] Quaranta *et al.* found similar IOP profiles (Fig. 1),[17-19] but other authors did not.[20-22] Discrepancies in the observed circadian IOP patterns among studies may be explained by differences in equipment (pneumotonometer vs Perkins or Goldmann tonometers) or study samples. The diagnosis of glaucoma and the use of topical IOP-lowering medication could per se influence 24-hour IOP rhythms. Moreover, age differences need to be taken into account when comparing IOP curves derived from different studies. Mansouri *et al.*[23] found that older healthy individuals in a sleep laboratory, irrespective of body posture, had a mean cosine-fitted peak IOP at around 10:20 AM, whereas the respective peak for younger healthy individuals was earlier, between 5:30 AM and 6:30 AM depending on body posture. Sleep lab conditions may also create an environment that affects biological rhythms. Contrary to hospital-based investigations, sleep laboratory studies may allow for some adjustment to the patient's usual routine of food intake or activities in the sitting or recumbent positions better simulating normal life.

Different levels of evidence regarding the role of IOP characteristics in glaucoma can be found in several reports.[24-30] Large, well-designed, prospective studies on the importance of circadian IOP fluctuation are currently lacking, and the existing literature has not produced consistent results. Moreover, actually there is no consensus about the way to define short-term IOP fluctuation: while it's generally defined as the difference between peak and through,[3] standard deviation (SD) of measurements has also been advocated.[31]
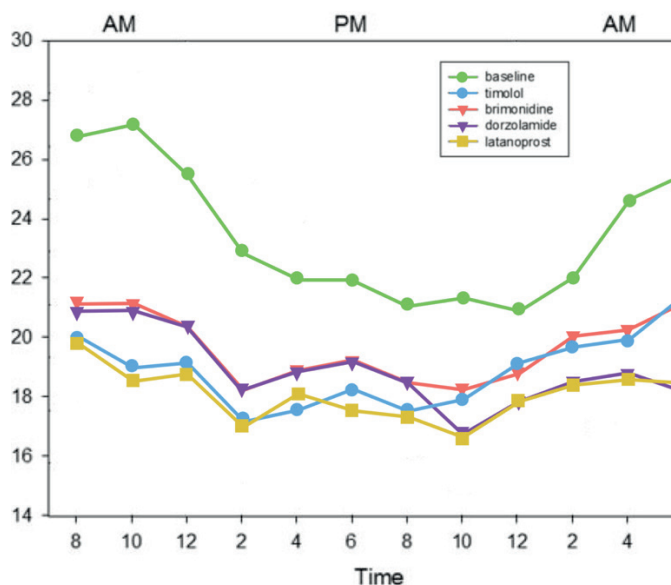
Fig. 1. 24-hour IOP profiles in treated POAG patients. (Adapted from Quaranta *et al.*[17])

Several reports found an increased short-term IOP fluctuation in patients affected by glaucoma than in controls, prevalently during office-hour.[32-34] Saccà *et al*. found that patients affected by POAG had a greater relative daily fluctuation (between -7 and +9.6%) than patients with normal-tension glaucoma (NTG, between -4.7 and +6.4%) or healthy eyes (between -3.4% and +6.9%).[35] On the other hand, following a cohort of 29 patients affected by ocular hypertension (OHT) for five years, Thomas *et al*. found that mean daily IOP fluctuation was 8.6 mmHg in patients progressed to POAG (n = 4), compared to 5.4 mmHg in patients not progressed.[36] In agreement with these results, Asrani *et al*. showed a strong association between diurnal fluctuation of IOP and disease progression in 105 eyes of 64 treated POAG patients using self-to-nometry.[37] Both the diurnal IOP and the short-term fluctuation over multiple days were significant predictors of progression. The mean office IOP had no predictive value, and the mean home IOP showed a weak association with progression. Indeed, this study was largely criticized, due to the use of self-tonometry and no stringent criteria for visual field progression evaluation. Moreover, an abnormally high rate of visual field progression was found.

In the Handan study, 47 Chinese patients affected by POAG underwent a 24-hour IOP curve, before starting any medication.[38] Mean IOP fluctuation was 6.0 ± 2.2 mmHg (range, 2-11 mmHg), and 72% of the patients had IOP fluctuation ≥ 5 mmHg. No correlation was found between 24-hour IOP fluctuation and Humphrey mean deviation (MD) (r = -0.166, P = 0.32). Interestingly, in patients with unilateral POAG, Authors found no difference in mean 24-hour IOP, peak IOP, trough IOP, or IOP fluctuation when comparing the glaucomatous eye with the nonglaucomatous eye (P>0.05). Results from this study should be interpreted with caution, taking into account that all patients enrolled were from oriental ethnicity and that over 90% of subjects from Handan had IOP below the cut-off of 21 mmHg.

Jonas *et al*.[39] performed a retrospective chart review of 855 eyes from 458 treated patients with NTG, POAG, or OHT. They investigated the potential correlation between 24-hour IOP parameters and progression of the disease, after a mean follow-up time of 55.6 months (range 5.4–124.9 months). In a multiple Cox pro-portional hazards model, progression of the disease was associated with age and neuroretinal RIM area. For the POAG group specifically, only age (p < 0.001) was a significant prognostic factor, whereas in the NTG group, higher mean IOP (p = 0.036) and lower fluctuation (p = 0.045) were identified as predictors of disease progression. Participants were receiving topical medication that is known to reduce IOP levels and its fluctuation, and the effect of 24-hour IOP variation may have been blunted.

In a recent study by Fogagnolo *et al*., 52 patients affected by POAG under topical therapy were followed-up for two years, after a 24-hour IOP baseline curve.[31] Authors registered visual field progression endpoint and investigated baseline IOP characteristics correlated with visual field progression. Regarding 24-hour IOP char-acteristics, only IOP peak was correlated to visual field progression, while 24-hour IOP fluctuation was not an independent risk factor. Indeed, 24-hour mean, peak

and fluctuation were associated with each other and a strong correlation was found between mean and peak IOP, and between fluctuation and peak IOP.

Twenty-four-hour IOP fluctuation could be a risk factor for glaucoma patients with low IOP and could influence ocular perfusion pressure. In a small cohort of 33 patients affected by NTG, Sakata et al. found that 24-hour IOP fluctuation was negatively correlated to visual field MD at baseline.[40] However, Choi et al. found opposite results in a retrospective study on 113 patients affected by NTG.[41] In this study, no correlation was found at baseline between 24-hour IOP fluctuation, visual field functional variables (MD and pattern standard deviation (PSD)) and anatomical variables (scanning laser polarimetry, GDX-VCC). Only fluctuation of mean ocular perfusion pressure (MOPP) was significantly correlated with decreased MD, increased PSD, and increased Advanced Glaucoma Intervention Study scores. Besides the correlation with functional outcome variables, the model identified MOPP fluctuation as an important predictor of structural damage, such as a thinner retinal nerve fiber layer. Similarly, Sung et al. published a retrospective chart review of 101 NTG patients with at least four years of follow-up and 24-hour sitting IOP and MOPP tracings.[42] Multivariate regression analysis identified baseline PSD and 24-hour MOPP fluctuations as significant predictors of visual field progression, but no correlation between VF progression and either 24-hour or follow-up IOP fluctuation was found. According to the model, each mmHg increase in MOPP fluctuation was associated with approximately 27% greater hazard ratio of glaucoma progression during follow-up.

As a result of all these studies, no conclusive evidences about the role of short-term IOP fluctuation in glaucoma can be drawn. Moreover, other points remain to be addressed. While 24-h IOP monitoring may provide the most accurate measurements, it is often limited by expense and doubts persist about stability of IOP patterns and IOP fluctuation from one day to the next, or between fellow eyes. Realini et al. found fair to good agreement of IOP values at each time-point in treated POAG patients who underwent two daytime IOP curves, one week apart (intraclass correlation coefficients (ICCS) ranging from 0.45 to 0.71 in right eyes and from 0.51 to 0.71 in left eyes).[30] However, poor agreement was found when IOP changes over time periods were considered (e.g., the change in IOP from 8 AM to 10 AM on visit 1 compared with the change in IOP from 8 AM to 10 AM on visit 2), with ICCS coefficients ranging from -0.08 to 0.38 in right eyes and from -0.11 to 0.36 in left eyes. These results show that IOP data collected on a single day could inadequately characterize diurnal or 24-hour IOP variability over time, making IOP curve repetition a new task to explore.

Another inherent problem with circadian IOP investigations is the assumption that awakening patients at night for IOP measurements does not significantly affect their endogenous IOP rhythm. To further compound the problem, patients are often asked to walk to a nearby slit-lamp and have their IOP measured in the sitting position. A newly developed 24-hour telemetric contact lens-embedded IOP

sensor could allow undisturbed tonometry of glaucoma patients at home[43] and may corroborate some of the existing evidence regarding the circadian IOP pattern found in sleep laboratory studies.[20-22] However, data provided by this instrument are not in mmHg and do not correlate with IOP values in mmHg.

In conclusion, further research is needed to establish the role of 24-hour IOP fluctuation in glaucoma, and to understand if 24-hour IOP fluctuation can influence our therapeutic decisions. Since current data suggest that repeatability of IOP change over time is uniformly poor, it's important to repeat diurnal IOP recordings in case a patient continues to deteriorate, in spite of an adequate diurnal IOP control, and in all patients with advanced disease. IOP is not a static number, but tends to fluctuate throughout the 24 hours. Mean IOP is a strong predictor of glaucomatous damage. A desired therapeutic target is therefore a uniform reduction of IOP throughout the 24 hours. A reliable method of continuous IOP measurement would be desirable, making 24-hour IOP phasing easier and opening new pathways for research.

References

1. Drance SM. The significance of the diurnal phasic variation of intraocular pressure in normal and glaucomatous eyes. Trans Can Opthalmolog Soc 1960;23:131-140.
2. Kitazawa Y, Horie T. Diurnal variation of intraocular pressure in primary open-angle glaucoma. Am J Ophthalmol 1975;79(4):557-566.
3. Lee PP, Sultan MB, Grunden JW, et al. Assessing the Importance of IOP Variables in Glaucoma Using a Modified Delphi Process. J Glaucoma 2010;19(5):281-287.
4. Quaranta L, Katsanos A, Russo A, Riva I. 24-hour intraocular pressure and ocular perfusion pressure in glaucoma. Surv Ophthalmol 2013;58(1):26-41.
5. Heijl A, Leske MC, Bengtsson B, et al. Reduction of intraocular pressure and glaucoma progression: results from the Early Manifest Glaucoma Trial. Arch Ophthalmol 2002;120(10):1268-1279.
6. The Advanced Glaucoma Intervention Study (AGIS): 7. The relationship between control of intraocular pressure and visual field deterioration.The AGIS Investigators. Am J Ophthalmol 2000;130(4):429-440.
7. De Moraes CG, Juthani VJ, Liebmann JM, et al. Risk factors for visual field progression in treated glaucoma. Arch Ophthalmol 2011;129(5):562-568.
8. Garway-Heath DF, Crabb DP, Bunce C, et al. Latanoprost for open-angle glaucoma (UKGTS): a randomised, multicentre, placebo-controlled trial. Lancet 2015;385(9975):1295-1304.
9. Drance SM. Diurnal Variation of Intraocular Pressure in Treated Glaucoma. Significance in Patients with Chronic Simple Glaucoma. Arch Ophthalmol 1963;70:302-311.
10. Duke-Elder S. The phasic variations in the ocular tension in primary glaucoma. Am J Ophthalmol 1952;35(1):1-21.
11. Langley D, Swanljung H. Ocular tension in glaucoma simplex. Br J Ophthalmol 1951;35(8):445-458.
12. Loewen NA, Liu JH, Weinreb RN. Increased 24-hour variation of human intraocular pressure with short axial length. Invest Ophthalmol Vis Sci 2010;51(2):933-937.
13. Konstas AG, Mantziris DA, Stewart WC. Diurnal intraocular pressure in untreated exfoliation and primary open-angle glaucoma. Arch Ophthalmol 1997;115(2):182-185.
14. Konstas AG, Mantziris DA, Cate EA, Stewart WC. Effect of timolol on the diurnal intraocular pressure in exfoliation and primary open-angle glaucoma. Arch Ophthalmol 1997;115(8):975-979.

15. Konstas AG, Lake S, Economou AI, et al. 24-Hour control with a latanoprost-timolol fixed combination vs timolol alone. Arch Ophthalmol 2006;124(11):1553-1557.
16. Konstas AG, Tsironi S, Vakalis AN, et al. Intraocular pressure control over 24 hours using travoprost and timolol fixed combination administered in the morning or evening in primary open-angle and exfoliative glaucoma. Acta Ophthalmol 2009;87(1):71-76.
17. Quaranta L, Gandolfo F, Turano R, et al. Effects of topical hypotensive drugs on circadian IOP, blood pressure, and calculated diastolic ocular perfusion pressure in patients with glaucoma. Invest Ophthalmol Vis Sci 2006;47(7):2917-2923.
18. Quaranta L, Konstas AG, Rossetti L, et al. Untreated 24-h intraocular pressures measured with Goldmann applanation tonometry vs nighttime supine pressures with Perkins applanation tonometry. Eye (Lond) 2010;24(7):1252-1258.
19. Quaranta L, Miglior S, Floriani I, et al. Effects of the timolol-dorzolamide fixed combination and latanoprost on circadian diastolic ocular perfusion pressure in glaucoma. Invest Ophthalmol Vis Sci 2008;49(10):4226-4231.
20. Liu JH, Zhang X, Kripke DF, Weinreb RN. Twenty-four-hour intraocular pressure pattern associated with early glaucomatous changes. Invest Ophthalmol Vis Sci 2003;44(4):1586-1590.
21. Liu JH, Kripke DF, Hoffman RE, et al. Nocturnal elevation of intraocular pressure in young adults. Invest Ophthalmol Vis Sci 1998;39(13):2707-2712.
22. Liu JH, Bouligny RP, Kripke DF, Weinreb RN. Nocturnal elevation of intraocular pressure is detectable in the sitting position. Invest Ophthalmol Vis Sci 2003;44(10):4439-4442.
23. Mansouri K, Weinreb RN, Liu JH. Effects of aging on 24-hour intraocular pressure measurements in sitting and supine body positions. Invest Ophthalmol Vis Sci 2012;53(1):112-116.
24. Bengtsson B, Heijl A. Diurnal IOP fluctuation: not an independent risk factor for glaucomatous visual field loss in high-risk ocular hypertension. Graefes Arch Clin Exp Ophthalmol 2005;243(6):513-518.
25. Bengtsson B, Leske MC, Hyman L, et al. Fluctuation of intraocular pressure and glaucoma progression in the early manifest glaucoma trial. Ophthalmology 2007;114(2):205-209.
26. Deokule SP, Doshi A, Vizzeri G, et al. Relationship of the 24-hour pattern of intraocular pressure with optic disc appearance in primary open-angle glaucoma. Ophthalmology 2009;116(5):833-839.
27. Gumus K, Bozkurt B, Sonmez B, et al. Diurnal variation of intraocular pressure and its correlation with retinal nerve fiber analysis in Turkish patients with exfoliation syndrome. Graefes Arch Clin Exp Ophthalmol 2006;244(2):170-176.
28. Musch DC, Gillespie BW, Niziol LM, et al. Intraocular pressure control and long-term visual field loss in the Collaborative Initial Glaucoma Treatment Study. Ophthalmology 2011;118(9):1766-1773.
29. Nouri-Mahdavi K, Hoffman D, Coleman AL, et al. Predictive factors for glaucomatous visual field progression in the Advanced Glaucoma Intervention Study. Ophthalmology 2004;111(9):1627-1635.
30. Realini T, Weinreb RN, Wisniewski S. Short-term repeatability of diurnal intraocular pressure patterns in glaucomatous individuals. Ophthalmology 2011;118(1):47-51.
31. Fogagnolo P, Orzalesi N, Centofanti M, et al. Short- and long-term phasing of intraocular pressure in stable and progressive glaucoma. Ophthalmologica 2013;230(2):87-92.
32. David R, Zangwill L, Briscoe D, et al. Diurnal intraocular pressure variations: an analysis of 690 diurnal curves. Br J Ophthalmol 1992;76(5):280-283.
33. Sihota R, Saxena R, Gogoi M, et al. A comparison of the circadian rhythm of intraocular pressure in primary phronic angle closure glaucoma, primary open angle glaucoma and normal eyes. Indian J Ophthalmol 2005;53(4):243-247.
34. Tajunisah I, Reddy SC, Fathilah J. Diurnal variation of intraocular pressure in suspected glaucoma patients and their outcome. Graefes Arch Clin Exp Ophthalmol 2007;245(12):1851-1857.
35. Sacca SC, Rolando M, Marletta A, et al. Fluctuations of intraocular pressure during the day in open-angle glaucoma, normal-tension glaucoma and normal subjects. Ophthalmologica 1998;212(2):115-119.
36. Thomas R, Parikh R, George R, et al. Five-year risk of progression of ocular hypertension to primary open angle glaucoma. A population-based study. Indian J Ophthalmol 2003;51(4):329-333.

37. Asrani S, Zeimer R, Wilensky J, et al. Large diurnal fluctuations in intraocular pressure are an inde-
     pendent risk factor in patients with glaucoma. J Glaucoma 2000;9(2):134-142.
38. Wang NL, Friedman DS, Zhou Q, et al. A population-based assessment of 24-hour intraocular
     pressure among subjects with primary open-angle glaucoma: the handan eye study. Invest Ophthal-
     mol Vis Sci 2011;52(11):7817-7821.
39. Jonas JB, Budde WM, Stroux A, et al. Diurnal intraocular pressure profiles and progression of chronic
     open-angle glaucoma. Eye (Lond) 2007;21(7):948-951.
40. Sakata R, Aihara M, Murata H, et al. Intraocular pressure change over a habitual 24-hour period after
     changing posture or drinking water and related factors in normal tension glaucoma. Invest Ophthal-
     mol Vis Sci 2013;54(8):5313-5320.
41. Choi J, Kim KH, Jeong J, et al. Circadian fluctuation of mean ocular perfusion pressure is a consistent
     risk factor for normal-tension glaucoma. Invest Ophthalmol Vis Sci 2007;48(1):104-111.
42. Sung KR, Lee S, Park SB, et al. Twenty-four hour ocular perfusion pressure fluctuation and risk of
     normal-tension glaucoma progression. Invest Ophthalmol Vis Sci 2009;50(11):5266-5274.
43. Mansouri K, Shaarawy T. Continuous intraocular pressure monitoring with a wireless ocular te-
     lemetry sensor: initial clinical experience in patients with open angle glaucoma. Br J Ophthalmol
     2011;95(5):627-629.

Integrated Multidisciplinary Approaches in the Study and Care of the Human Eye

Integrated Multidisciplinary
Approaches in the Study
and Care of the Human Eye

EDITED BY
PAOLA CAUSIN
GIOVANNA GUIDOBONI
RICCARDO SACCO
ALON HARRIS

EDITED BY

PAOLA CAUSIN
GIOVANNA GUIDOBONI
RICCARDO SACCO
ALON HARRIS

ISBN 978-90-6299-241-6
Dec. 2015. x and 185 pages. Hardbound.
Many figures and photos. 16x24 cm
List price € 80.00 / US $ 100.00*

Discount price: € 72.00 / US $ 90.00*
* excl. 6% VAT (only applicable for EU customers) and shipping costs

The human eye offers the possibility to non-invasively observe and quantify many morphological and hemodynamical data in real time. The interpretation of these dynamic data, however, remains a challenging task.

Mathematical models provide quantitative representations of the biomechanics and fluid-dynamics of the eye and their relationship with systemic conditions providing a valuable investigative tool. While inevitably presenting complex mathematics, this volume is not intended solely for mathematicians, rather it facilitates a new and exciting interdisciplinary field and approach to eye disease.

CORNEAL BIOMECHANICS

from theory to practice

Edited by

Cynthia J. Roberts
Jun Liu

CORNEAL
BIOMECHANICS
from theory to practice

CORNEAL BIOMECHANICS
from theory to practice
Edited by
Cynthia J. Roberts and **Jun Liu**

ISBN: 978-90-6299-248-5
2016, 315 pages, with numerous full color illustrations, hardbound, 16x24cm

List price: € 125 ($ 150)
DISCOUNT PRICE: € 112,50 ($ 135)*
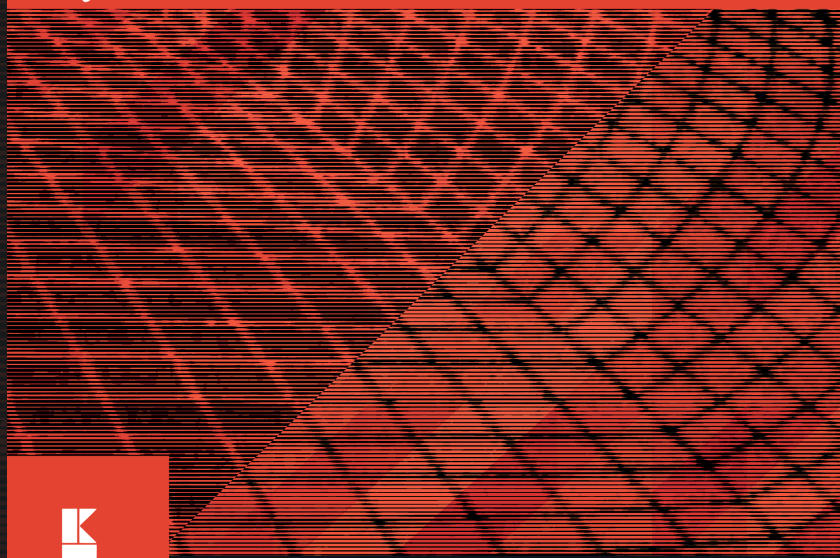
Please use discount code **CB1678** when ordering at
www.kuglerpublications.com

*excl. 6% VAT (only applicable for European Union customers) and shipping costs

SPECIAL OFFER | 10% DISCOUNT

Corneal Biomechanics: From Theory to Practice represents the first comprehensive book on corneal biomechanics, with clinicians as the target audience. The book is divided into three sections: **Basics**, **Devices**, and **Applications**. The **Basics** section includes an introduction to important biomechanical concepts and vocabulary, as well as laboratory techniques for quantifying biomechanical properties and a comparison of properties between human and porcine eyes.

The **Devices** section includes chapters written by representatives of the manufacturers of the Ocular Response Analyzer and the Corvis ST, the only two commercial devices available for characterizing biomechanical deformation response to an air puff, as well as three other promising technologies with which data has been acquired on living human eyes, written by the main developer(s) of the respective technology. The **Applications** section starts with a chapter on interpretation of deformation characteristics, followed by two chapters relevant for glaucoma specialists, and four chapters relevant for cornea and refractive surgeons.

CORNEAL TOPOGRAPHY
from theory to practice

Edited by: A. Kılıç & C.J. Roberts

List Price: € 125 / US $ 156.25
Discount Price: € 100 / US $ 125

ISBN 13: 978-90-6299-230-0
2013. Book. xxxii and 370 pages.
With numerous full color illustrations,
hardbound, 16x24cm (6.3x9.4in)

"Kılıç and Roberts have assembled a strong team of experts to create a treatise of extraordinary value to the eye care professionals. Modern corneal topography is presented from the fundamental concepts, to the descriptions of representative instruments available, to a selection of the many applications to which this technology has applied itself"
Stephen D. Klyce, taken from the preface.